2002-09-01

Diffusion Based Grating Formation in a Photopolymer Material

Justin R. Lawrence
Technological University Dublin

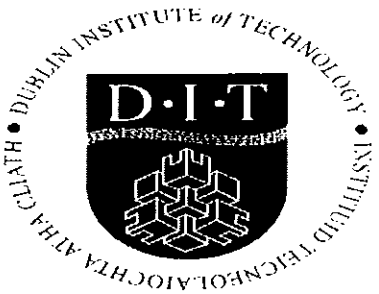

Diffusion Based Grating Formation in a Photopolymer Material

September 2000

Justin R. Lawrence B.Sc.

Supervisor

Dr. John T. Sheridan

Submitted in partial fulfilment
of the institute requirements
for the award of M.Phil.

School of Physics
Dublin Institute of Technology
Kevin Street, Dublin 8, Ireland.

Declaration

I certify that this thesis which I now submit for examination for the award of M.Phil is entirely my own work and has not been taken from the work of others save and to the extent that such work has been cited and acknowledged within the text of my work.

This thesis was prepared according to the regulations of postgraduate studies by research of the Dublin Institute of Technology and has not been submitted in whole or in part for an award in any other Institute or University.

The Institute has permission to keep, to lend or to copy this thesis, in whole or in part, on condition that any such use of the material has been duly acknowledged.

Signature: Justin Lawrence Date: August 2001

Acknowledgements

Firstly, I would like to express my gratitude to my supervisor Dr. John T. Sheridan* for his advice, encouragement and friendship. Thanks Sean.

I would also like to thank Prof. Yves Lion, Prof. Yvon Renotte and Mr. Vincent Moreau for their kind help during my visit to the University of Liege, Belgium. Thanks also to my co-worker Ms. Silvia Soler-Hernandez.

Many thanks to Dr. Hugh Byrne, Dr. Alan Dalton, Gordon Chambers and Kieran Henderson for advice and help with polymer science, photochemistry and Raman spectroscopy. I would like to thank Dr. Surendra Ponrathnam and Dr. Andy Davey for advice on polymer retarders.

Thanks to all the School of Physics postgrads. especially Feidhlim, Alan, Robert and Fran.

Finally, thanks to my family, Robert, Marion and Jean and to all my friends for their support and encouragement.

*Current address: Dept. of Electronic and Electrical Engineering, University College Dublin, Belfield, Dublin 4.

Contents

Abstract

Photopolymers are promising materials for use in holography. They have many advantages such as ease of use and are capable of efficiencies of up to 100%. However, the main disadvantage to these materials is their inability to record high spatial frequency gratings when compared to other materials such as dichromated gelatin and silver halide emulsion. This poor spatial frequency response is not predicted by any of the current physical models.

In this study, it is proposed that this effect is due to polymer chains growing away from their initiation point and causing a 'smearing' of the profile to be recorded. This is termed a non-local response. The model introduced by Zhao et al. [Zhao, 94] is extended to include this non-local effect. The predictions of the new non-local model are examined. The model predicts a fall off in spatial frequency repsonse which is easily observable by experiment but not predicted by any other theory

This model is then manipulated to give simple analytic expressions. These expressions are then applied to experimental data using a number of techniques. This allows values to be estimated for material parameters such as the diffusion coefficient of monomer, the ratio of polymerisation rate to diffusion rate and the distance that the polymer cahins spread during holographic recording. The model is then adjusted to take account of a new form of intensity dependence proposed by Kwon et al. [Kwon, 99].

Commercially available DuPont photopolymer was used to fabricate Holographic Optical Elements. Experimental work was carried out in an attempt to improve the spatial frequency response of an acrylamide based photopolymer material. This involved changing the molecular weights of the chemical components and the addition of a retarder in order to shorten the polymer chains, thereby decreasing the non-local effect. No significant change in spatial frequency response was observed. However, with further work, the use of retarders could lead to an improvement in response for a range of photopolymers.

Chapter 1 Introduction

Many types of materials are used as holographic recording media. The most well known include Silver Halide photographic emulsion [Soly, 81] and Dichromated Gelatin [Syms, 90]. Photopolymer materials are also promising candidates for use in holography because of their self-proccessing nature [Mani, 94]. However there are several problems with this class of material. The high performance, commercially available photopolymers are very expenxsive and their compositions are proprietary [Ingw, 89; Smot, 90; Webe, 90; Monr, 91a]. The photopolymers developed mainly by university research groups and smaller companies are in general cheaper and non–propriatory but have poorer performance. Many attempts have been made to improve the performance of these materials but the mechanisms which give rise to holographic recording are in many cases not well understood. An example of this lack of understanding is that the best theories of hologram formation in diffusion based photopolymer materials predict no maximum spatial frequency cut-off contrary to the simplest experimental results [Zhao, 94].

To enable development of improved materials, a better understanding of the recording mechanism is required. This is the primary motivation of this work and so the three main aims of this study are as follows.

1. To provide a consistent model which predicts a maximum spatial frequency cut-off.
2. To compare this model with experimental data and estimate physical parameters which govern the the diffusion process of holographic recording.
3. To propose and experimentally explore material improvements suggested by the model.

In order to systematically present the results of this study, the report is structured as follows;

1. Chapter 1 introduces holography, the basic models of light diffraction by gratings including Kogelnik's coupled wave theory [Koge, 69]. The historical development of various types of holographic recording material is reviewed with emphasis on photopolymers. A detailed discussion of the photochemical proccess in acrylamide based photopolymer systems is presented.
2. Chapter 2 introduces the theory of grating formation by diffusion. An extension of current models by the introduction of a non-local response term is presented [Sher. 00]. The non-local response represents the growth of polymer chains away from their point of initiation. It is shown that this model predicts a maximum spatial frequency cut-off.
3. Chapter 3 presents the procedures used to determine the spatial frequency response of an acrylamide based photopolymer material. The basic composition of the material is changed to include different molecular weights binders dyes and a number of inhibitors. The effects of these changes on the spatial frequency response are discussed.
4. Chapter 4 contains a comparison between the new model and experimental data This involves the derivation of an approximate analytic solution which enables the estimation of physicsal parameters governing grating formation. The results of experiments involving the addition of inhibitor to influence the non-local response are examined.
5. Chapter 5 presents several improvements to the model in order to take account of a different dependence of monomer concentration on intensity which was proposed recently by Kwon et. al. [Kwon, 99].
6. Chapter 6 describes applications of the commercially available DuPont photopolymer recording material along with a general comparison of with an acrylamide based material.
7. Chapter 7 contains the conclusions of this study along with future work to be carried out.

8. A section containing a full list of references is then presented.
9. Appendix A. contains the derivation of the coupled differential equations from the diffusion equation presented in Chapter 2.
10. Appendix B. contains a detailed set of graphs comparing the numerical non-local Zhao model presented in Chapter 2 and the analytic non-local Zhao model introduced in Chapter 4.
11. Appendix C. contains details of the polynomial curve fitting procedure introduced in Chapter 4, which is used to extract physical parameters from experimental data.
12. Appendix D. contains the derivation of the coupled differential equations from the diffusion equation allowing for any form of intensity dependence as introduced in Chapter 2.
13. Appendix E. shows the derivation of the non-local Kwon model.
14. Appendix F contains a list of the parameters used in this thesis and their units.
15. Finally, a list of publications from this study is given.

1.1 Introduction to Holography

The technique of wavefront reconstruction or *holography* was first demonstrated by Denis Gabor in 1948 [Gabo, 48] while attempting to improve the resolution of an electron microscope. The development of holography at this time was hampered by the lack of a light source with sufficient coherence length. Such a light source became available in the early 1960's with the invention of the laser [Ohan, 89]. In 1962 Leith and Upatnieks [Leit, 63] showed that transmission holography was a practical technique using an off-axis geometry. Denisyuk demonstrated reflection geometry holography in 1962 [Soly, 81].

Holography is a method of recording the total light field diffracted by a subject illuminated with coherent light. This can be achieved as follows. The complex diffracted waves are caused to interfere with an easily reproduced reference wave. The relative phase between subject and reference wave must remain constant in time, producing a three-dimensional interference pattern. This interference pattern can be stored in any one of a number of holographic recording materials such as dichromated gelatin, silver halide emulsion or photopolymer films. When the hologram is illuminated during replay with the reference beam, the subject wave is reconstructed due to the phase and amplitude information stored by the hologram [Coll, 71]. The image formed by this reconstructed wave has the depth and parallax properties normally associated with real objects. Holography has applications in many areas such as non-destructive testing [Coll, 71; Finc, 80; Carr, 92], information storage [Dhar, 98; Shah, 98; Stec, 98] and integrated optics [Syms, 90; Gamb, 94]. The next section contains a mathematical description of holographic recording and replay.

1.1.1 Holographic Recording

A typical set-up for holographic recording is shown in Figure 1.1 below. Highly coherent, collimated light from a laser is divided so as to produce a reference wave and to illuminate the object, creating an object wave. The two waves interfere in the plane of the recording medium producing a complex interference pattern. Figure 1.2 shows the reconstruction stage, where the original reference wave is used to illuminate the hologram and is diffracted by the recorded interference pattern so as to form an image of the object.

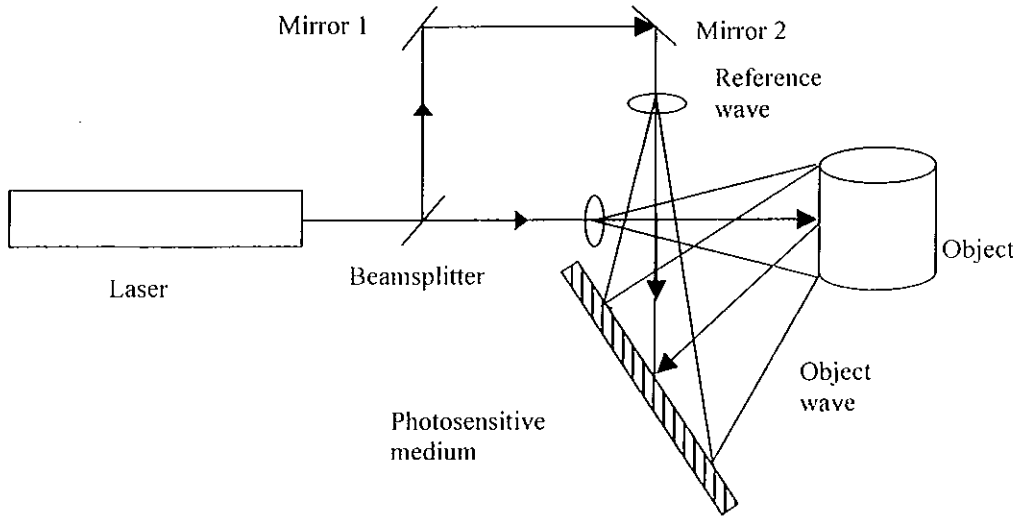

Figure 1.1 Experimental set-up for recording a transmission hologram.

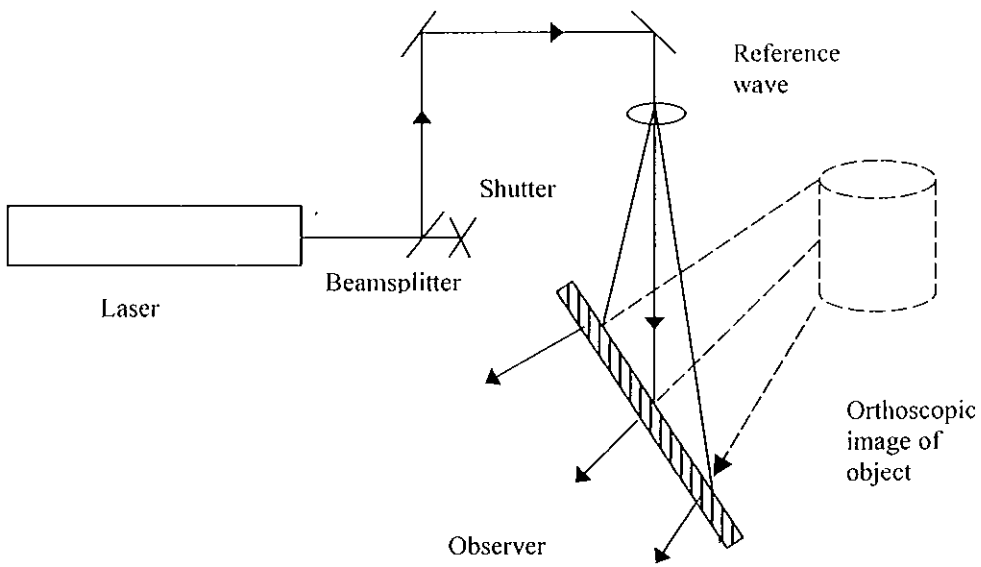

Figure 1.2 Reconstruction requires the illumination of the recorded hologram with the reference beam to produce an image of the object. An observer sees an image of the object through the hologram.

The process may be explained mathematically in simple terms as follows [Coll, 71; Syms, 90]. The object wave can be given as

$$a(x,y)\exp[j\phi(x,y)] \tag{1.1}$$

where a(x,y) is the wave amplitude and $\phi(x,y)$ is its phase. The reference wave is represented by

$$b \exp[-jky\sin\theta] \tag{1.2}$$

at an angle θ to the normal to the recording medium, which is positioned so that the object and reference waves overlap in its plane.

The total field distribution in the plane of the medium due to interference of the two waves is given by

$$a^2 + b^2 + a\,b \exp[\, j\,\phi\,(x,y) + k\,y\,\sin\theta\,] + a\,b \exp[-j\,\phi\,(x.y) + k\,y\,\sin\theta\,] \tag{1.3}$$

Some recording media react so that its *amplitude transmittance* is proportional to the original illuminating intensity distribution. These media form what is known as amplitude holograms. In these cases, during replay with the reference beam the expression for the output light amplitude can be given in as

$$b(a^2 + b^2) \exp[-jky\sin\theta] + b^2\, a(x,y) \exp[j\phi(x,y)]$$

$$+ b^2\, a(x,y) \exp[-j(\phi(x,y) + 2ky\sin\theta)] \tag{1.4}$$

The first term is directly proportional to the reference wave and constitutes the zero order wave. The second term is directly proportional to the complex amplitude of the diffracted wave from the original object. Therefore it contains the phase information which is responsible for the reconstruction of a three-dimensional virtual image of the object, known as the orthoscopic image as shown in Figure 1.2. The third term represents a conjugate version

of the original object wave. If a wave conjugate to the original reference wave illuminates the hologram then a conjugate version of the original object is produced, represented by

$$b^2 a(x,y) \exp [-j\phi(x,y)] \qquad (1.5)$$

Thus an image of the object is produced in front of the recording medium, known as the pseudoscopic or conjugate image.

The above treatment describes the production of an amplitude hologram where the amplitude transmittance of the hologram is proportional to the original illuminating intensity distribution. Other recording materials react to the light by producing a refractive index modulation which is proportional to the intensity distribution, referred to as a phase hologram [Jenn, 71]. As the material used in this study records volume type holograms, they will be discussed further in the next section.

1.1.2 Volume Holography

In most experimental studies of holographic recording materials, the sample is exposed to a simple sinusoidal interference fringe pattern having a single spatial frequency of up to several thousand lines per millimetre (l/mm) [Suga, 75]. The resulting diffraction gratings are relatively easy to record and analyse as the light emitted in the diffraction orders can be independantly measured. The efficiency with which the gratings diffract the incident light into these diffraction orders is a parameter that is used to provide valuable information for both optimisation and characterisation of the material [Down, 96; Weis, 96]. It is important to

differentiate between thin and volume gratings as the reconstruction process for volume (thick) gratings are more stringent than that of the thin grating [Soly. 81].

To illustrate this, Figure 1.3 shows a reference beam incident on a thin grating. A thin grating can be imagined as having only one scattering layer. The output is diffracted waves produced in the direction of the object beam such that

$$\sin\theta_1 = \sin\theta_2 + n\,\frac{\lambda}{\Lambda} \tag{1.6}$$

Where $n = 0, \pm 1, \pm 2....$ This is the well known Fraunhofer grating equation [Coll. 71]. θ_1 and θ_2 are the angles of incidence and diffraction respectively, λ is the wavelength of the incident light and Λ is the period of the grating. According to Equation (1.6) the light diffracted by each period of the thin grating adds in phase, to produce a diffracted wave. It is also evident that the larger the spatial period, the greater the number of diffracted orders that will propagate result. However, the grating equation only produces information about the number of diffraction orders present and their spatial frequency, it does not describe the intensity in the diffracted orders.

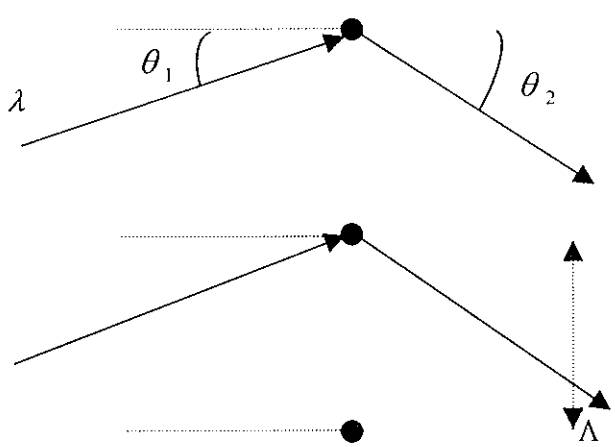

Figure 1.3 Fraunhofer (thin) grating diffraction.

In order for the diffracted waves to propagate outside the medium $\theta_2 < \pm\pi/2$. The holograms discussed in this study are volume gratings. Unlike thin gratings, volume gratings have multiple diffracting layers. The conditions for the reconstruction of a volume grating are collectively known as Bragg's law

$$2\Lambda\sin(\theta_2 - \phi) = n\lambda \tag{1.7}$$

Where θ_1 and θ_2 are the angles of incidence and diffraction respectively, λ is the wavelength of the incident light, Λ is the period of the grating and ϕ is the grating slant angle. In the case of an unslanted grating the fringes shown in Figure 1.4 below are parallel to the normal and ϕ becomes zero.

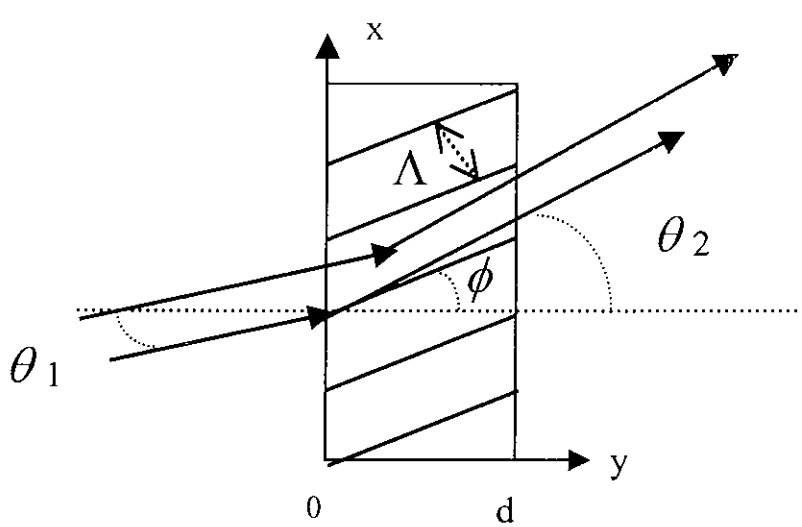

Figure 1.4 Bragg (volume) diffraction from a slanted transmission grating.

The Bragg condition is stricter than the grating equation. For any incident angle, the grating equation predicts the existence of many diffraction orders over a wide range of output angles. If the wavelength of light incident on a holographically recorded volume grating with fixed fringe width, is different to that used in recording, the angle of incidence of the reconstructing beam must be altered to satisfy Bragg's law. How this fact may be applied in order to obtain information in the analysis of volume holograms is discussed in more detail in section 1.3.

The parameter Q [Syms, 90] is frequently used to distinguish between volume and thin gratings.

$$Q = (2n\lambda d)/n\Lambda^2 \qquad (1.8)$$

In this equation, n is the average refractive index of the volume holographic medium. λ is the recording wavelength, d is the thickness of the medium and Λ is the period of the grating. When $Q \leq 1$ a hologram can be regarded as thin, for $Q \geq 10$, volume hologram theory is appropriate. When Q is between 1 and 10 the hologram is considered to be in an intermediate regime [Syms, 90]. However Kaspar, Magnusson and Gaylord showed that this was incorrect for strongly modulated gratings [Syms, 90]. Instead the parameter Q'/ν is used where $Q' = Q/\cos\theta_1$ and $\nu = \kappa d/\cos\theta_1$ where $\kappa = n_1$. A grating is considered thick if Q'/ν is greater than 20. In this study all the holograms recorded are considered thick or volume holograms. The most commonly used approach to describe these volume gratings is Kogelnik's first-order two-wave coupled wave theory. This approach is discussed in the next section.

1.1.3 Coupled Wave Theory

As stated earlier, the holographic interference pattern is usually stored in the form of a spatial modulation of the absorption constant and / or the refractive index of the medium. Kogelnik's coupled wave theory [Koge, 69] considers the efficiency with which thick holograms can diffract incident light and the angular dependence of this diffraction efficiency as the incident light deviates from the Bragg angle θ_1.

The theory is based on a number of assumptions. It is assumed that the total field inside a thick grating can be described by two waves travelling through the grating, the reference and signal (diffracted) waves. Any higher order waves produced by the grating are considered negligible. It is also assumed that power is coupled back and forth slowly between these two waves as they travel through the grating, so that any second derivatives produced in the theory may also be considered negligible. This means that any Fresnel boundary effects are also neglected. Based on these assumptions, the theory yields a pair of first-order coupled differential equations, which may be solved by applying appropriate boundary conditions. The boundary conditions differ according to the geometry of the grating recorded/replayed.

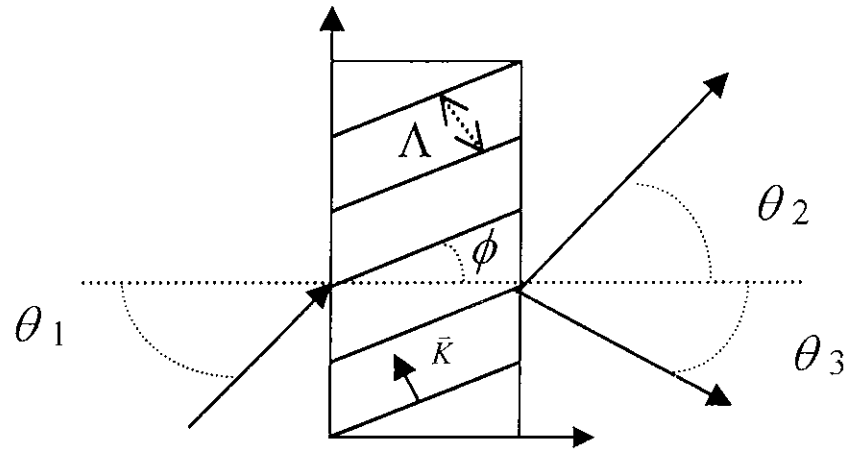

Figure 1.5 Kogelnik model representation of a slanted volume grating. θ_I is the angle of incidence inside the medium, $\vec{K} = 2\pi/\Lambda$ is the grating vector, Λ is the grating period, ϕ is the grating slant angle, d is the grating thickness.

The theory yields equations, which may be used to relate the diffraction efficiency of the grating to a number of parameters that may be extracted experimentally. In the case of an unslanted, phase transmission grating replayed on-Bragg it can be shown that the diffraction efficiency, η, can be expressed as

$$\eta = \sin^2\left[\frac{d\pi n_1}{\cos\theta_1 \lambda}\right] \tag{1.9}$$

where *d*, represents grating thickness, n_1 the refractive index modulation of the grating. θ_1 is the Bragg angle of incidence and λ, the wavelength of the incident light inside the grating.

This expression describes the diffraction efficiency of the grating when it is illuminated at the Bragg angle. This means that the incident beam satisfies Bragg's Law (Equation 1.7). The 'off-Bragg' parameter, ξ may be introduced which determines the diffraction efficiency of the grating in terms of angular deviation from the Bragg condition [Coll, 71].

$$\eta = \frac{\sin^2 \sqrt{\nu^2 + \xi^2}}{1 + (\xi/\nu)^2} \tag{1.10}$$

where $\nu = \frac{\pi n_1 d}{\lambda \sqrt{\cos\theta_1 \cos\theta_2}}$ and $\xi = \frac{d\pi}{\Lambda \cos\theta_1}$.

It can be noted that when $\xi = 0$, Equation (1.10) reduces to Equation (1.9). Diffraction efficiency may be plotted as a function of the off-Bragg parameter in order to predict the angular response of a grating for small deviations from θ_1, for specific values of ν.

Figure 1.6 illustrates the angular response of a grating, with a diffraction efficiency of unity, (at the Bragg angle) corresponding to $\nu = \pi/2$. When this value for ν is exceeded the grating is said to be overmodulated with the result that the power in the diffracted wave is coupled back into the reference wave. As the diffraction efficiency is a measure of the light in the diffracted beam this results in a decrease in the central peak and an increase in the side-lobes. Further over-modulation causes the diffraction efficiency for the central peak to drop back down to zero. The response of a grating with maximum modulation, then subsequent over-modulation, is illustrated in Figures 1.6.a, b, c and d, for varying values of ν.

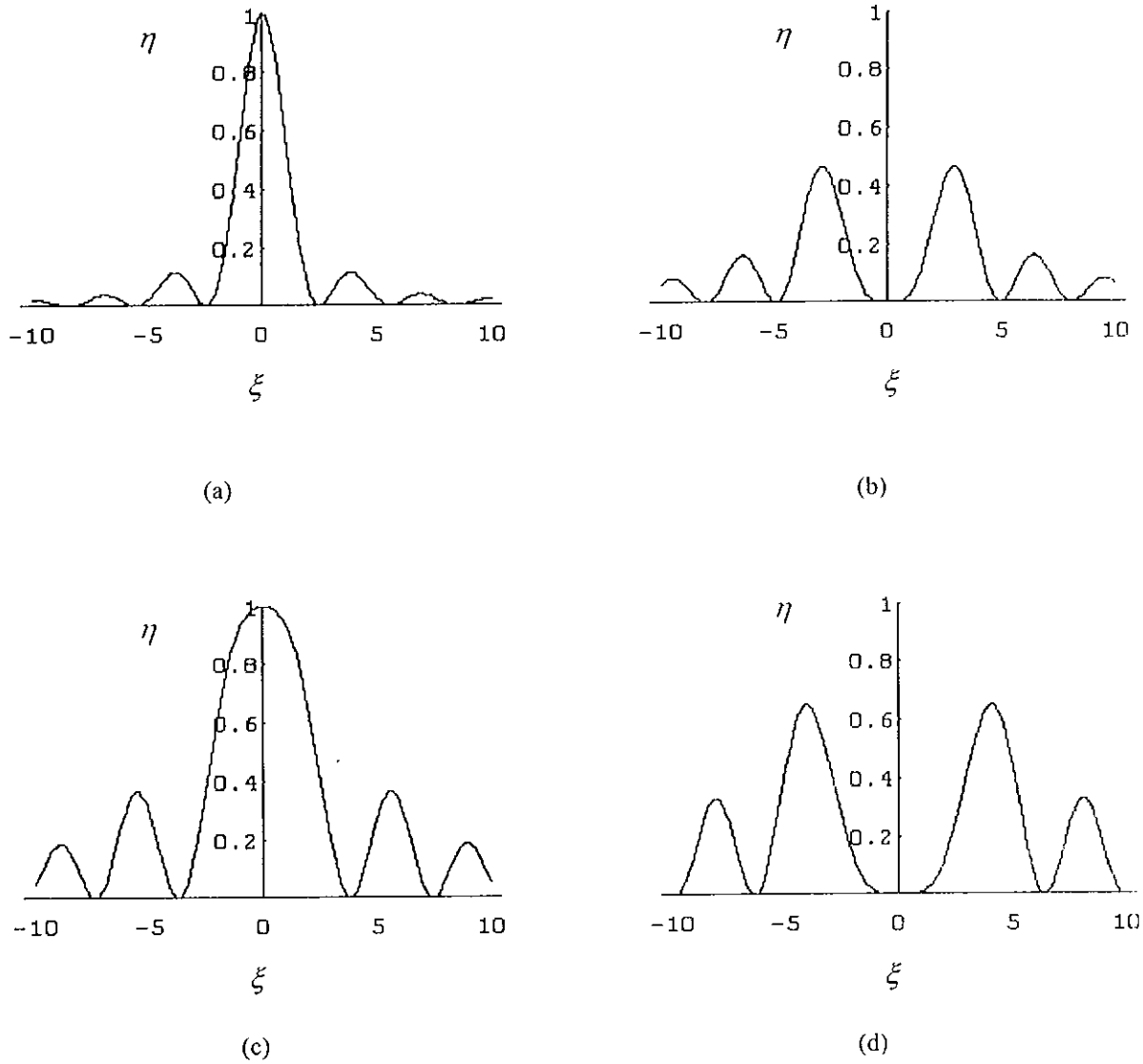

Figure 1.6 Theoretical curves illustrating effect of varying v parameter: (a) Maximum modulation at $v = \pi/2$, (b) Overmodulation at $v = \pi$, (c) $v = 3\pi/2$, (d) $v = 2\pi$

The following graph (Figure 1.7) shows the theoretical growth curve. The first peak corresponds to Fig. 1.6 (a), the first trough corresponds to Fig. 1.6 (b). The second peak corresponds to Fig. 1.6 (c) and the second trough to Fig. 1.6 (d).

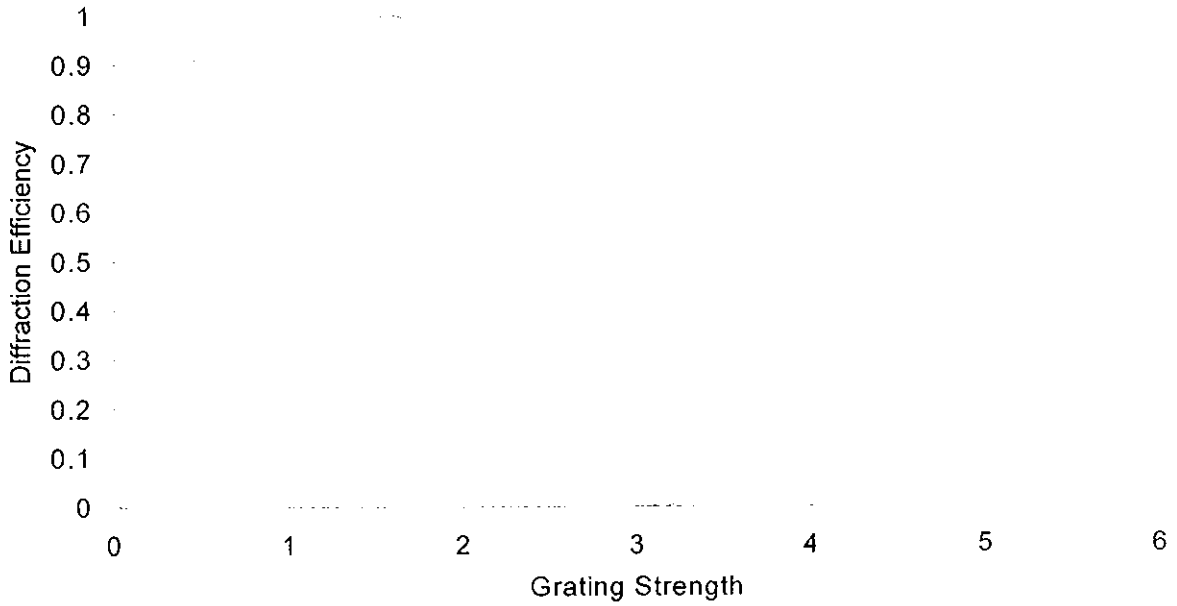

Figure 1.7 Theoretical growth curve for on-Bragg replay.

The refractive index modulation for phase gratings can be easily determined under varying experimental conditions using Equation (1.8), which relates diffraction efficiency, grating thickness, recording wavelength and the on-Bragg reconstruction angle. This will be used in Chapter 3 to analyse experimental data.

There are a number of other theories used in holography such as modal theory, transparency theory and the optical path method [Syms, 90]. However, as the coupled wave theory provides all the information needed for this study, these alternative theories will not be considered here. The next section will discuss the various types of holographic recording materials.

1.2 Holographic Recording Materials

In this section, the properties of an ideal holographic recording material will be discussed along with those of the most commonly used actual materials. The properties of the ideal and the real materials will be compared. The materials examined in this section include silver halide photographic emulsion, dichcromated gelatin and various photopolymer systems.

1.2.1 The Ideal Material

There are several criteria, which must be met before a material could be considered ideal:

1. The material must have a high resolution and a flat spatial frequency response. This will ensure that the desired interference pattern is completely stored. i.e. that no fine detail is lost.
2. There must be a linear relationship between exposure and the amplitude of the reconstructed wave. This ensures the fidelity of the image at replay.
3. The material's dynamic range must be large enough for a sufficient modulation to be formed during recording, which will lead to a good signal to noise ratio.
4. The material should be of high optical quality and lossless. This will lead to high optical efficiencies (bright images).
5. Changes in environmental conditions should not effect the material and the recorded hologram should be stable for long periods of time.
6. The material should be sensitive enough to react to a low energy exposure.

In reality no single material meets all these requirements. In the next section the most commonly used real materials are described.

1.2.2 Silver Halide Photographic Emulsion (SHPE)

Silver halide photographic emulsion is one of the oldest and most commonly used recording materials. It was the original material used in the early 1960's as it was the only inexpensive material available that was sensitive to Helium–Neon laser light. SHPE can be used to record holograms in reflection and transmission mode and is suitable for both amplitude and phase holograms [Kron, 94].

It is popular because of its very high sensitivity (10^{-5} to 10^{-3} mJcm^2) compared to other materials and can also record with good resolution (greater than 6000 lines/mm) [Syms, 90]. Its main drawbacks are the need for wet chemical post-processing and scatter due to particles dispersed in the material. Post exposure processing can lead to shrinking or swelling of the material which affects its replay wavelength.

SHPE consists of a gelatin layer in which microscopic grains of silver halide (usually AgBr) are dispersed. This layer is coated onto a glass or film substrate. Typical layer thicknesses are between 5 and 15 μm. The material works by recording a latent image, which is then developed by chemical post–processing.

The latent image is formed when an incident photon is absorbed by the material. This causes ionisation of the halide (bromine in this example) [Syms, 90].

$$Br^- + h\nu \rightarrow Br + e^- \qquad (1.11)$$

The resulting free electron can move through the crystal lattice until it is trapped by a crystal defect. It then combines with a silver ion to form what is known as a silver atom prespeck.

$$Ag^+ + e^- \rightarrow Ag \qquad (1.12)$$

If another electron arrives before the prespeck dissociates back to an ion, a larger speck is formed.

$$Ag + Ag^+ + e^- \rightarrow Ag_2 \qquad (1.13)$$

The speck is now stable, i.e. it will not thermally dissociate at room temperature. However it is too small to be developed. It is thought that a speck needs to contain at least four silver atoms to be developable [Soly, 81]. The speck can grow by the addition of further atoms in a process known as nucleation.

$$Ag_2 + Ag^+ + e^- \rightarrow Ag_3 \qquad (1.14)$$

$$Ag_3 + Ag^+ + e^- \rightarrow Ag_4 \qquad (1.15)$$

If nucleation occurs the speck will become a latent image speck which can be developed. The number of developable specks is proportional to the exposure that an area receives, so that the layer records a latent image of the spatial variation of intensity across the film.

The latent image can be developed by reducing each grain with a latent image speck into silver. The exact mechanism of this reduction reaction is not well understood. It is known that the speck itself catalyses the reaction which explains the very high sensitivity of SHPE

relative to other materials. This amplification effect depends on the size of the speck but is usually in the order of 10^6 [Syms, 90].

There are a number of procedures that can be carried out after development. Each one produces a different type of hologram. These procedures are outlined below.

Fixing produces an absorption hologram. This involves removing all the undeveloped silver halide. The layer is therefore rendered insensitive to further exposure but reduces the refractive index and shrinks the layer by about 15%. Shrinkage can alter both reflection and transmission holograms. For this reason other methods are normally used.

The *tanning bleach* process the developed silver grains are removed and the gelatin nearby becomes hardened due to crosslinking. When the layer is dried the hardened area do not shrink as much as the unhardened areas. In this way a thickness modulation is formed. The hologram formed is therefore a lossless phase hologram. The maximum resolution achievable with this process is about 1200 lines/mm due to the decrease in modulation depth at higher spatial frequencies.

An alternative bleaching process can be used when higher spatial frequencies are required. The developed silver in a fixed (absorption) hologram is replaced by a transparent silver salt, which has a higher refractive index, e.g. AgI. This process increases the diffraction efficiency of the original hologram. Noise levels are higher with this method due to increased scattering. Figure 1.8 below summarises the development process.

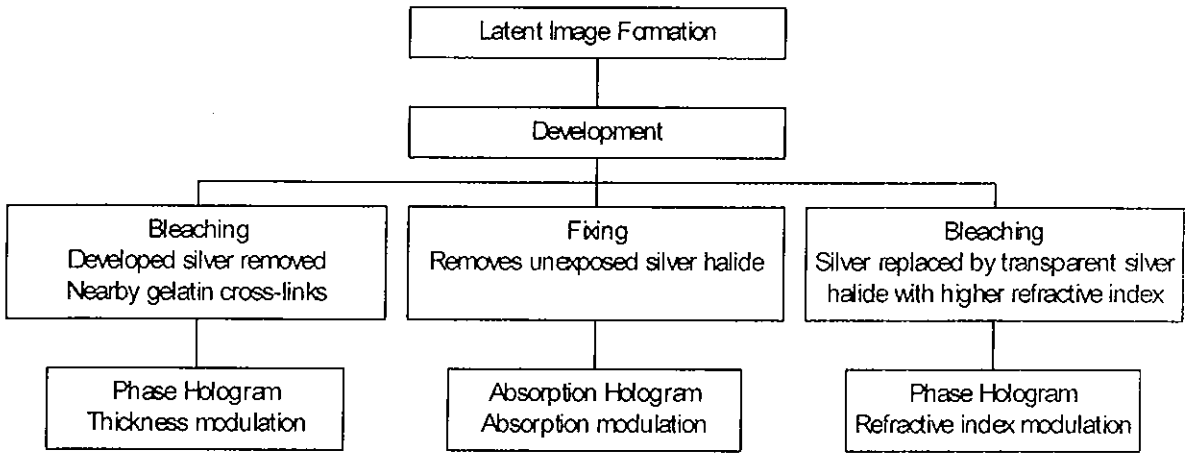

Figure 1.8 SHPE recording / development processes.

Because of the high sensitivity and good resolution, silver halide photographic emulsions are one of the most popular holographic recording materials presently in use. However, it's main disadvantage is the need for cumbersome chemical processing and development. Holograms were recorded in silver halide during this study.

1.2.3 Dichromated Gelatin (DCG)

The first serious rival to silver halide emulsion as a holographic recording material was dichromated gelatin (DCG). It was originally used in the printing industry but was first applied to holography in the late 1960's. It has high diffraction efficiency and good resolution [Chan, 79a]. Because of it's almost grainless character it is of high optical quality and has low noise when compared to SHPE [Chan, 80]. However DCG is not available commercially. It must be prepared in the laboratory before use as it has a useful life of only a few hours [Soly, 81].

DCG consists of a gelatin layer that contains ammonium dichromate. Like SHPE a hologram is recorded by the formation of a latent image and chemical development. The exact mechanism of latent image formation is not precisely known but one common idea is that the absorption of a photon reduces the hexavalent dichromate ion to the trivalent Cr [Syms. 90].

$$Cr_2O^{2-}_7 + 14H^+ + 6e^- + hv \rightarrow 2Cr^{3+}\ 7H_2O \qquad (1.16)$$

The Cr^{3+} ions formed during this reaction crosslink the gelatin in areas exposed to light. The crosslinked gelatin has a different solubility and hardness than the uncrosslinked material. A number of different post-processing steps can be carried out to produce different types of hologram. These are summarised in Figure 1.9 below.

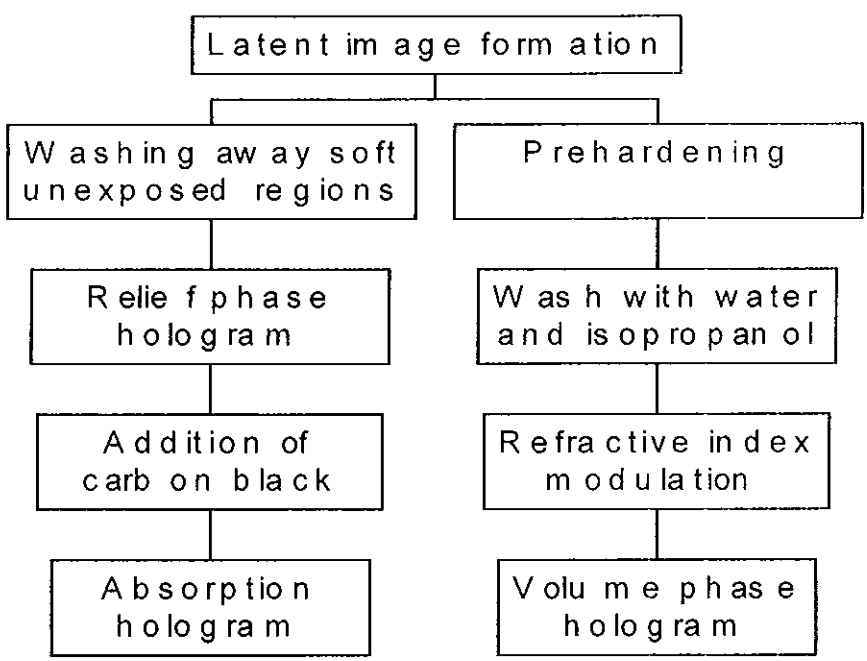

Figure 1.9 DCG recording / development processes.

To obtain a relief phase hologram the uncrosslinked gelatin is washed away which results in a thickness variation in the layer. Carbon black may then be incorporated into the material to form an absorption hologram.

For holographic recording DCG is usually developed to give a volume hologram. This is achieved by washing with water and isopropanol to give a cross sectional refractive index modulation in the layer. Exactly how this modulation occurs is not clearly understood. It is thought that swelling with water and drying with isopropanol causes submicroscopic cracks and voids to form in the softer, less exposed regions. This induces a refractive index modulation between the different regions [Syms, 90].

DCG is not as sensitive as SHPE because it has no self-amplifying reaction but it has higher efficiency and better resolution. It is however very sensitive to environmental changes and also needs chemical processing [Chan, 79b]. Another disadvantage is that it must be prepared in the laboratory before use because of its short shelf life. No experimental work was carried out using DCG during this study.

1.2.4 Photopolymers

Photopolymers were first introduced as a holographic recording material by Close et al. in 1969 [Clos, 69]. Since then numerous systems have been examined, but only a small number have become commercially available. These materials have several advantages. Because thick layers can be fabricated they act as a true volume materials giving high diffraction efficiency and good angular selectivity. Most of the materials are self–developing or require only some simple post–processing such as an exposure to light or heat treatment. This eliminates the need for wet chemical development, which makes photopolymers suitable for

applications such as holographic interferometry [Coll, 71; Finc, 80; Carr, 92] and information storage [Dhar, 98; Shah, 98; Stec, 98]. However, the resolution of these materials are usually not as high as for DCG and the thick layers lead to scattering which lowers the signal–to–noise ratio.

Photopolymers generally consists of a monomer, a photosensitive dye and an initiator. They can either be liquid or dry layer systems. The dry photopolymers usually contain a polymeric binder in addition to the other components. As an acrylamide-based material was used in this study, the discussion will begin with these materials.

As mentioned above the first photopolymer material used for holographic recording was reported by Close et. al. [Clos, 69]. This material consisted of a mixture of acrylamide and metal acrylate monomers and a photocatalyst such as methylene blue and p–toluene sodium salt. This material was a liquid and was trapped between two glass plates for recording. Diffraction efficiencies as high as 45 % were achieved with exposures of around 300 mJ/cm^2. The resolution of the photopolymer was found to be about 3000 lines/mm. The material also had a very short shelf life. Jenney [Jenn, 70; Jenn, 71] characterised and improved the sensitivity of the system, reducing the necessary exposure to 0.6 mJ/cm^2 by using lead or barium acrylate along with acrylamide as the monomer

A second liquid system was developed by Sugawara and Sugegawa [Suga, 75]. It consisted of an acrylamide monomer, a crosslinker (N,N methylene bisacrylamide), sensitiser (methylene blue) and either triethanolamine or acetylacetone as an initiator. Diffraction efficiencies of 65 % were obtained with exposure energies of 50 mJ/cm^2 and resolution of 550 lines per millimetre. A material based on the same monomer and crosslinker but using ferric ammonium citrate as sensitiser and t-butyl hydrogen peroxide was also examined [Suke, 75].

This system gave diffraction efficiencies of 80% with an exposure of 20 mJ/cm^2 at a resolution of 1500 lines per millimetre.

Sadlej and Smolinska [Sadl, 75] improved the original system proposed by Close and Jenney by including a poly-vinylalcohol binder. A binder allows the production of dry photopolymer layers which are easier to use then the earlier liquid systems. In this way the shelf life of the original material was greatly improved, proving conclusively that a binder can improve the stability of recorded holograms. The sensitvity of this system was 10 mJ/cm^2. Spatial frequencies of up to 4700 lines/mm could be recorded. The main disadvantage was the low diffraction efficiency reported, only up to 4% with surface relief modulation and 0.5% with volume effects.

Jeudy and Robillard [Jeud, 75] reported an interesting version of the liquid Sugawara system which included a reversible photochrome (indolino-spiropyran), as sensitiser and poly-vinylalcohol as binder. The photochrome, which was fully transparent in visible light, could be activated by ultra-violet (UV) light shifting its absorption band to allow recording at 633nm. When recording was completed the UV was switched off and the photochrome was rendered inactive resulting in a highly transparent, stable hologram of typically 90% diffraction efficiency with an exposure energy of 100mJ/cm^2 and a resolution of 3000 lines per millimetre.

Calixto [Cali, 87] continued the work on acrylamide-based systems. The material contained acrylamide monomer, triethanolamine as electron donor, methylene blue dye and poly-vinylalcohol as binder. Although exposure energy was low at approximately 94 mJ/cm^2, the maximum diffraction efficiencies reported were poor at 10%.

Fimia et al. [Fimi, 92; Fimi, 93] devised a method for increasing the sensitivity of acrylamide photopolymers by reducing the inhibition time caused by oxygen. The material contained two dyes, Methylene Blue which is sensitive to 633 nm and Rose Bengal which absorbs at 546 nm. The layer was pre-exposed to a 546 nm beam before actual recording. The Rose Bengal dye produces radicals, which then react with oxygen within the layer. When recording takes place at 633nm, there is a reduced amount of oxygen and sufficient Methylene Blue dye to polymerise the monomer. Using this system, diffraction efficiencies of 40% at a spatial frequency of 1000 lines/mm could be obtained with an exposure of 3 mJ/cm^2.

The Calixto photopolymer was optimised by Martin et al. [Mart, 94] for recording in the 514 nm region by the addition of a xanthene dye. Diffraction efficiencies of greater than 80% were obtained with an exposure energy of 80 mJ/cm^2. The limiting spatial frequency of the material is approximately 2750 lines / mm.

Weiss et al. [Weis, 96] improved the sensitivity of the Close and Sugawara material at 514 nm by adding diphenyl iodonium chloride to act as a sensitiser along with TEA. The addition of glutaraldehyde as a second crosslinker was found to increase the refractive index modulation. Diffraction efficiencies of greater than 90% at 2000 lines/mm were shown to be achievable with an exposure of 12 mJ/cm^2.

Blaya et al. [Blay, 98] improved the sensitivity of the acrylamide material for recording at 633 nm by changing the crosslinker used. This new crosslinker, N,N-dihydroethylene bisacrylamide, caused an increase in the rate of polymerisation which lowers the exposure energy required. Diffraction efficiencies of 70% at a spatial frequency of 1000 lines/mm were achieved with an exposure energy of 5 mJ/cm^2.

A new hybrid material containing acrylamide and acrylic acid as monomers was proposed by Zhao et al. in 1998 [Zhao, 98]. The material uses Methylene Blue as the dye, TEA and p-toluenesulfonic acid as sensitisers and gelatin as a binder. This material was capable of recording up to 4000 lines/mm. The maximum diffraction efficiency obtainable was greater than 80% and the exposure energy required is 2 mJ/cm^2.

Figure 1.10 below, shows the major steps in the development of acrylamide–based holographic recording materials.

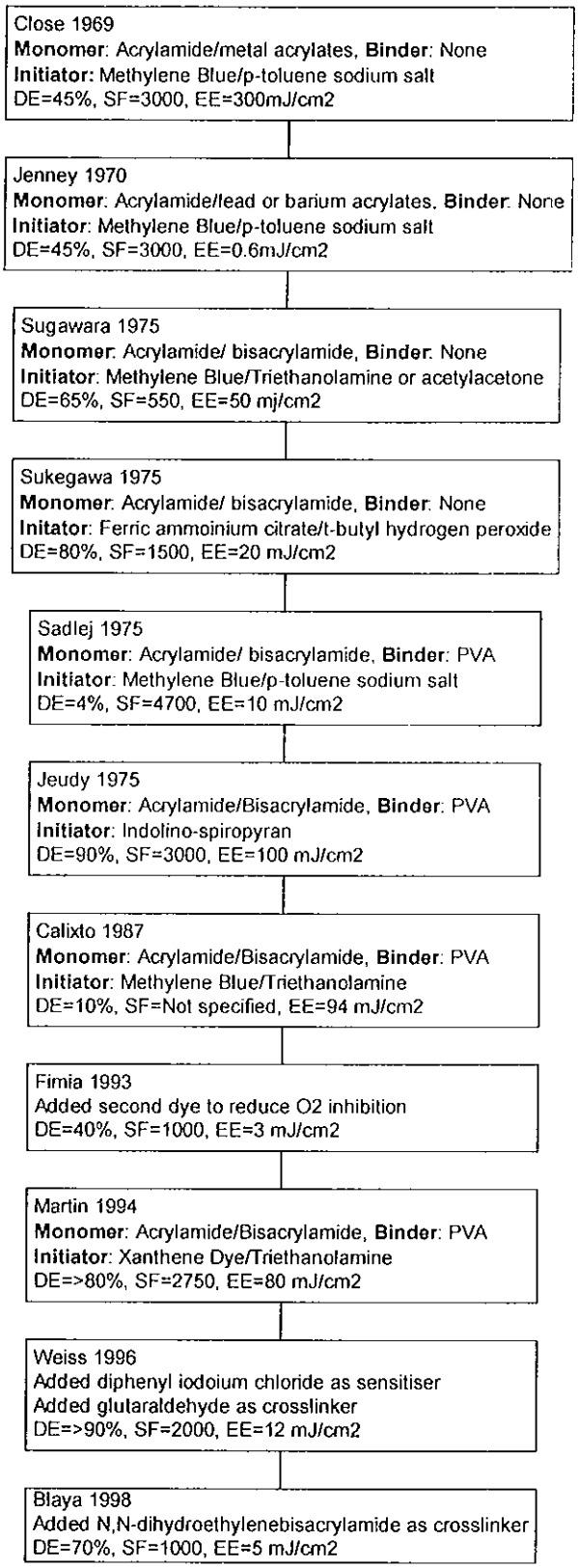

Figure 1.10 Development of acrylamide-based holographic recording materials. EE=Exposure Energy, SF=Spatial Frequency in lines per millimetre and DE=Diffraction Efficiency.

It should be noted that the materials listed in Figure 1.10 above as having no binder are used in liquid form while those with binders are used in dry form.

1.2.5 Commercially Available Photopolymers

Probably the best known photopolymer systems are those commercially available from Polaroid and DuPont. These two systems are discussed next.

A commercial material named DMP–128 was developed by Ingwall et al. [Ingw. 89] of the Polaroid Corporation. It consists of a mixture of methlyenebisacrylamide and lithium acrylate as the monomer and a poly–N–vinylpyrrolidone binder. The dry material must be incubated in a 50% humidity environment before use. Post recording treatment involves a uniform white light exposure, immersion in a special developer/fixer bath, rinsing and drying. These steps are needed to increase the efficiency from 0.1% to 80%. The material can be used to record transmission and reflection holograms with exposure energies between 5 and 30 mJ/cm^2. Although it is more sensitive than the DuPont material the need for wet chemical processing is a significant disadvantage.

Perhaps the most popular commercially available photopolymers is the family of acrylate based system developed by E.I. DuPont Nemours and Co. The original material consists of an acrylate based monomer, an initiator system and a cellulose binder [Boot, 72; Boot, 75]. The exact composition of these materials is proprietary. Diffraction efficiencies of up to 90% can be obtained with an optimum exposure of 30 mJ/cm^2 and the material has a resolution of

3000 lines/mm. The diffraction efficiencies can be improved by post exposure with a fluorescent lamp even though the material is self-developing

Because of its limited resolution this material could not be used for reflection holograms. To rectify this DuPont developed the Omnidex photopolymer system [Monr, 91a; Monr, 91b]. This material has a resolution of about 6000 lines /mm and efficiencies of 99% have been obtained. These results can be achieved with exposure energies of 50–100 mJ/cm^2. The material is a dry layer consisting of an acrylic monomer, a photosensitising dye, an initiator, a chain transfer agent, a plasticizer and a polymer binder coated onto a polyethyleneterephtalate film substrate. The exact monomer and binder used has not been disclosed but the following were investigated [Monr, 91b].

Binders	Cellulose acetate butyrate (CAB) Poly(methyl methacrylate) (PMMA) Poly(styrene – methyl methacrylate) (PS – MMA) Poly(styrene – acrylonitrile) (PS - AN)
Monomers	2 - phenoxyethyl acrylate (POEA) Triethyleneglycil diacrylate (TEGDA)
Initiator	Hexaarylbiimidazole (HABI)
Chain transfer agent	2 - mercaptobenzoxazole (MBO)
Dye	2,5 {bis [4-(dimethylamine)-phenyl] methylene cyclopentanone} (DEAW)

Figure 1.11 Materials reported as having been investigated by DuPont.

The material is capable of producing a high refractive index modulation ($n_1 = 0.07$) relative to other systems. This thought to be due to the large difference in refractive index between the aromatic binder and the aliphatic monomer [Monr, 91b]. As with the earlier DuPont material, the efficiencies of the Omnidex system can be increased with post exposure to a uniform

beam and a simple heat treatment. Because of their high diffraction efficiency, high sensitivity and good resolution these photopolymers are generally considered to be the best commercially available at this time.

In the next section the mechanism of holographic recording in acrylamide photopolymers is discussed

1.3 Mechanism of Recording in Acrylamide Material

This section will describe the chemical processes by which the material is made sensitive to the wavelength of the recording light. It will also describe the initiation of the polymerisation, which is responsible for the change in refractive index that allows holographic information to be stored.

1.3 1 Photosensitisation and Initiation

Photopolymer materials can be made sensitive to a particular wavelength of light by the use of a sensitising dye. For example, the material developed by Monroe et al. [Monr, 91] uses 2,5 bis[4-(dimethylamine)-phenyl]methylene cyclopentanone to sensitise it to light in the 488 nm region. The photopolymer in this study uses a xanthene dye (Erythrosin B) so holographic recording can be carried out using a 514 nm argon–ion laser [Mart. 94]. Acrylamide based systems have also been sensitised to 633 nm light using Methylene Blue, a thiazine dye [Clos, 69].

Photosensitisation and initiation in this material depend on the dye and the electron donor (triethanolamine). The reaction between these two components leads to the production of free radicals (highly reactive species) which initiate the polymerisation process.

When the dye molecule, D, is exposed to light of a suitable wavelength, it absorbs a photon of light and is promoted into a singlet excited state, $^1D^*$ [Birk, 75].

$$D + h\nu \rightarrow {}^1D^* \qquad (1.17)$$

This singlet excited dye can return to the ground state by radiationless transfer to another molecule such as the electron donor, ED. This process is known as fluorescence quenching [Gilb, 91].

$$^1D^* + ED \rightarrow D + ED \qquad (1.18)$$

It can also revert back to the ground state, D, by the emission of a photon by a process called fluorescence [Gilb, 91].

$$^1D^* \rightarrow D + h\nu \qquad (1.19)$$

The singlet state can also undergo inter–system crossing into the more stable and longer lived triplet excited state

$$^1D^* \rightarrow {}^3D^* \qquad (1.20)$$

This triplet state dye molecule can return to the ground state by radiationless transfer or by the delayed emission of a photon. At high dye concentrations it can be deactivated by collision with another dye molecule.

$$^3D^* + D \rightarrow 2D \qquad (1.21)$$

The dye molecule can also undergo a reaction whereby it abstracts two hydrogens from the electron donor to form the transparent (leuco) form of the dye.

The actual production of free radicals takes place when the triplet state dye reacts with the electron donor. The electron donor used in this study was triethanolamine $(HOCH_2CH_2)_3N$:. The reaction between a xanthene dye and triethanolamine have been studied by Zakrezewski and Neckers [Zakr, 87]. The triethanolamine (TEA) donates an electron to the excited triplet state of the dye leaving the dye with one unpaired electron and an overall negative charge.

$$^3D^* + (HOCH_2CH_2)_3N: \rightarrow D^{\cdot -} + (HOCH_2CH_2)_3N^{\cdot +} \qquad (1.22)$$

The TEA radical cation then loses a proton and becomes a free radical.

$$(HOCH_2CH_2)_3N^{\cdot +} \rightarrow (HOCH_2CH_2)_2NCH^{\cdot}CH_2OH + H^+ \qquad (1.23)$$

When the acrylamide monomer is present the free radical can undergo two different reactions.

The first possible reaction is the initiation of the acrylamide (ACR) polymerisation. The exact mechanism of this reaction will be discussed in the next section.

$$TEA^{\cdot+} \rightarrow TEA\text{-}ACR^{\cdot} \qquad (1.24)$$

The second reaction the radical can undergo is dye bleaching. This occurs when the dye radical formed in (1.22) abstracts a hydrogen from the TEA free radical. An unstable TEA intermediate and the transparent dihydro dye are formed by this reaction.

$$(HOCH_2CH_2)_2NCH^{\cdot}CH_2OH + H^{+} + D^{\cdot-} \rightarrow (HOCH_2CH_2)_2NCH{=}CHOH + H_2D \qquad (1.25)$$

The unstable intermediate then rearranges to form a more stable intermediate.

$$(HOCH_2CH_2)_2NCH{=}CHOH \rightarrow (HOCH_2CH_2)_2NCH_2CHO \qquad (1.26)$$

Dye bleaching is an important process because it allows a hologram to be fixed after recording. By bleaching any remaining dye no extra free radicals can be formed. This means that no unwanted polymerisation occurs after holographic recording. It also makes the final hologram transparent. In the next section the mechanism of polymerisation is discussed.

1.3.2 The Polymerisation Mechanism

The free radicals initiate the polymerisation of acrylamide/methylene–bis–acrylamide which forms a polyacrylamide network. This occurs via a mechanism known as free radical polymerisation [Odia, 70]. There are other mechanisms such as cationic or anionic polymerisation but they as they are not significant for this study they will not be considered

here. Free radical polymerisation consists of three separate steps, *initiation*, *propagation* and *termination*.

The first step of this process is *initiation*. This is when the free radical initiator attaches to the monomer by addition across the carbon–carbon double bond

(1.28)

When forming the bond to attach itself to the monomer, the free radical uses its own unpaired electron and a π electron from the C=C bond. This leaves one of the carbons with an unpaired electron therefore the monomer becomes a free radical.

The new radical will attach itself to another monomer by addition across the double bond by the same method as above. The second monomer now becomes a radical and in this way a polymer chain grows. This is the *propagation* step.

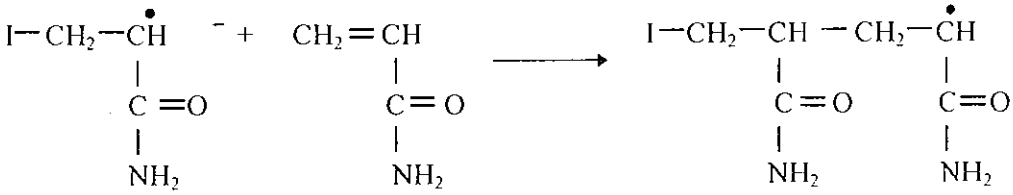

(1.29)

The newly formed chain will continue growing one link at time until it is stopped by a termination reaction. *Termination* can occur by two reactions known as disproportionation or combination. Disproportionation happens when a hydrogen is abstracted from one propagating chain by another. The hydrogen reacts with the free radical and the original double bond is reformed. This process results in two separate chains.

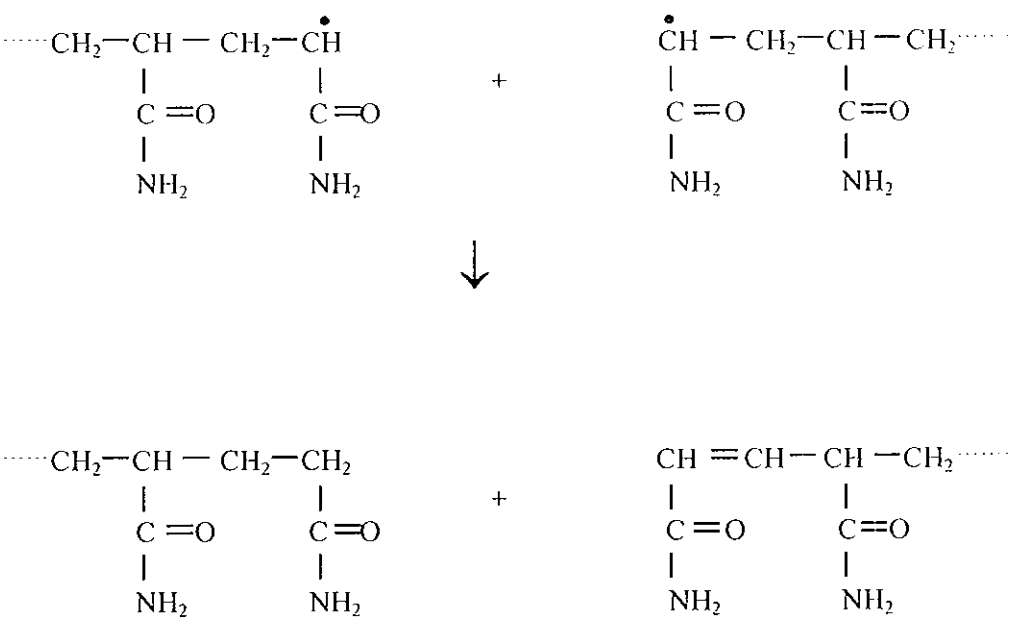

(1.30)

The second method of termination is combination. Combination occurs when the radicals at the ends of two propagating chains react forming one long chain.

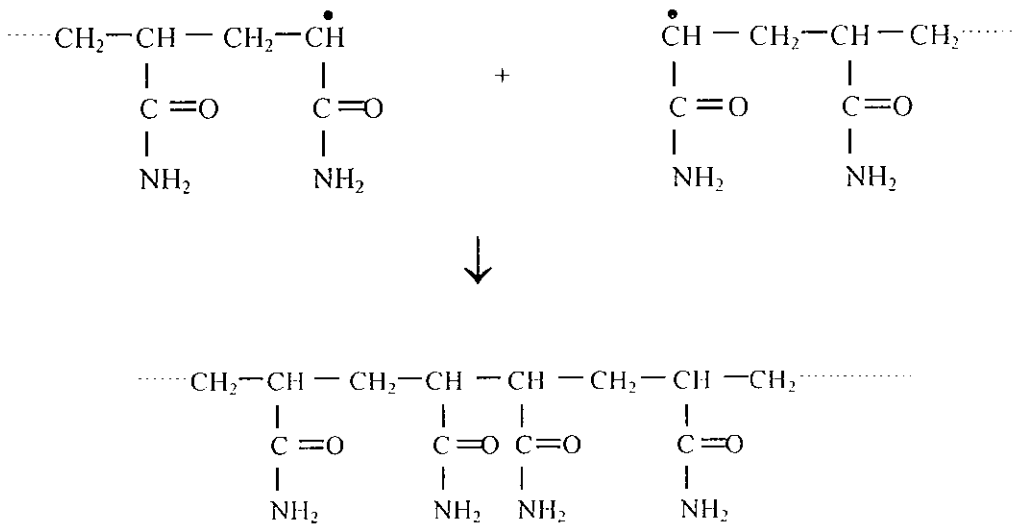

(1.31)

On polymerisation each carbon double bond is converted into a carbon single bond lowering the molar refractivity from approximately 4.16 cm^3 to 2.15 cm^3 [Pitt, 80]. This lowers the refractive index of the material. This is usually accompanied by an increase in density (10–15%) which leads to an increase in refractive index [Pitt, 80]. The combination of these two processes results in a higher refractive index in polymerised regions compared to unpolymerised regions so that a refractive index modulation exists between exposed and unexposed areas. It is also thought that during exposure monomer diffuses into bright regions as a result of the concentration gradient induced by the depletion of these components [Colb, 71]. This causes a further difference in density (and so refractive index) between bright and dark regions. The type of hologram recorded by this process is a lossless phase hologram.

1.4 Conlcusions

In this chapter the aims of this study were presented along with an outline of the structure of the work carried out.

A general introduction to holography was given the basic models of light diffraction by gratings including Fraunhofer and Bragg diffraction. Kogelnik's coupled wave theory [Koge. 69] was introduced and its use in the calculation of various parameters was outlined. This theory will be applied to experimental data in Chapter 3. There are a number of other theories used to in holography such as modal theory, transparency theory and the optical path method which will not be considered further as the first-order two wave coupled wave theory provides all the necessary information.

The properties of an ideal holographic material were then outlined and the two most commonly used materials silver halide emulsion and dichromated gelatin were presented. The historical development and properties of various types of on photopolymers was given with emphasis on the acrylamide based systems. The photochemical and polymerisation process in acrylamide based photpolymer systems was discussed.

In the next chapter, a diffusion based model of grating formation in a photopolymer material is presented.

Chapter 2 Diffusion Theory

In this chapter the basic principles of diffusion are discussed. The concept of a non-local medium response in photopolymer materials is also introduced.

2.1 Introduction

It is generally recognized that the mechanism of recording in most photopolymer materials involves diffusion of one or more of the components [Colb, 71; Syms, 90; Mani. 94]. For example, recording in the acrylamide based system examined in this study is thought to involve the diffusion of monomer molecules away from unexposed dark areas and into exposed bright areas, leading to a density change which contributes to the formation of a refractive index modulation.

A diffusion-based mechanism of recording in these materials was first proposed by Colburn and Haines [Colb, 71]. Monomer diffusion was examined experimentally by Wopschall and Pampalone [Wops, 72]. The technique know as Holographic Grating Relaxation has been used to verify that dyes can diffuse through polymer matrices under conditions similar to those that occur during holographic recording [Wang, 88].

Most of the work on photopolymers carried out during the 1970's and 1980's was experimental in nature. The groups involved in photopolymer research concentrated on formulating and characterising new materials. It was not until the 1990's that detailed work on mathematical models of hologram formation began. Adhami et al. [Adha, 91] solved the diffusion equation by

considering the absorption of the modulated illumination and predicted changes in the monomer concentration. Piazolla and Jenkins [Piaz, 96] derived an analytic solution for the temporal change in refractive index modulation assuming that the grating formation process is much slower than the diffusion process. A more complete model of hologram formation was then developed by Zhao and Mouroulis [Zhao, 94]. This model can be used to describe how the ratio between the diffusion and polymerisation rates controls the process of grating formation. Colvin et al. [Colv, 97] studied the process of hologram formation in a material of their own formulation. They refined the model presented by Zhao and Mouroulis by including the effects of photoreaction kinetics and monomer diffusivity. However, these models do have failings, most seriously, they predict no maximum spatial frequency cut-off contrary to the simplest experimental results [Zhao, 94]. In this section the basic principles of diffusion are discussed. The model presented by Zhao.et al. and Colvin et al., are generalised using the concept of a non-local response in photopolymers [Sheri, 00]. The standard one-dimensional diffusion equation is extended to include such a response. Finally a comparison is made between the existing and the non-local models.

2.2 Basic Principles of Diffusion

Diffusion is a material transport property. This is the ability of a material to transfer matter, energy or some other specified property from one location to another [Atki, 92]. In the case of photopolymers monomers, dyes and initiators are consumed faster in the bright exposed regions than dark regions. This leads to a concentration gradient, which causes diffusion of these components from dark to bright regions. They will continue to diffuse until uniform concentration is achieved.

2.2.1 Fick's Law

In the following derivation, the method of Atkins is followed [Atki, 92]. Diffusion is a transport property, which may be measured by its flux J, which is defined as the amount of that property, (in this case, the number of diffusing molecules) passing through unit area per unit time. In our case, the flux of matter J_x diffusing parallel to some axis x is proportional to the concentration gradient along that axis:

$$J_x \propto \frac{d\mathrm{N}}{dx} \tag{2.1}$$

where N represents the number of molecules.

This relation is known as Fick's first law of diffusion. If $J_x > 0$, the flux is towards increasing x, if $J_x < 0$ the flux is towards decreasing x. Matter flow will usually occur down a concentration gradient so if $dN/dx < 0$, J_x is positive as illustrated in Figure 2.1. This means that the constant of proportionality must be negative and is denoted $-D$, where D is referred to as the diffusion coefficient. When the diffusion coefficient is included, Fick's first law becomes

$$J_x = -D\frac{dN}{dx} \tag{2.2}$$

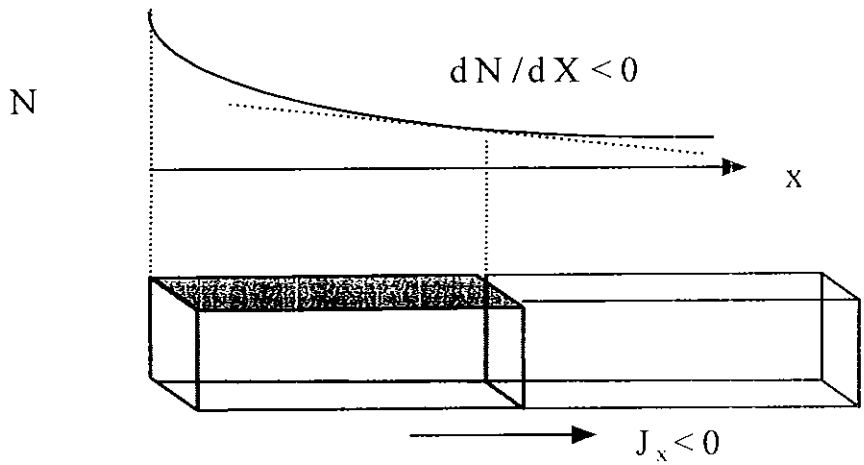

Figure 2.1 Diagram of increasing flux following [Atki, 92].

Fick's law for particle flux in terms of moles of molecules per unit area per unit time may be written as

$$J_x = -D\frac{dc}{dx} \tag{2.3}$$

where dc/dx represents the molar concentration gradient. This relation now must be generalised in order to take account of time-dependent diffusion processes. The aim is to obtain an expression that may be applied to the rate of change of the concentration of particles in an inhomogeneous region.

Consider a thin slab of cross-sectional area A, extending a distance Δx, from x to $x + \Delta x$, as illustrated in Figure 2.2.

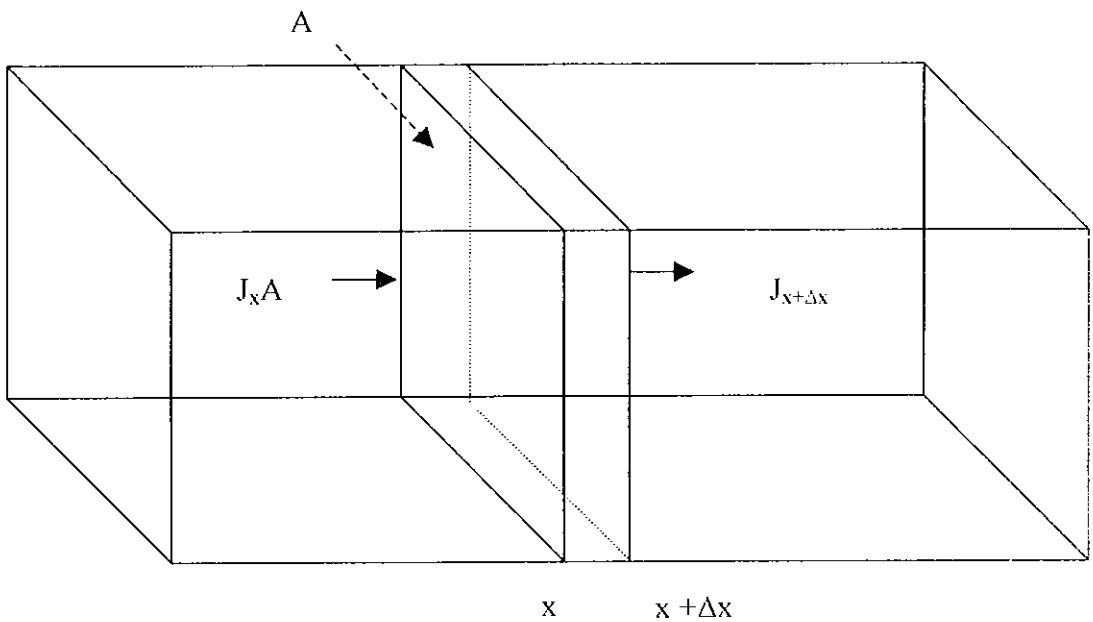

Figure 2.2. To illustrate flux for deriving the diffusion equation.

Let the concentration at position x be c_x at time t. The number of moles of particles entering the slab per unit time is $J_x A$. The increase in concentration inside the slab with volume $A\Delta x$ arising due to the flux from the left is

$$\frac{dc_x}{dt} = \frac{J_x A}{A\Delta x} = \frac{J_x}{\Delta x} \tag{2.4}$$

There is also an outflow towards the right. This outflow is represented by $J_{x+\Delta x}$ and can be represented by

$$\frac{dc_{x+\Delta x}}{dt} = \frac{-J_{x+\Delta x}A}{A\Delta x} = \frac{-J_{x+\Delta x}}{\Delta x} \tag{2.5}$$

The net rate of change in concentration, c, can be given as

$$\frac{dc}{dt} = \frac{d\left(c_x + c_{x+\Delta x}\right)}{dt} = \frac{J_x - J_{x+\Delta x}}{\Delta x} \tag{2.6}$$

The flux is proportional to the concentration gradient within the slab and so may be written using Fick's first law as

$$J_x - J_{x+\Delta x} = -D\frac{dc_x}{dx} + D\frac{dc_{x+\Delta x}}{dx} = -D\frac{dc}{dx} + D\frac{d}{dx}\left\{c + \left(\frac{dc}{dx}\right)\Delta x\right\}$$

$$= D\frac{d^2c}{dx^2}\Delta x \tag{2.7}$$

Equation 2.7 now represents the change in flux. When this relation is substituted into the expression for the rate of change of concentration in the slab, the usual one-dimensional diffusion equation is obtained.

$$\frac{dc}{dt} = D\frac{d^2c}{dx^2} \tag{2.8}$$

The concentration $c(x,t)$ can now be clearly recognised as a function of both distance x and time t. We have now introduced the basic principles of diffusion and mass transfer. In the next section

the formation of holographic gratings will be discussed. In this case it is assumed that the concentration of interest is that of the monomer within the polymer matrix.

2.2.2 Holographic Grating Formation: Monomer Diffusion

In this study, the diffusion of monomer is assumed to be of primary interest. Following Zhao et al. [Zhao, 94] the motion of the other chemical components in the polymer matrix is also important but it will not be considered further. This is done in order to simplify the analysis. The diffusion equation derived above must now be applied to the monomer concentration. It is assumed that there are two main processes that will affect the concentration of monomer at any location within the material. The first is the removal of monomer from the location in question. This would occur physically by monomer being polymerised. The amount of monomer being removed by polymerisation can be represented by,

$$-F(x,t)u(x,t) \tag{2.9}$$

Where $F(x,t)$ is the rate of polymerisation at time t and location x while $u(x,t)$ is the monomer concentration at location x and time t. The second factor is the rate of 'addition' of monomer to the location. This occurs physically by monomer diffusing from nearby areas due to the concentration gradient induced by the removal of monomer to form polymer. If the diffusion constant is assumed to be a function of position and time [Zhao, 94] then this can be represented as follows:

$$\frac{\partial u(x,t)}{\partial t} = \frac{\partial}{\partial x}\left[D(x,t)\frac{\partial u(x,t)}{\partial x} \right] \tag{2.10}$$

Which is a generalisation of the usual one-dimensional diffusion equation (2.8). Combining the two equations above gives the standard one-dimensional diffusion equation for monomer concentration, which appears later in this study.

$$\frac{\partial u(x,t)}{\partial t} = \frac{\partial}{\partial x}\left[D(x,t)\frac{\partial u(x,t)}{\partial x} \right] - F(x,t)u(x,t) \tag{2.11}$$

2.3 Non-Local Response

As mentioned above a diffusion based mathematical model of grating formation has been developed by Zhao and Mouroulis [Zhao, 94]. Although this model provides insights into the physical processes taking place, it incorrectly predicts that the higher the spatial frequency of the interference pattern to be recorded, the more ideal the grating produced.

Several practical reasons can be given why this theoretical prediction disagrees with experimental results. The recording of high spatial frequency gratings requires vibration isolation during exposure. Poor isolation or long exposure times will cause a cumulative smearing of the grating profile. However, it seems reasonable to expect that there is a fundamental physical limit to the minimum grating period recordable, which depends on the material's recording mechanism.

In all previous models it is assumed that the response of the photopolymer to the incident light is local, i.e. the effect at a point is independent of effects at all other times and places in the

medium. In this study the case of a medium in which the response of the material is non-local, i.e. the response at point x at time t depends on what happened at a point x' at time t' is discussed. Such a non-local response can arise due to several physical effects, but in particular it may arise due to the recording mechanism. In the case of dry photopolymer, gratings are formed when varying numbers of polymer chains are simultaneously initiated in all illuminated areas within the material. The chains then grow away from their initiation point, which leads to a "spreading" of the polymer. In this study it is proposed that this chain growth is the physical reason for a non-local response. Other possible causes such as diffuse scattering of light during recording will not be considered further here.

In this section the mathematical representation of such non-local effects will be discussed. It is assumed that the growth of polymer chains outward from any initiation point is isotropic. It is also assumed that the length the chains grow away from their initiation point and the directions of the polymer's bond vectors can be described using a macroscopic distribution function [Doi, 97]. To represent the spreading of the polymer chains two macroscopic Probability Density Functions, (p.d.f.) are introduced, a chain length p.d.f. and a chain growth velocity p.d.f., which give the likelihood of a chain having a particular parameter value

The probability of the existence of a chain of effective length L is represented by

$$P[L] = \exp\left[-(L-L_m)^2 / 2\sigma_L\right] \Big/ \sqrt{2\pi\sigma_L} \tag{2.13}$$

While the probability of the existence of a chain growing with velocity v is given by

$$P[v] = \exp\left[-(-v - {}_{m}v)^2 / 2\sigma_v\right] / \sqrt{2\pi\sigma_v} \qquad (2.14)$$

Where L_m is the mean effective chain length and σ_L is the chain length distribution variance, while v_m is the mean chain growth velocity and σ_v the velocity variance. In both cases it is assumed that the p.d.f. of the two parameters are well approximated by normal Gaussian distributions [Elia, 77]. To ensure that nonphysical negative values have very low probabilities of existing, i.e. over 99% of the total population is positive valued and normally distributed. it is assumed that $L_m - 2\sqrt{2\sigma_L} > 0$ and $v_m - 2\sqrt{2\sigma_v} > 0$.

Now the case of two points x and x' separated by a distance $x - x'$ in the recording medium is examined. If $x - x' > L_m + 2\sqrt{2\sigma_L}$ then a negligible number (less than 1%) of chains originating at x' will be of sufficient effective length to reach x. But if $x - x' < L_m - 2\sqrt{2\sigma_L}$ effectively all chains which start to grow at x' will pass through x. In a similar manner effective maximum and minimum velocities can be defined. Dividing the effective maximum 'connectable' separation by the minimum effective velocity an expression for the maximum effective travel of time T_{MAX} between the points can be derived.

$$T_{\max} \approx \frac{(x - x')\big|_{MAX}}{v\big|_{MIN}} = \frac{L_m + 2\sqrt{2\sigma_L}}{v_m - 2\sqrt{2\sigma_v}} \qquad (2.15)$$

The time parameter T_{MAX} is of special significance. Given any length of time greater than T_{MAX} it is certain that more than 99% of all the chains which started to grow at x' and which are long

enough to reach x, will have given rise to an amount of polymer at x. In developing this model it is assumed that over this length of time the monomer concentration at x' varies very little. In this case, following an initial transient period within the system, the cumulative effect of position x' on position x will be 'instantaneously' governed by the amount of polymerisation at point x'. If the initiation of chains at position x' changes slowly as a function of time eventually a steady state is achieved at x. At any time following the initial transient time period, T_{MAX}, all possible x' initiated polymer chain length/velocity combinations which can reach the x position will be simultaneously present there. In this way an average over the time interval T_{MAX}, to find the accumulative effect of x' on x, can be used.

In other words, if chain growth is rapid compared to other temporal effects within the medium, i.e. the rates of monomer diffusion and polymerisation, then any change in the time averaged concentration of monomer at x' will effectively give rise to an instantaneous change in the time averaged amount of polymerisation at position x. In this section it is therefore assumed that the non-local temporal response arising due to the growth of the polymer chains can be modelled using an equivalent instantaneous non-local spatial response.

2.3.1 The Non-local Diffusion Model

Following the notation of Zhao and Mouroulis [Zhao, 94] the following extended non-local form of the one-dimensional diffusive transport equation for the concentration of monomer $u(x, t)$ in a dry layer is proposed.

$$\frac{\partial u(x,t)}{\partial t} = \frac{\partial}{\partial x}\left(D(x,t)\frac{\partial u(x,t)}{\partial x}\right) - \int_{-\infty}^{+\infty} \int_{0}^{t} R(x,x';t,t')F(x',t')u(x',t')dt'dx' \qquad (2.16)$$

In this equation $D(x, t)$ is referred to as the diffusion constant. $F(x', t')$ represents the rate of polymerisation [rate of removal of $u(x', t')$] at point x' and time t'. The non-local response function $R(x, x'; t, t')$ represents the effect of monomer concentration at location x' and t' on the amount of material being polymerised at location x at time t. The units of all these quantities are shown in Appendix F.

As discussed in the introduction it is argued that averaging takes place over the temporal effects and the material can therefore be assumed to have an equivalent instantaneous response. Now, based upon the introductory arguments regarding time scales, it is assumed that over the time interval T_{MAX} other processes vary very little.

$$F(x',t')u(x',t') \approx F(x',t'\pm T_{MAX})u(x',t'\pm T_{MAX}) \qquad (2.17)$$

It is assumed that the non-local response function can be broken up into the product of a spatial and a temporal response. $R(x,x';t,t') = R(x,x')T(t,t')$. The purely temporal response takes account of the effects of past events, over the time interval $0 \le t' < t$. In the local limit the time response function must have the following mathematical property:

$$\lim_{T_{MAX}\to 0}\{T(t',t)\} = \delta(t'-t) \qquad (2.18)$$

Furthermore it is argued that only events in the recent past, quantified using T_{MAX}, will give rise to significant non-local temporal effects. The time response must therefore have the properties that

$$\int_{-\infty}^{t} T(t',t)dt' = 1 \approx \int_{t-T_{MAX}}^{t} T(t',t)dt' \tag{2.19}$$

In Equation (2.19) the limits of integration indicate that the time response only operates over the range $t - T_{MAX} \le t' < t$.

Starting with Equation (2.16) and applying Equations (2.17) and (2.19) it is argued that

$$\int_0^t R(x,x';t,t')F(x',t')u(x',t')dt' \approx$$

$$\left[\int_{t-T_{MAX}}^{t} R(x,x')T(t,t')dt'\right]F(x',t)u(x',t) \approx R(x,x')F(x',t)u(x',t) \tag{2.20}$$

Combining these results the diffusion equation (2.11) becomes

$$\frac{\partial u(x,t)}{\partial t} = \frac{\partial}{\partial x}\left[D(x,t)\frac{\partial u(x,t)}{\partial x}\right] - \int_{-\infty}^{+\infty} R(x,x')F(x',t)u(x',t)dx' \tag{2.21}$$

Upon examination it can be seen that when the spatial response is local, i.e. $R(x,x') = \delta(x-x')$ we return to the standard one dimensional diffusion equation for monomer concentration, Equation (2.11) [Zhao, 94; Colv, 97].

$$\frac{\partial u(x,t)}{\partial t} = \frac{\partial}{\partial x}\left[D(x,t)\frac{\partial u(x,t)}{\partial x} \right] - F(x,t)u(x,t) \tag{2.22}$$

In order to solve Equation (2.21) a form for the spatial response function must be assumed. The response function must arise due to the growth of chains from the point at which they are initiated into adjacent regions. It will be related to, but not the same as, the p.d.f. of chain lengths. Furthermore it can be assumed that the growth of chains will be spatially isotropic, and therefore it is expected that the response will be an even function of x - x'. It would also seem physically reasonable to assume that the probability of a chain initiated at point x' influencing the process at x will decrease as the distance between the two points increases. Finally as the process approaches the local limit the response function must become a delta function. A mathematical function, which satisfies all these criteria, is:

$$R(x-x') = \frac{\exp\left[-(x-x')^2/2\sigma\right]}{\sqrt{2\pi\sigma}} \tag{2.23}$$

The squareroot of the variance $\sqrt{\sigma}$ is referred to as the *non-local response length* since it characterises the length scale over which the non-local effect is significant. It is noted that

$$\lim_{\sigma\to 0}\frac{\exp\left[-(x-x')^2/2\sigma\right]}{\sqrt{2\pi\sigma}} = \delta(x-x') \quad \text{and} \quad \int_{-\infty}^{+\infty}\frac{\exp\left[-(x-x')^2/2\sigma\right]}{\sqrt{2\pi\sigma}}dx' = 1 \tag{2.24}$$

Equation (2.21) is now solved following the method of Zhao and Mouroulis [Zhao, 94] including the non-local response presented in Equation (2.23), and under the following initial condition,

$u(x,0)=100$, for $-\infty < x < +\infty$. Following [Zhao, 94] we assume a recording intensity of the form

$$I(x,t)=I_0[1+V\cos(Kx)] \tag{2.25}$$

I_0 is the average intensity in the medium, V is the fringe visibility, $K=2\pi/\Lambda$ is the grating angular spatial frequency and Λ is the grating period. The validity of this assumption will be discussed later in Chapter 5. It is assumed that the rate of polymerisation is directly proportional to the exposing intensity and therefore

$$F(x,t)=F_0[1+V\cos(Kx)] \tag{2.26}$$

Where $F_0=\kappa I_0$, with κ as a fixed constant. The monomer concentration is written as a four harmonic expansion.

$$u(x,t)=\sum_{i=0}^{M=3} u_i(t)\cos(iKx) \tag{2.27}$$

While the 'diffusion constant' is expanded as a two harmonic expansion

$$D(x,t)=\sum_{i=0}^{M=1} D_i(t)\cos(iKx) \tag{2.28}$$

It is assumed that the variation of the diffusion coefficient can be expressed as a Fourier series. We now truncate this expansion assuming that only the first two terms must be retained.

$$D(x,t) = D_0(t) + D_1(t)\cos(Kx) \tag{2.29}$$

This assumption has previously been examined for the local response case and was shown to be acceptable, since the first or average term dominates except in cases of high non-linearity [Zhao, 94]. This assumption is re-evaluated here for the case of a non-local response. The diffusion constant is assumed to decay exponentially as a function of the polymerisation rate. The maximum and minimum of the diffusion rate, corresponding to the maximum and minimum of the exposing interference pattern, are then given by

$$D_{\max}(t) = D_a e^{-\alpha F_0(1-V)t} \tag{2.30}$$

$$D_{\min}(t) = D_a e^{-\alpha F_0(1+V)t} \tag{2.31}$$

D_a represents the initial diffusion constant. In the exponents the α term is a diffusion constant decay parameter. Comparing Equation (2.29), (2.30) and (2.31) it can be shown that

$$D_0(t) = \frac{1}{2}\left[D_{\max}(t) + D_{\min}(t)\right] = D_a e^{-\alpha F_0 t}\cosh(\alpha F_0 V t) \tag{2.32}$$

$$D_1(t) = \frac{1}{2}\left[D_{\max}(t) - D_{\min}(t)\right] = -D_a e^{-\alpha F_0 t}\sinh(\alpha F_0 V t) \tag{2.33}$$

We now introduce the variable ξ, which is proportional to the exposure energy.

$$\xi = F_0 t = \kappa I_0 t \tag{2.34}$$

Substituting these expansions into Equation (2.21) the following set of first order coupled concentration equations can be derived (See Appendix A).

$$\frac{du_0(\xi)}{d\xi} = -u_0(\xi) - \frac{V}{2} u_1(\xi) \tag{2.35}$$

$$\frac{du_1(\xi)}{d\xi} = -V \exp[-K^2\sigma/2]\, u_0(t) - \left[\exp[-K^2\sigma/2] + R\exp[-\alpha\xi]\cosh(\alpha V\xi)\right] u_1(\xi)$$

$$-\left[\frac{V}{2}\exp[-K^2\sigma/2] + R\exp[-\alpha\xi]\sinh(\alpha V\xi)\right] u_2(\xi) \tag{2.36}$$

$$\frac{du_2(\xi)}{d\xi} = -\left[\exp[-(2K)^2\sigma/2] + 4R\exp[-\alpha\xi]\cosh(\alpha V\xi)\right] u_2(\xi)$$

$$-\left[\frac{V}{2}\exp[-(2K)^2\sigma/2] - R\exp[-\alpha\xi]\sinh(\alpha V\xi)\right] u_1(\xi)$$

$$-\left[\frac{V}{2}\exp[-(2K)^2\sigma/2] - 3R\exp[-\alpha\xi]\sinh(\alpha V\xi)\right] u_3(\xi) \tag{2.37}$$

$$\frac{du_3(\xi)}{d\xi} = -\left[\exp[-(3K)^2\sigma/2] + 9R\exp[-\alpha\xi]\cosh(\alpha V\xi)\right] u_3(\xi)$$

$$-\left[\frac{V}{2}\exp[-(3K)^2\sigma/2]+3R\exp[-\alpha\xi]\sinh(\alpha V\xi)\right]u_2(\xi) \qquad (2.38)$$

Where u_0, u_1, u_2 and u_3 are the first four monomer concentration harmonics, σ is the non-local variance, α is a constant that characterises the rate of decrease of the diffusion coefficients [Zhao, 94]. $R = DK^2/F_0$ where $D=D_a$ [not to be confused with the response function $R(x-x')$] is the ratio of the diffusion rate and the polymerisation rate. $\xi = F_0 t = \kappa I_0 t$ it is the illumination time, t, multiplied by irradiance.

The resulting concentration of polymerized monomer, after an exposure of duration t seconds, is given by a modified version of the driving function of Equation (2.21), [Zhao, 94].

$$N(x,t)=\int_0^t\int_{-\infty}^{+\infty}R(x-x')F(x',t'')u(x',t'')dx'dt'' \qquad (2.39)$$

Giving the following polymerisation concentration spatial harmonic components:

$$N_0(\xi)=\int_0^{\xi}[u_0(\xi'')+(V/2)u_1(\xi'')]d\xi'' \qquad (2.40)$$

$$N_1(\xi)=\exp[-K^2\sigma/2]\int_0^{\xi}[Vu_0(\xi'')+u_1(\xi'')+(V/2)u_2(\xi'')]d\xi'' \qquad (2.41)$$

$$N_2(\xi)=\exp[-4K^2\sigma/2]\int_0^{\xi}[(V/2)u_1(\xi'')+u_2(\xi'')+(V/2)u_3(\xi'')]d\xi'' \qquad (2.42)$$

$$N_3(\xi)=\exp\left[-9K^2\sigma/2\right]\int_0^{\xi}\left[(V/2)u_2(\xi'')+u_3(\xi'')\right]d\xi'' \tag{2.43}$$

It is now assumed that the modulation of the refractive index induced during recording is approximately linearly related to the polymer concentration. Therefore each of the above terms corresponds to a change in the size of a spatial frequency component of a grating pattern recorded in the volume.

$$n(x,\xi)=n_{av}+C\sum_{i=0}^{M=3}N_i(\xi)\cos(iKx) \tag{2.44}$$

Where C is the constant relating polymerised concentration to refractive index. The numerical predictions of this model are discussed in the next section.

2.3.2 Numerical Results of Model

In this section changes to the local response diffusion model predictions which arise due to the introduction of the non-local response will be explored. This is achieved by carrying out a set of calculation analogous to those previously presented in the literature for the local response case and then comparing these to the non-local predictions [Zhao, 94; Colv, 97]. A single parameter the variance, σ is used to change the non-local effect. Three values of σ are normalised to the period of the grating squared. The values used in the following calculations are: σ = 0 (local case), σ = 1/32 and σ = 1/64. These last two values were chosen for two main reasons. To understand the first reason it is necessary to note that all length scales used in the following

section are, for the sake of generality, normalised with respect to the grating period length. Since the values of variance correspond to the square of a length within the grating. A normalised variance of $\sigma = 1/64$ corresponds, in the grating material, to a response length scale of one eight of a period and indicates the length range over which the effects of one point on another are significant. Besides simplicity, the second reason these values of variance were chosen was that they were found to provide clearly visible and typical results.

Equations (2.35, 2.36, 2.37 and 2.38) and (2.40, 2.41, 2.42 and 2.43) are solved numerically using *Mathematica* [Wolf, 96] run on a personal computer. Using the four harmonic expansion of the monomer concentration the harmonic amplitudes for the case when $V = 1$, $\alpha = 0.1$ and $R = 1$, are presented in Figure 2.3. As stated, all length scales are normalised with respect to the grating period length. In Figure 2.3.a the variation of the amplitudes of the zeroth, u_0, and first, u_1, harmonics as functions of exposure energy, ξ, are presented. In each case the curves for three values of non-local variance are presented: $\sigma = 0$ (local response case), $\sigma = 1/32$ and $\sigma = 1/64$. The corresponding graph for the second order monomer concentration harmonic are shown in Figure 2.3.b. The amplitudes of all the monomer harmonics are seen to decrease with time, also the larger the value of σ, the more rapidly the monomer is polymerised.

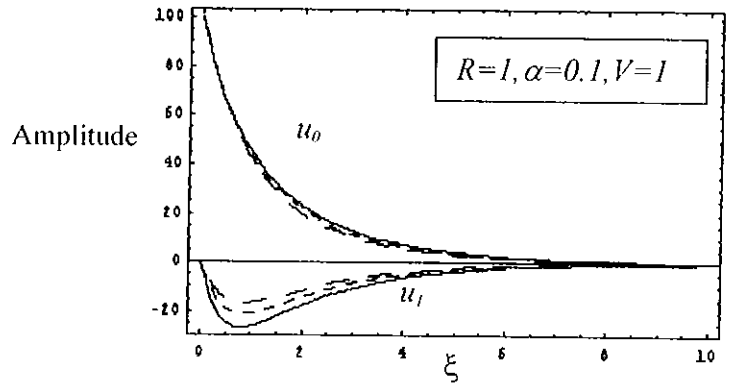

(a)

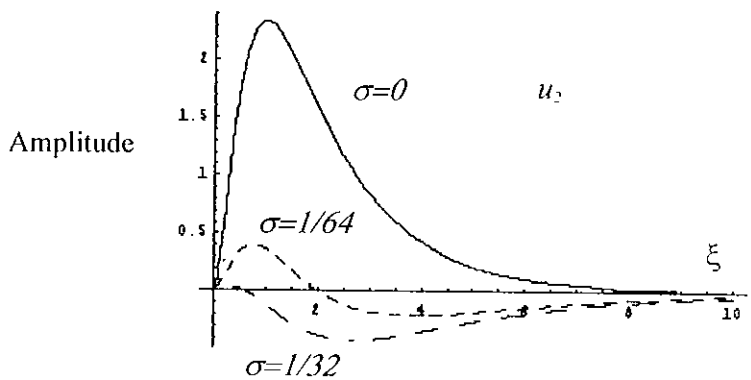

(b)

Figure 2.3 Monomer concentration amplitudes: (a) u_0 and u_1 and (b) u_2 versus exposure ξ. Solid lines $\sigma = 0$. Fine dashed lines $\sigma = 1/64$. Wide dashed lines $\sigma = 1/32$.

The corresponding harmonics of polymer concentration are shown in Figure 2.4. The effect of σ is to decrease the saturation levels of the higher order harmonics. Thus decreasing the amplitude but improving the sinusoidal purity of the profile shape.

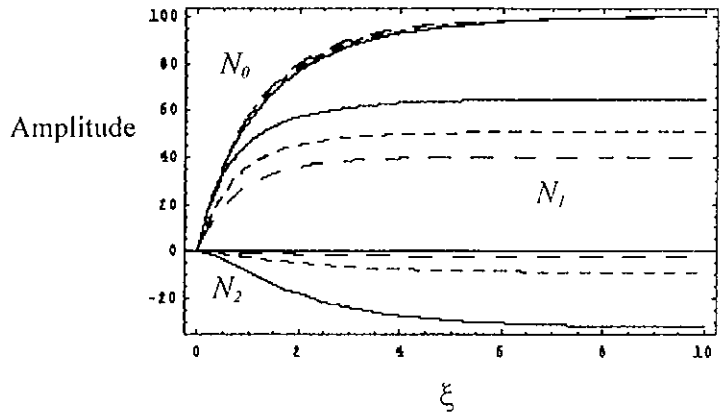

Figure 2.4 Polymer concentration amplitudes versus ξ for $R=1$. Solid lines $\sigma = 0$. Fine dashed lines $\sigma = 1/64$. Wide dashed lines $\sigma = 1/32$.

In Figure 2.5 the same sets of curves are plotted but in this case with the ratio of diffusion rate to polymerisation rate is decreased to the value $R = 0.05$. This smaller value of R corresponding to a higher rate of polymerisation and/or a lower rate of diffusion than in the previous case. The result is a slower decrease in monomer concentration and the smaller R the lower the saturation value of the first harmonic of the polymer profile. The effects of varying σ are qualitatively the same as above, e.g. increasing σ decreases the sizes of the saturation values.

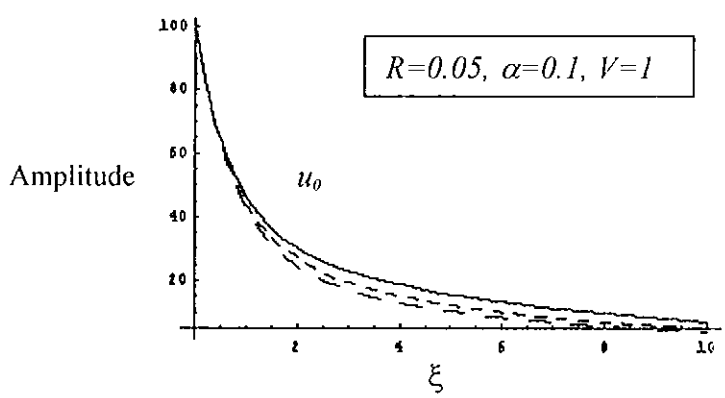

(a)

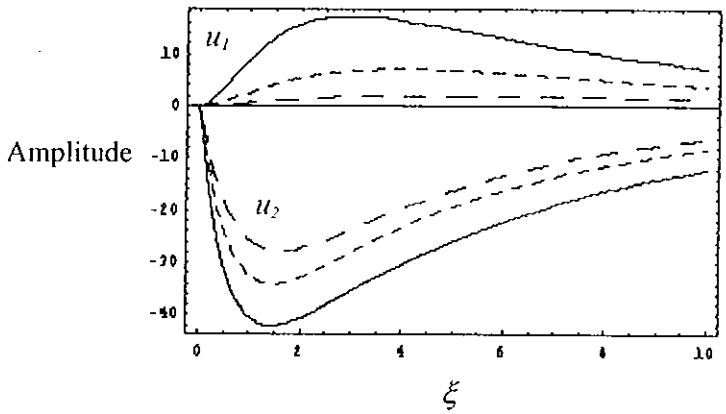

(b)

Figure 2.5 Monomer concentration amplitudes: (a) u_0 and (b) u_1 and u_2, versus exposure ξ. Solid lines $\sigma = 0$. Fine dashed lines $\sigma = 1/64$. Wide dashed lines $\sigma = 1/32$.

Clearly R is very important in determining grating formation. To investigate its effects, in Figure 2.6 three sets of figures showing the variations of the saturation values (calculated for $\xi = 40$) of the first three harmonics of the polymer profile are presented. The saturation values are presented for the cases when $\alpha = 0$ (solid line) and when $\alpha = 1$ (dashed line). The parameter α, characterises the rate of decrease of the diffusion constants [Zhao, 94].

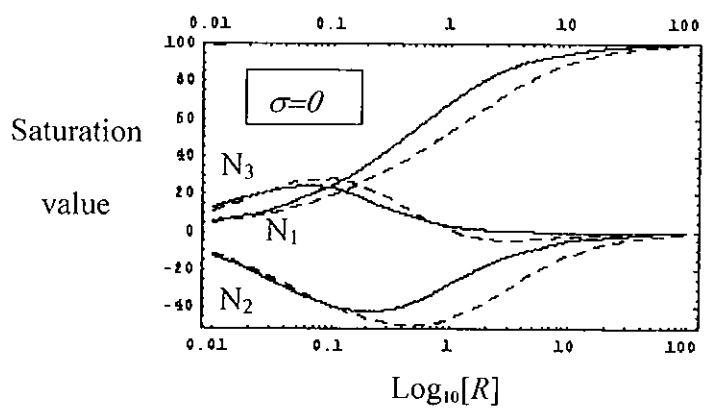

(a)

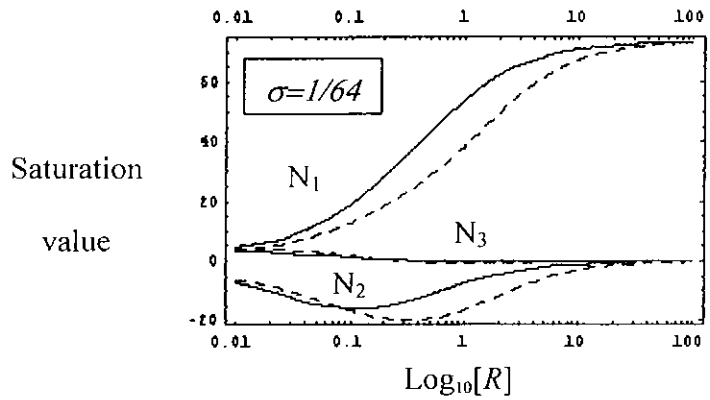

(b)

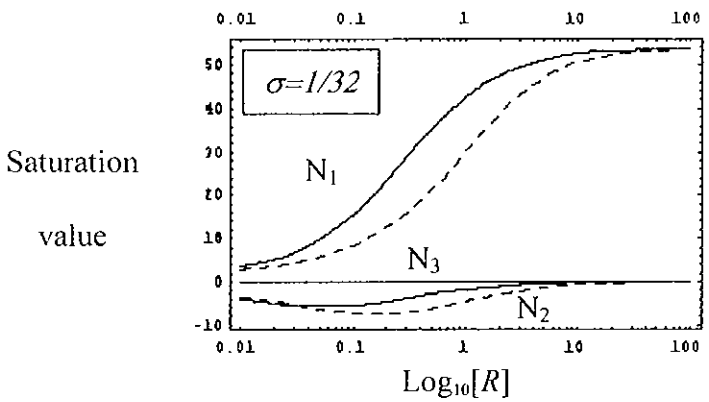

(c)

Figure 2.6 Saturation values ($\xi = 40$), of the first three harmonics of polymer concentration as a functions of R. Non-local response variances: (a) $\sigma = 0$, (b) $\sigma = 1/64$, and (c) $\sigma = 1/32$. In all cases $V = 1$. Solid lines $\alpha = 0$. Dashed lines $\alpha = 1$.

Three regions of behaviour have been identified for material exhibiting a local response [Zhao, 94].

In Region I., $R >> 1$, the diffusion rate is larger than the rate of polymerisation and the first harmonic achieves its maximum value while all higher orders go to zero.

In Region II. $R \sim 1$, N_1 increases as R increases while both N_2 and N_3 achieve their maximum values and then decrease in size.

In Region III. $R << 1$, the polymerisation rate dominates and monomers can be polymerised without any diffusion taking place, all the harmonics have low values in this region.

The effect of varying α, Equation (2.30) and (2.31), is to shift the saturation curves to the right. The strongest effect of increasing α occurs in Region II, where it reduces the size of N_1 while increasing the sizes of N_2 and N_3 for a given value of R. When $\alpha = 0$, $D_1 = 0$ and so a constant rate of diffusion D_0 exists in the material. The fact that any increase in α can be compensated for by an increase in R implies that including the sinusoidal variation of the diffusion constant is not essential to modelling the grating formation process [Zhao, 94].

Most noticeably as σ increases the saturation value of N_1 decreases. Both the second and third orders harmonics also have smaller maximum values and decrease more rapidly as a function of R. Although the percentage changes in the harmonic saturation values become larger in Region II. as the value of α increases, the behaviour is still that of a simple shifting of the curve to the right. Therefore in the non-local regime the diffusion constant, Equation (2.28), can still be modelled satisfactorily using a first order sinusoidal expansion, with $M=1$.

The effects of varying the illuminating fringe visibility on the saturated amplitude of the first order harmonic of the polymer concentration profile is now examined using the graphs in Figure 2.7. Results for three values of R and three values of σ are presented. For $R = 50 >> 1$, Figure

2.7.a, the response for all three values of σ is linear, with decreasing maximum N_1 as σ increases. As R and σ increase further the relationship becomes less linear and N_1 decreases rapidly in amplitude.

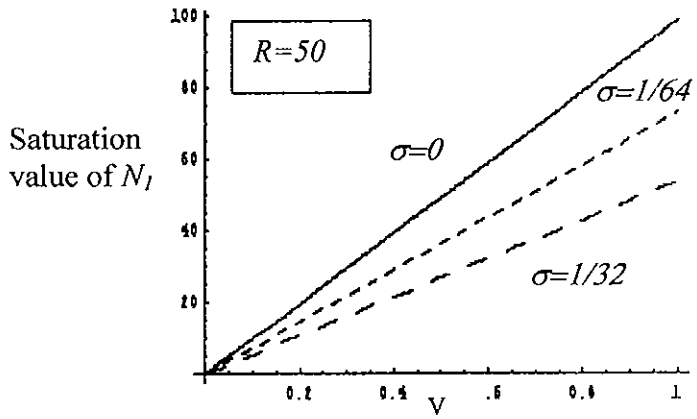

(a)

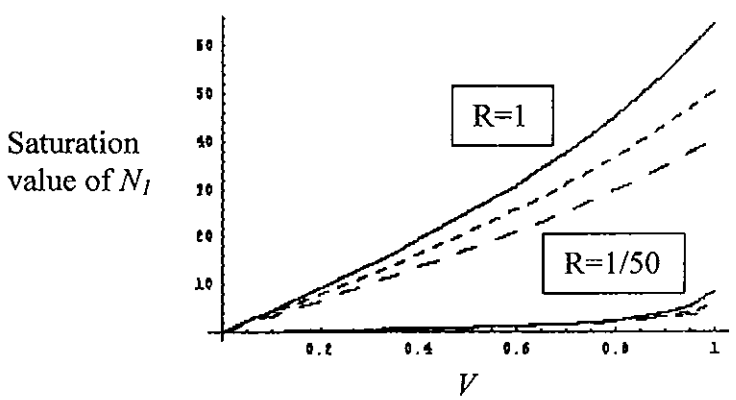

(b)

Figure 2.7 *Saturation values of the N_1 polymer concentration as a function of V. Solid lines $\sigma = 0$. Fine dashed lines $\sigma = 1/64$. Wide dashed lines $\sigma = 1/32$.*

2.3.3 Grating Profiles and Diffraction Efficiencies

For a range of physical parameters, the amplitudes of both the monomer and the resulting polymer concentration harmonics have been examined. In Figure 2.8 the corresponding polymer concentration profiles are presented, following an exposure of $\xi = 20$, plotted over one grating period, with $V = 1$ and $\alpha = 0.1$. In Figure 2.8: (a) $R = 1$, (b) $R = 50$ and (c) $R = 0.05$. In each case the profiles for values of normalised variance $\sigma = 0$, 1/64 and 1/32 are presented.

In Figure 2.8.a, $R=50$, there is significant distortion in the local response profile recorded. Increasing the non-local variance smoothes the profile and while the profile visibility decreases, it's harmonic purity increases. When $R = 50$, Figure 2.8.b, the largest visibility and most pure sinusoidal grating profiles are achieved. Increasing σ decreases the profile visibility. In Figure 2.8.c, $R = 0.05$, the most non-linear profiles with the most frequency components and the lowest visibility occur. Once again increasing σ produces a more purely sinusoidal profile but also decreases the profile visibility.

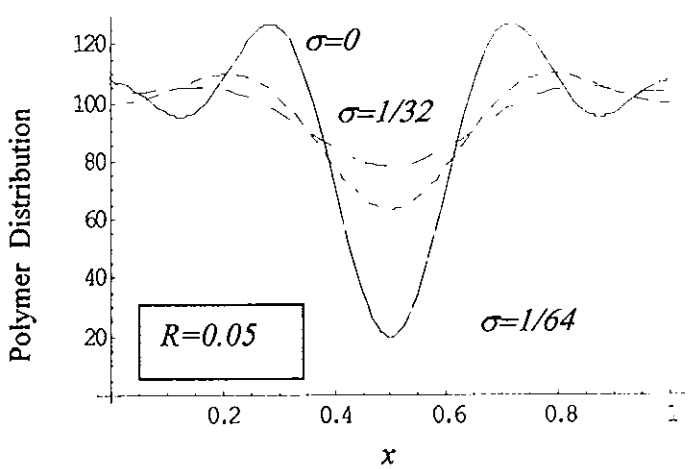

(a)

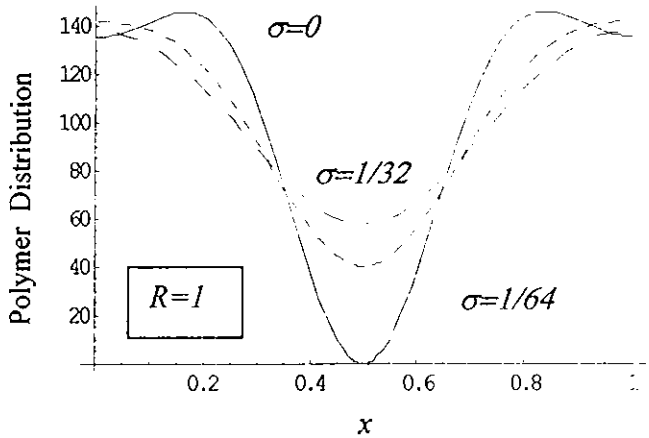

(b)

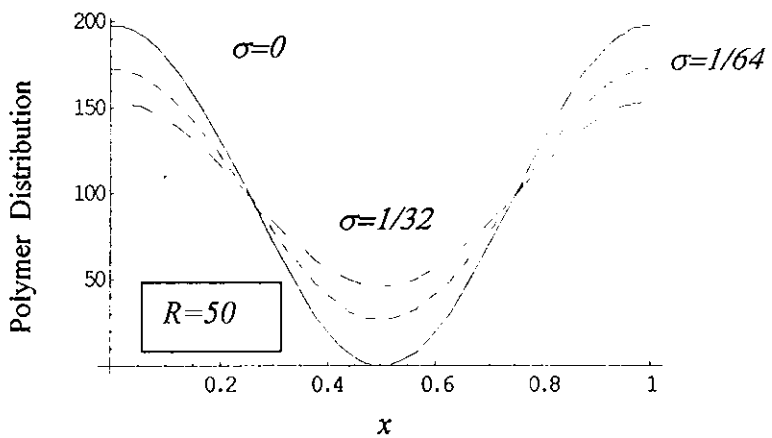

(c)

Figure 2.8 Spatial distribution profiles of polymer concentrations : (a) R = 0.05, (b) R = 0.05 and (c) R = 50. In all figures V=1, and α = 0.1. Non-local variances: Solid lines σ = 0. Fine dashed lines σ = 1/64. Wide dashed lines σ = 1/32.

It should be noted that the results in Figures 2.8.a correspond to those in figures 2.3 and 2.4 while those in Figure 2.8.c correspond to those in Figures 2.5 and 2.4.

As stated earlier, it is assumed that a linear relationship exists between the strength of the refractive index changes, which occur in the material and the strength of the polymer concentration. Rigorous electromagnetic models of diffraction by gratings exist [Syms, 90], however these are cumbersome and in the limiting case of volume gratings several adequate approximate models exist. The first-order two wave coupled-wave model [Koge, 69] predicts that the diffraction efficiency of a volume unslanted transmission phase grating replayed at the Bragg condition is given by

$$\eta = \sin^2\left(\frac{\pi n_1 d}{\lambda \cos\theta_1}\right) \tag{2.45}$$

Where d is the grating thickness, λ the replay wavelength, θ_1 the on-Bragg replay angle and n_1 the amplitude of the refractive index modulation (see Chapter 1). Physical values of these parameters are $d = 100\mu m$, $\lambda = 500nm$, $\theta_1 = 30^o$, which will produce a grating of period, $\Lambda = \lambda/(2\sin\theta_1) = 500nm$. It is assumed that $n = CN_1(\xi)$ and that therefore

$$\eta \approx \sin^2\left[725.5 \times CN_1(\xi)\right] \tag{2.46}$$

In Figure 2.6 it was shown that the range of N_1 saturation amplitudes between a maximum of 100 and a minimum of 50 over the full range of R. Given that a value of n_1 of about 0.002 will provide a diffraction efficiency close to 100%, a value of C of $4.3\text{x}10^{-5}$ l/mol substituted into Equation (2.46) will provide an experimentally achievable diffraction efficiency result.

Using these parameter values the diffraction efficiency growth curves, corresponding to the polymer profiles shown in Figure 2.8, are presented in Figure 2.9. The diffraction efficiency is shown as a function of ξ (exposure energy = illumination time by irradiance). From the model, an increase in diffraction efficiency up to a maximum value of 1, (100%), followed by a decrease to zero etc. as expected. Once n has increased beyond this first maximum value the medium is over-modulated.

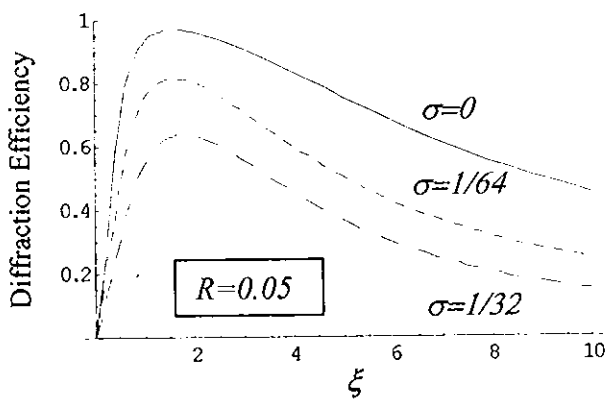

(a)

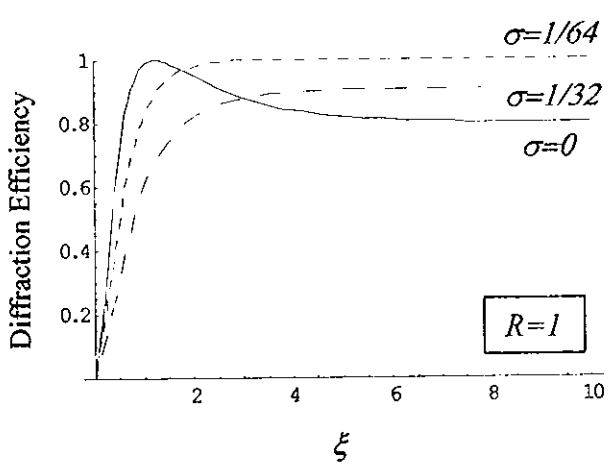

(b)

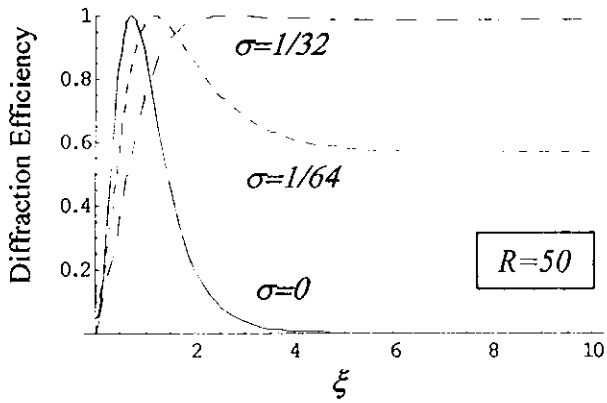

(c)

Figure 2.9 First-order two-wave coupled wave model prediction of the diffraction efficiency growth curves of the gratings:(a) R = 0.05, (b) R = 1, and (c) R = 50.

It can be noted from Figure 2.9 that both R and σ have very strong effects on the diffraction efficiency of the grating. In general the larger R the faster the growth of the grating and the higher the modulation achievable. Increasing the non-local variance always acts to slow down the growth of the diffraction efficiency and to reduce the maximum saturation modulation achievable. Examining these figures, in combination with all the previous results, the connection between changes in the first harmonic polymer concentration and the diffraction efficiency growth curves can be identified.

Finally, we present a spatial frequency response curve in Figure 2.10 below. The curve is plotted as polymer concentration against spatial frequency. For the local case (solid line) $\sigma = 0$ while for the non-local case (dashed line) $\sigma = 80$ nm. In Chapter 4 this will be shown to be a reasonable value for $\sqrt{\sigma}$.

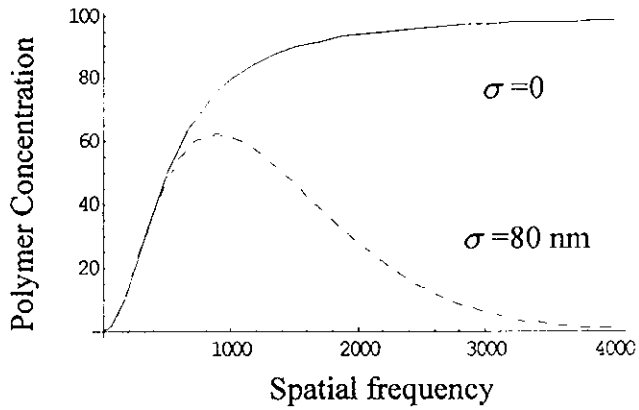

Figure 2.10 Theoretical spatial frequency response curve. Solid line is local (σ=0). while dashed line is non-local (σ=80nm).

The drop off in spatial frequency response for the non-local case can be clearly seen from Figure 2.10. This fall off which can be observed experimentally is not predicted by any of the current diffusion based models.

2.4 Conclusions

The diffusion model for hologram formation in photopolymer has been extended to include the non-local spatial response effect. This was done as previous models were not satisfactory. In particular, they failed to predict a cut-off in spatial frequency, which is observable experimentally. In order to do so it has been assumed that non-local temporal effects occur on a short time-scale, which, following averaging, allows them to be treated as effectively instantaneous.

The predictions of the local diffusion model, $\sigma = 0$, [Zhao, 94; Colv, 97] might be stated as follows. In general the larger the value of R the stronger the first order grating and the more closely the resulting grating profile matches the illuminating fringe pattern. These results can be summarised as follows:

(i) As I_0 increases $F_0 = \kappa I_0$ increases and $R = DK^2/F_0$ decreases.

(ii) As Λ increases $K = 2\pi / \Lambda$ decreases and R decreases.

Therefore the lower the illuminating intensity, I_0 (the longer the exposure, t) and the finer the fringe period the larger R and so the better the profile.

In the non-local response regime, $\sigma > 0$, further qualifications must be noted. The larger the non-local response variance the lower the visibility of the profile but also the more closely the profile recorded resembles the exposing sinusoidal interference pattern. Experimentally, one usually works with a fixed material in which the chain length and chain growth velocity p.d.f.s are fixed. As the recording fringe pattern period decreases the ratio of the non-local response variance to the period squared increases. In this situation eventually the grating amplitude is so weak as to be negligible. Therefore two additional results are predicted.

(iii) As Λ decreases, $K^2\sigma$ increases, $n_1 = CN_1$ decreases and the first order grating is suppressed.

(iv) As Λ decreases, $(mK)^2\sigma$ increases more rapidly and so $n_m = CN_m$ decreases and the higher order grating harmonics are even more heavily suppressed.

In (iii) and (iv) N_m is the m^{th} order polymer concentration harmonic.

Finally a spatial frequency response curve was shown. This clearly shows a drop off in spatial frequency response for the non-local case, which is not predicted by the local diffusion models.

The diffusion model has been extended in a way, which should make it applicable to a wider range of observable phenomena. This simple monomer diffusion and polymerization model is insufficient to explain all aspects of hologram formation. For example the diffusion of other components also effects the process. A model of much greater complexity may be required to fully predict the material behaviour.

In Chapter 4 this non-local diffusion model will be refined so it can be applied to experimental data. The equipment and procedures used to obtain such data are discussed in the next chapter.

Chapter 3 Experimental Work

In this chapter the experimental work carried out will be described. For each set of experiments the aims, methods, results and conclusion will be laid out. There were five sets of experiments carried out in this study. These experiments are summarised below.

1. The spatial frequency response of the material without any changes was measured.
2. The spatial frequency response of the material with different xanthene dyes was measured.
3. A set of experiments was carried out to find the effect of different molecular weight PVA binders on the spatial frequency response of the material.
4. A set of experiments was carried out to test the effect of various retarders on the response of the material.
5. A set of Substrate Mode Holograms (SMH) and Polarisation Selective Holograms (PSH) were recorded in DuPont photopolymer. This experimental work will be discussed in Chapter 6.

Before each of these experiments are examined in more detail, the method used to prepare the material and plates used in all procedures is presented.

3.1 Material Composition and Preparation

The acrylamide based photopolymer material used in this study was made up of the components presented in Table 3.1.

Component	Function	Amount per 100cm^3	Supplier
Poly-vinylalcohol	Binder	70 cm^3 of 10% sol.	Riedel de Haen
Acrylamide	Monomer	2.4g	Sigma–Aldrich
Bis–acrylamide	Crosslinker	0.8g	Sigma–Aldrich
Erythrosin B	Dye	16 cm^3 of 2x10^{-4} M	Sigma–Aldrich
Triethanolamine	Electron donor	8 cm^3	Riedel de Haen

Table 3.1 Composition of photopolymer material.

The material was prepared as follows with all chemicals being used as supplied.

1. 10 g of poly vinylalcohol were added to 100 cm^3 of deionised water. The PVA was dissolved using a heater/stirrer apparatus. Dissolution took about 45 minutes. The solution was allowed to cool and 70 cm^3 were then transferred into a beaker using a pipette.
2. 8 cm^3 of triethanolamine were added to the PVA solution and stirred thoroughly.
3. 2.4 g of acrylamide and 0.8 g of bis-acrylamide were added to the PVA solution and stirred until fully dissolved.

4. 16 cm^3 of $2x10^{-4}$ M Erythrosin B were added to the beaker. This and following steps were carried out under a safety light as the material was now sensitive to green light.
5. The solution was made up to 100 cm^3 in a volumetric flask with deionised water.
6. All solutions were stored in a sealed box away from light.

For holographic recording dry layers were prepared from the above liquid photopolymer. This was carried out as follows.

1. The substrates on which the layers were deposited were 5 cm by 5 cm glass plates.
2. The glass plates were cleaned thoroughly using acetone and deionised water. The plates were then placed on a clean and levelled marble slab. This allowed the photopolymer layers to adhere to the substrate evenly.
3. 2 mls of the liquid photopolymer were spread evenly on the plate using a syringe.
   This method typically gave layers 120 microns thick. Different thicknesses could be obtained be using larger or smaller amount of the solution. The thickness of the layers could be measured using a micrometer screw gauge.
4. The plates were left in the dark to dry for 12 --24 hours. The drying time depends on the thickness of the layer and the humidity of the room.
5. After drying, the plates could be sealed by coverplating or spraying them with an aerosol sealant to provide protection from humidity [Onei, 00c].
6. The dry layers were stored in a light-proof dessicator cabinet until needed for later use.

3.2 Measurement of the Spatial Frequency Response

The spatial resolution of a material can be defined as the highest spatial frequency grating which can be recorded with an diffraction efficiency of half of that at its maximum value. Spatial frequency is the numbers of lines per mm in an interference pattern. The spatial frequency response of the material describes how the diffraction efficiency that can be achieved using the material varies as a function of the fringe spacings recorded. A material with a good response will be capable of producing high diffraction efficiencies over a large range of fringe spacings. All real materials show a decline in maximum achievable diffraction efficiency outside a certain range of spatial frequencies. In practice this means the photopolymer must be capable of forming polymer chains corresponding to a bright and dark fringe interference pattern.

The aim of this work was to establish the spatial frequency response of the photopolymer material under study. It was also hoped to improve this response by changing the chemical composition of the material.

3.2.1 Method

The apparatus used to test the spatial frequency response of the material is shown in Figure 3.1 below:

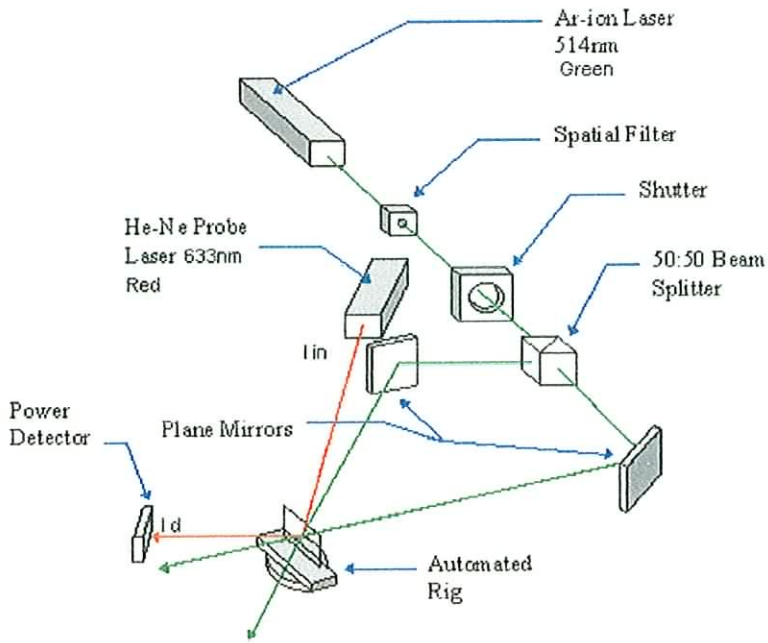

Figure 3.1 Apparatus for measuring spatial frequency response.

The set-up consists of a 200 mW Lexel (Model No. 95) Argon ion laser $\lambda = 514$ nm, a spatial filter and collimating lens. The beam passes from the lens through a Uniblitz shutter and into a 50:50 beam-splitter. The two beams are steered onto the layer using two plane mirrors. The glass plate which holds the layer was mounted on an Oriel rotation stage. A 1 mW He-Ne laser $\lambda = 633$ nm (Uniphase Model 1508-0) was used to probe the diffraction grating. The diffracted beam power is measured using a Newport optical power meter (Model No. 840).

The recording and probing of the gratings is controlled using a PC with the LabVIEW software package. The LabVIEW program has been developed in–house [Ryan, 98; Onei, 00b], it controls the shutter and rotation stage and also with data acquisition from the optical power meter and aall subsequent data processing. In this way angle scans and growth curves of gratings can be obtained quickly and easily. The processing software then fits theoretical curves to the data and

estimates the refractive index modulation size and thickness of the grating layer. The control software also allows the monitoring of grating decay and the recording and testing of arrays of gratings.

The spatial frequency of the gratings being recorded can be changed by varying the angle between the recording beams. This was achieved in practice by changing the distance from the plate to the plane mirrors and overlapping the beams on the plate. In this way, gratings with spatial frequencies from 750 up to 3000 lines / mm were recorded.

In the experiments carried out a number of gratings were recorded at different spatial frequencies. The exposure intensity of each beam was $2mW/cm^2$ and the exposure time was 20 seconds. These values were kept constant for all the gratings reported here.

3.2.2 Results

Figure 3.2 below shows the spatial frequency response of the original photopolymer material without any changes to its chemical composition [Mart, 94].

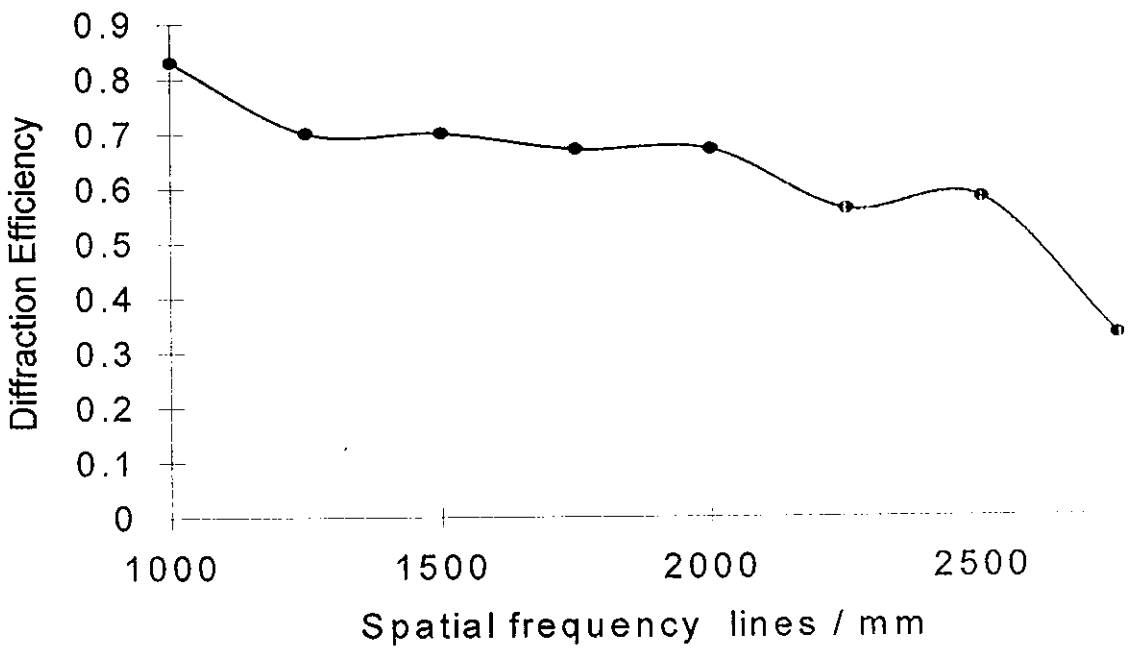

Figure 3.2 Spatial frequency response of the standard photopolymer material.

The curve shows a peak diffraction efficiency of about 80% at around 1000 lines/mm and then a gradual decay down to about 30% at 2750 lines/mm. Compared to the performance of other photopolymers this is quite a low value for the highest recordable number of fringes.

This result could be due to several factors, which are outlined below:

1. The inability to record gratings with small fringe spacing could be due to vibrations in the experimental set-up. These could be caused by mirrors or holders moving due to man-made sources of vibration or external noise. However the results do not vary significantly when carried out on a fully floated optical table or when the experiments are carried out in the evening when there are less people moving around. This would seem to suggest that there is a material-related cause related of an enviromental cause for the observed results. Further evidence to support a material-related cause is that various workers have recorded reflection holograms in silver halide emulsion using the same optical bench and equipment.

2. It is well known that diffusion of monomers and other components lead to grating formation in photopolymers [Colb, 71; Wops, 72]. It can be assumed that the greater the rate of diffusion, the more polymer will be formed in exposed regions. This in turn would lead to a higher difference in refractive index modulation between exposed and unexposed regions leading to a higher diffraction efficiency. The low diffraction efficiencies observed could be due to a low rate of diffusion, which prevents necessary material from moving in time to where it is required. This will be discussed in Section (3.3) and (3.4).

3. Finally it is also possible that the fall off in diffraction efficiency at high spatial frequencies could be due to polymer chains which have been initiated inside a bright region but grow into an adjoining dark region. This would lead to a "smearing" or averaging of the recording refractive index profile. This type of response which was discussed theoretically in Chapter 2, can be described as non-local since a refractive index change (polymer chain) initiated at one point produces a change at a point some distance away. Such an effect would produce a weaker refractive index modulation and a correspondingly lower diffraction efficiency at high

spatial frequencies, that would decrease further as the frequency increased. This view would seem to be consistent with the fall-off seen in the results such as those in Figure 3.2.

In the following section, the second possibility outlined above will be examined by varying the weights of the molecules in the photopolymer.

3.3 Spatial Frequency Response of Material with Different Xanthene Dyes

The dye used to sensitise the acrylamide based material under study is Erythrosin B. This is one of a class of compounds called xanthene dyes. They have been examined extensively in the literature [Oste, 60; Zakr, 87]] and they were first used in an acrylate based holographic recording material by Carre et al. [Carr, 90]. The xanthene dyes examined in this study were Eosin Y, Phloxine B, Erythrosin B and Rose Bengal. The molecular weights of these dyes are shown below in Table 3.2.

Xanthene Dye	Molecular Weight g/mol.
Eosin Y	691.88
Phloxine B	829.66
Erythrosin B	879.87
Rose Bengal	1017.65

Table 3.2 Molecular weights of the four xanthene dyes used in this study.

It can be seen that there is a large difference in molecular weight between the four dyes. It is reasonable to assume that barring usual geometry the smaller the molecule, the quicker it would diffuse through any given polymer matrix. As stated in Section 3.2, the faster the rate of

diffusion, the more polymer that will be formed in the exposed areas. This would lead to a greater difference in refractive index modulation and hence a higher spatial frequency. Therefore the effect of the four different size xanthene dyes on the spatial frequency response is examined.

3.3.1 Experimental

The material was prepared as described in Section 3.1 with $2x10^{-4}$ moles of each of the different dyes being used. The spatial frequency response was measured as shown in Section 3.2.

3.3.2 Results.

The spatial frequency responses of the four materials are shown below in Figure 3.3.

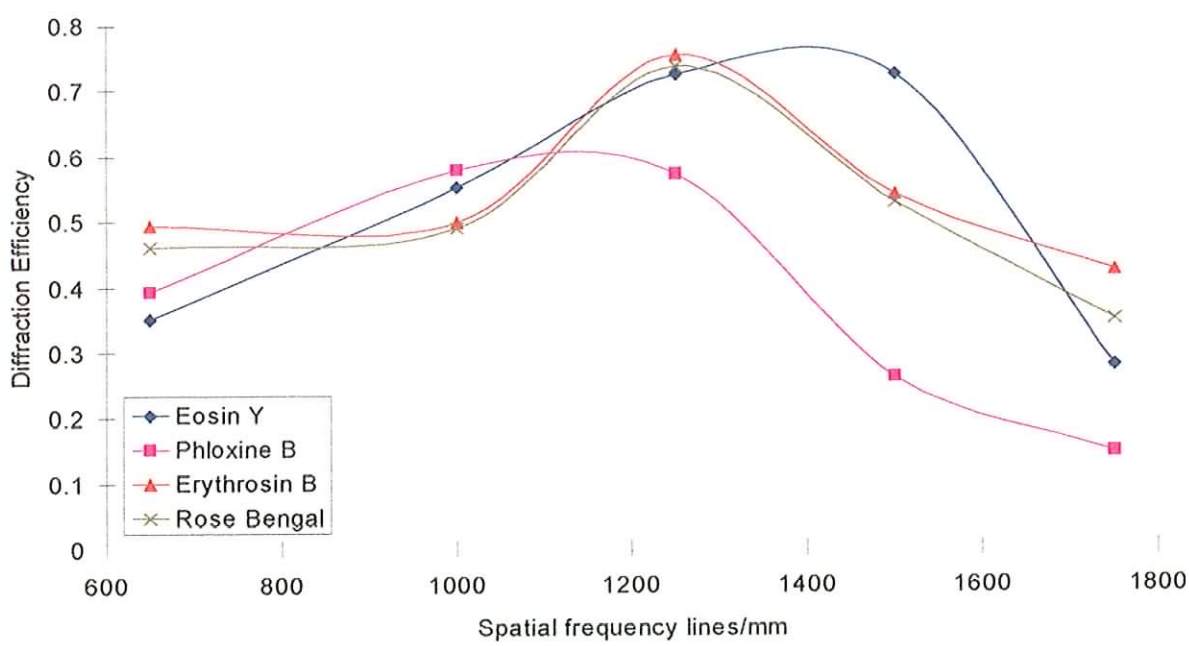

Figure 3.3 Spatial frequency response of material with different xanthene dyes.

It should also be noted that the curve above for the Erythrosin B sensitised material can be compared to the curve for the same material as shown in Figure (3.2). It can be seen that Figure (3.2) shows a much flatter response then Figure (3.3). This indicates the difficulties encountered in obtaining reproducible results when working with this material.

It can be seen from Figure (3.3) that there are no clear trends in the spatial frequency response behaviour as the molecular weights vary between 691 g/mol and 1017 g/mol. This would seem to indicate that the spatial frequency response is not primarily dependent on the rate of diffusion of these molecules. As the four xanthene dye molecules have basically the same shape, the geometry and shape of the molecules should not significantly affect the diffusion [Sigm, 99]. However, it is possible that the difference in the molecular weights of the dyes is too small to have a clear effect on the observed results. It would appear necessary to dramatically change the molecular weight of one of the components in order to examine the effects of diffusion on spatial frequency response.

3.4 Spatial Frequency Response of Material with Different Molecular Weight Binders.

It is well known that the binder plays an important role in dry photopolymer systems [Sadl, 75]. The molecular weight, refractive index and other properties of the binder have a major effect on the characteristics of the material. For example changing the binder to one which has a different refractive index than that of the polymer can lead to higher refractive index modulation and therefore higher efficiencies [Pitt, 80]. In a previous study of the acrylamide based system used

here, it was indicated that varying the molecular weight of the PVA binder used could cause the rate of diffusion in the photopolymer to change [Feel, 98]. This was in agreement with the general findings of Kokes and Long [Bove, 78]. Therefore it was decided to examine the spatial frequency response of the material using different molecular weight binders. As the available binders had a much wider variation in molecular weights than the xanthene dyes examined above, it was hoped an unambiguous effect on the spatial frequency response could be observed.

3.4.1 Experimental

The procedure used to measure the spatial frequency response has already been described. The material used and its preparation were as described in section 3.2.1. Four materials were made up, each containing a different molecular weight PVA binder. The binders used are described in Table 3.3 below.

PVA	Molecular Weight g/mol
A	9000-10000
B	12000-23000
C	50000
D	Not specified.

Table 3.3 Molecular weights of PVA binders used in binder study.

All the PVAs were supplied by Riedel de Hahn. There was no indication of the molecular weight range of Type D on the packaging. A fifth type of PVA was also available with a weight range of 124,000 to 180,000 g/mol. However, it was not possible to dissolve the required amount in water, so it was not examined further.

3.4.2 Experimental Results

Figure 3.4 (a) and (b) shows the spatial frequency response of four materials with different molecular weight PVA binders.

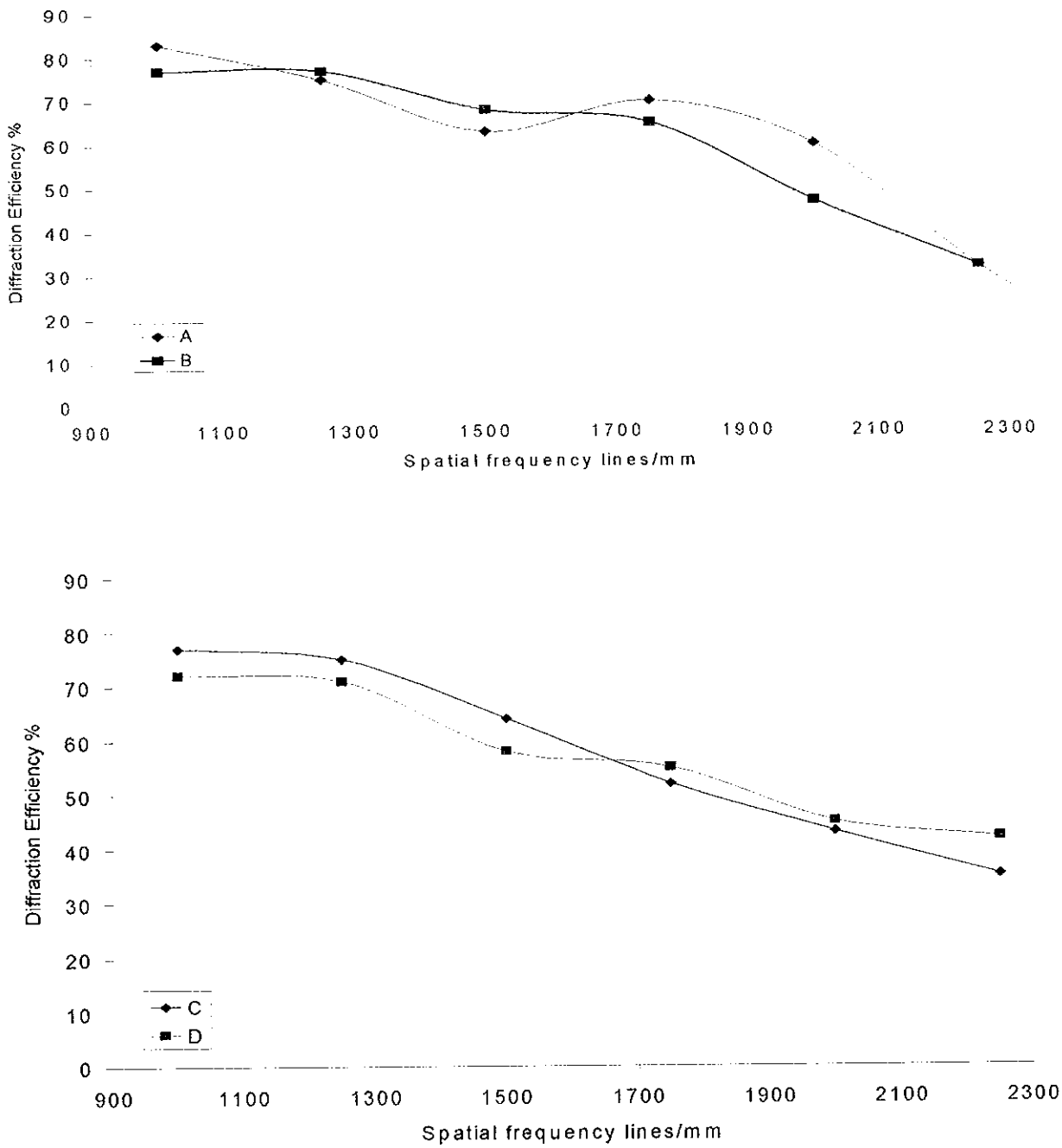

Figure 3.4 Spatial frequency response of photopolymer with different binders.

From this figure it can be seen that the lowest molecular weight binder, A, generally gives higher efficiencies for a given spatial frequency. However, the spatial frequency response does not change significantly with different binders. This would seem to suggest that changing the rate of diffusion of the mobile components will not change the spatial frequency response of the material. It might be possible that a poly-vinylalcohol binder with a molecular weight much larger or much smaller may have some effect. Experimentally, it was found that dry layers could not be formed with PVA's of a molecular weight higher than 50,000 g/mol.

Based on the results presented in Sections (3.3) and (3.4) it seems possible that other processes may determine the maximum spatial frequency recordable.

3.5 Control of Polymer Chain Length: Retarders

As shown earlier photopolymer materials store interference patterns by forming polymer chains in bright fringes regions. The difference in refractive index between polymerised bright regions and unpolymerised dark regions is the cause of light diffraction when the hologram is replayed. We propose that the fall-off in diffraction efficiency at high spatial frequencies could be due to polymer chains, which have been initiated inside the bright regions but continue growing into the adjacent dark regions. At high spatial frequencies this would lead to a "smearing" of the refractive index profile. To investigate whether this actually occurs in a photopolymer material it was necessary to find a method of controlling the lengths of polymer chains formed in the bright

regions. If the chain lengths could be shortened then the "smearing" effect due to polymer chain growth should decrease [Pont, 98]..

3.5.1 Methods of Controlling Polymer Chain Lengths.

One method of controlling chain lengths is by the addition of a chemical known as a *retarder* or *inhibitor*. These work by reacting with the radical at the end of a propagating polymer chain thereby stopping the chain from adding any more monomer units [Conr, 67]. The difference between inhibitors and retarders is the extent to which this process occurs. If the inhibitor attacks every polymer radical just after it has formed then no polymerisation will take place. This is known as inhibition. If the concentration of the inhibitor is lower then the polymer chains have a chance to grow before they are attacked and terminated by the inhibitor. This process is called retardation.

The retarder chosen for use in this study was 4-ethoxyphenol. This chemical was picked because it is used by chemical companies to stop acrylamide monomer polymerising during transport [Sigm, 99]. Its structure is shown in Figure 3.5 below. All of the following structure diagrams were produced using Chemsketch Version 3.5 from Advance Chemistry Development Inc. [Acdi, 98].

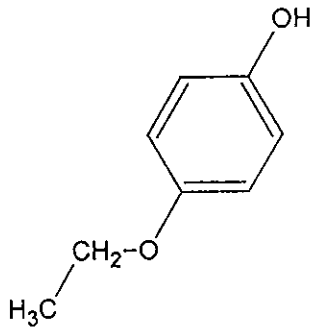

Figure 3.5 Structure of 4-ethoxyphenol.

A second chemical called para-benzoquinone was also examined as it is a commonly used inhibitor of vinyl polymerisation [Conr, 67]. Its structure is shown in Figure 3.6

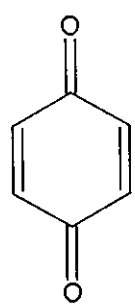

Figure 3.6 Structure of para-benzoquinone.

There are two mechanisms by which these molecules are thought to cause inhibition or retardation. Both are shown below following [Conr, 67]. The first involves the polymer radical reacting with a quinone to produce inactive free radicals by nuclear substitution.

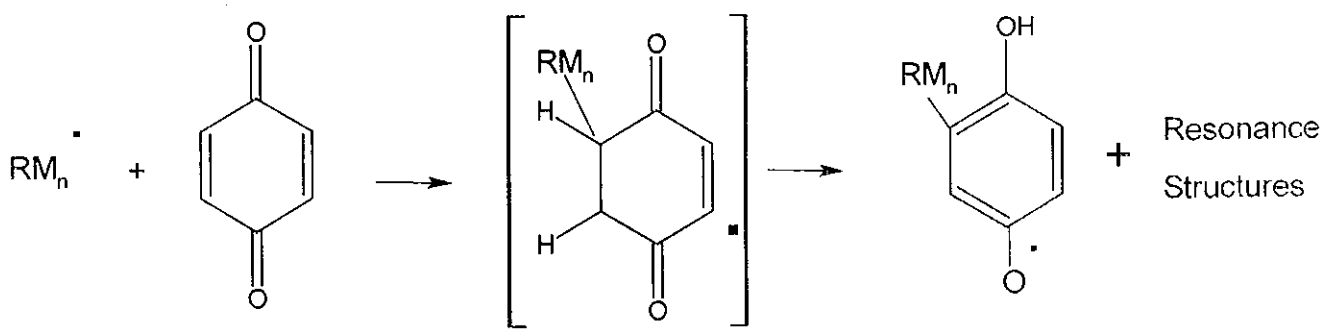

Figure 3.7 Mechanism of polymer chain addition to retarder.

The "inactive" free radicals do not have the ability to react with monomer molecules. However they can react with another quinone molecule to produce a substituted quinone and a quinhydrone radical as shown in Figure 3.8.

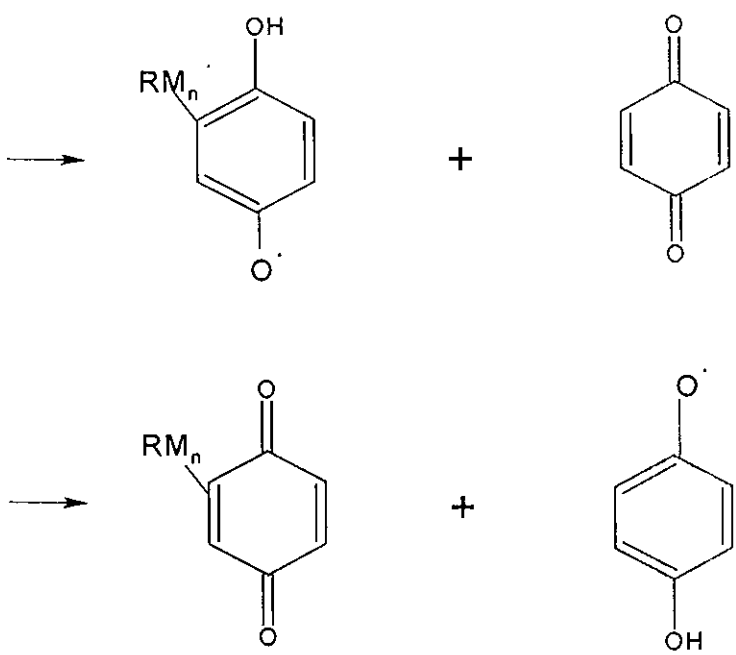

Figure 3.8 Mechanism of "inactive" free radical reaction.

These undergo equilibrium disproportionation to hydroquinone and quinone.

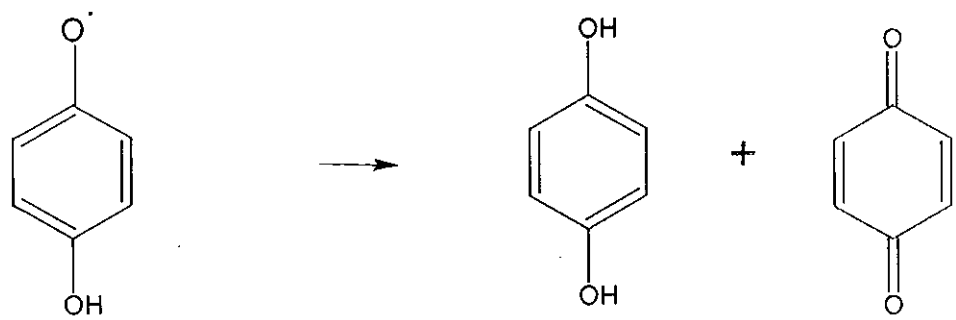

Figure 3.9 Mechanism of disproportionation to hydroquinone and quinone.

The second suggested mechanism involves the polymer radical attacking the quinone molecule at one of the oxygen atoms. This reaction produces diethers of hydroquinone.

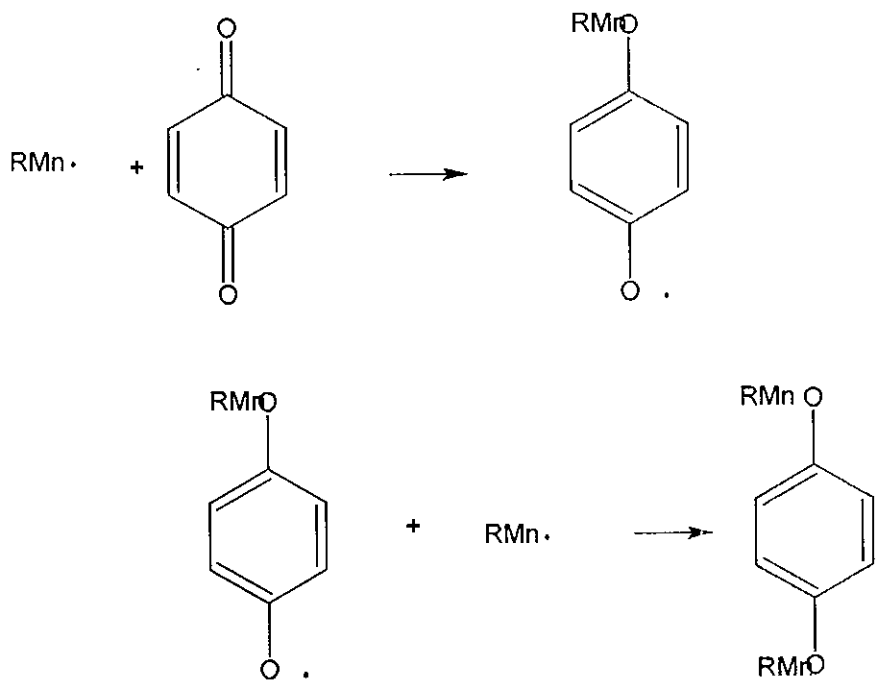

Figure 3.10 Polymer radical attack on quinone oxygen atom.

The polymer radical could also disproportionate with a quinone molecule to form ethers and hydrogenated products.

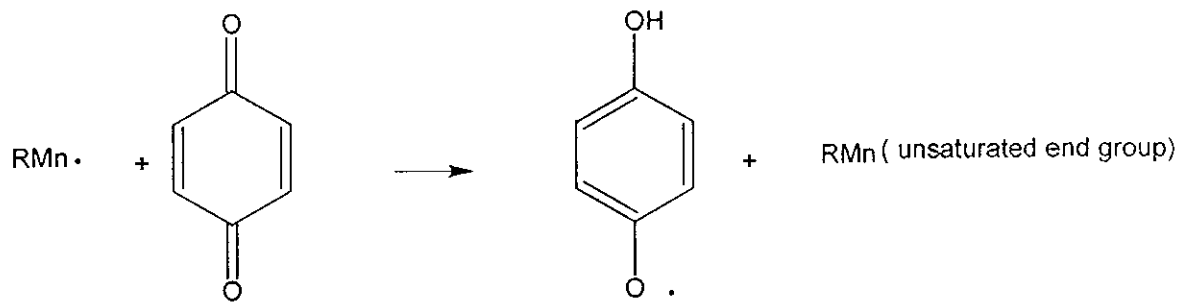

Figure 3.11 Mechanism of polymer radical/quinone disproportionation.

In this section we have introduced retarders and described the mechanism by which it can control the length of polymer chains. Next we examine the experimental results produced when specific retarder concentrations are introduced into the material.

3.5.2 Experimental

The spatial frequency response was measured using the apparatus and procedures already described in section 3.2.1. The type and amount of retarder added to the standard material is shown in Table 3.4 below.

Retarder	Concentration % weight/volume
4-ethoxyphenol	0.5 1.5 3.0 6.0
p-benzoquinone	0.01

Table 3.4 Types and concentrations of retarder added to the standard material for initial studies.

These retarder concentrations were added to the standard material in the hope of being able to clearly identify the effects on the spatial frequency response of reducing the average length of the polymer chains.

3.5.3 Experimental Results

Figure 3.12 (a) and (b) shows the spatial frequency response of the standard photopolymer material with four different concentrations of 4-ethoxyphenol added.

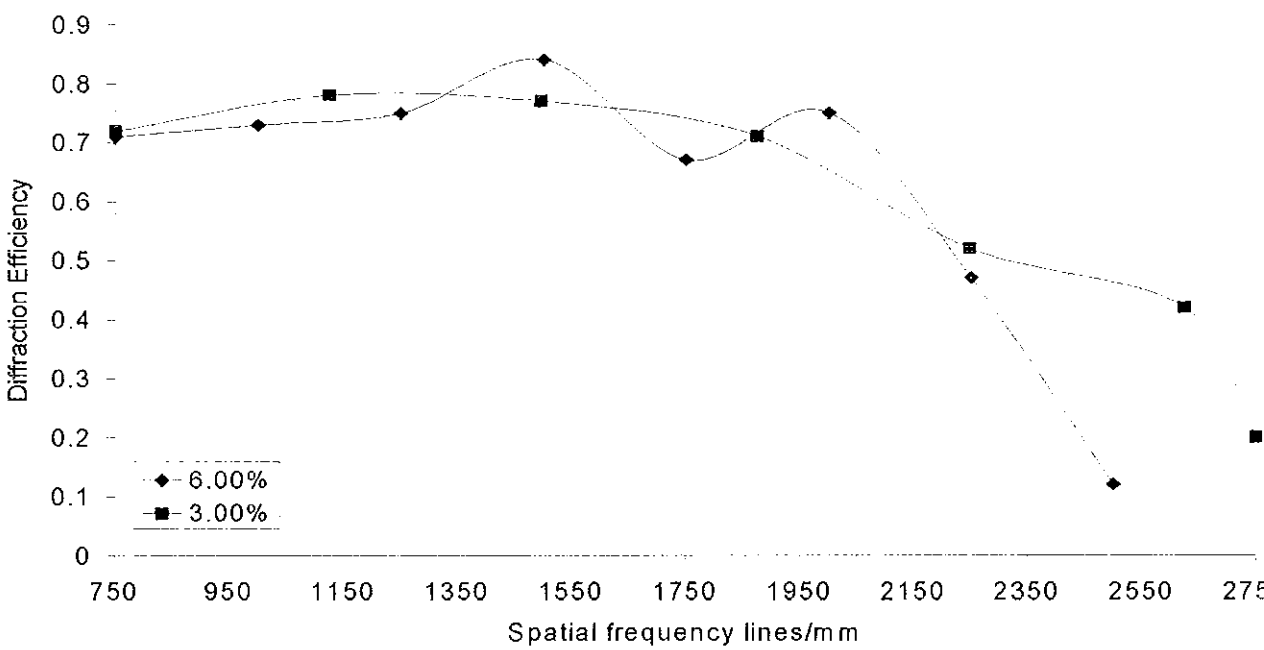

(a)

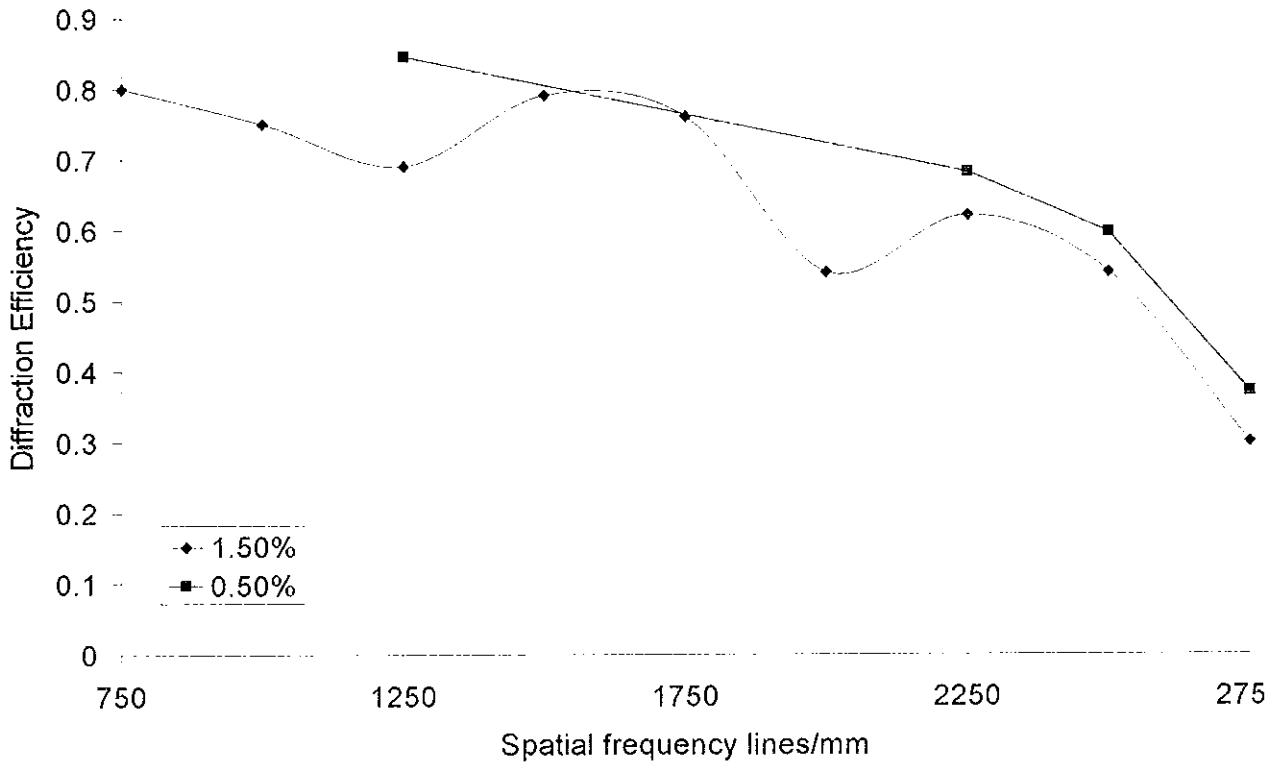

(b)

Figure 3.12 Spatial frequency response of material with 4-ethoxyphenol added.(a)=6.0% and 3.0%, (b) 1.5% and 0.5%.

The graph shows that there is no significant change in the spatial frequency at which the diffraction efficiency drops off when compared to the response of the standard material as shown in Figure (3.2). The material with 6% retarder added shows a sharper decrease of diffraction efficiency versus increased spatial frequency when compared to the other materials. At frequencies higher than about 2000 lines per mm the material with the lowest concentration was found to give the highest diffraction efficiency for a particular fringe spacing.

Figure 3.13 shows the spatial frequency response of the standard material with of p-benzoquinone added.

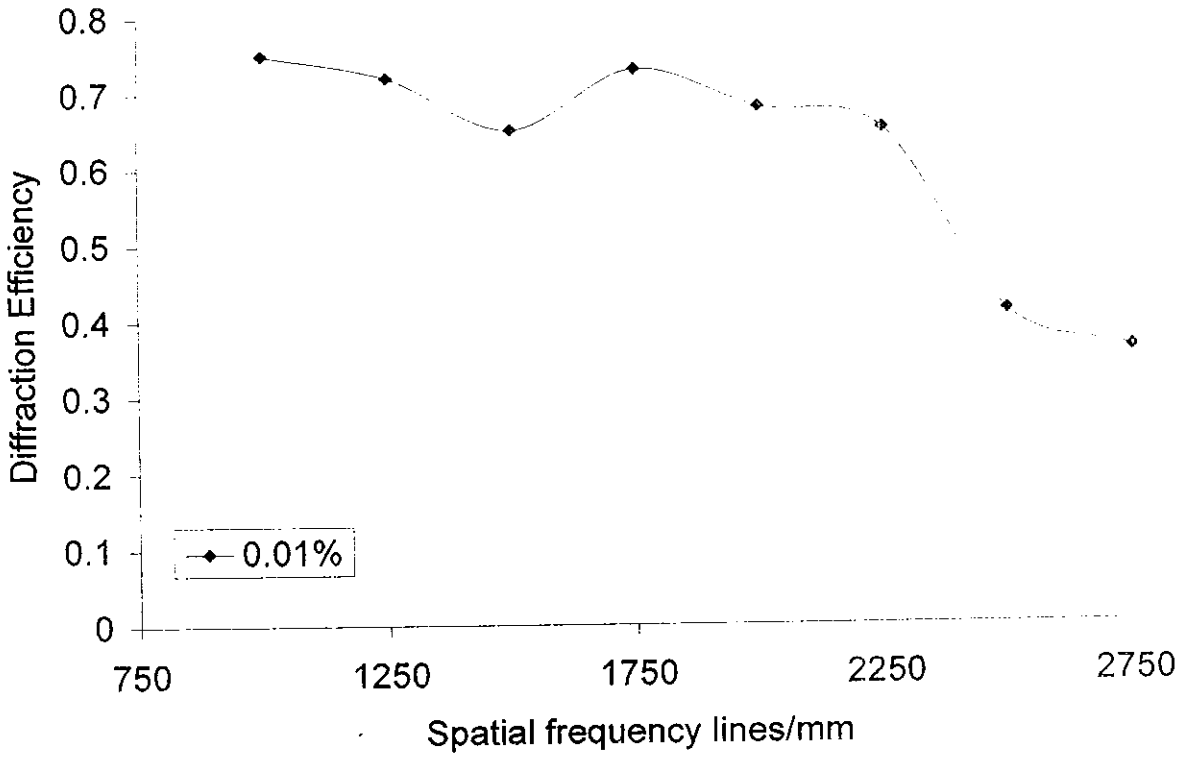

Figure 3.13 Spatial frequency response of material with a 0.01% concentration of para-benzoquinone added.

The response of this material is similar to the material with 4-ethoxyphenol added. No significant change can be seen in the spatial frequency at which the diffraction efficiency drops off when compared to the standard material in Figure (3.3). However, it is known that the concentration of retarder added is critical [Dave, 99]. Up to a certain concentration there is no observable effect. Then only over a small range of concentrations of retarder is an effect on the polymer chain length noticed. At higher concentrations the polymerisation reaction will be totally inhibited and no polymer will form. It is possible that for the experiments carried out to date, a sample of which are shown above, too low a concentration of retarder was being used. It

is also possible that there are more suitable retarders for an acrylamide-based material than the two proposed for use in this study.

3.6 Conclusions

In this chapter, the procedures used to determine the spatial frequency response of the photopolymer material were presented. The composition of the material and the methods used to prepare it were outlined.

A number of experiments were carried out to establish the effect of changing the material composition on the spatial frequency response:

First, the spatial frequency response of the material sensitised with four different xanthene dyes was measured. There was no significant difference in the responses. This is thought to indicate that dye diffusion or the shape of the dye molecules does not have a major role to play in determining spatial frequency response. However, it is possible that the difference in shape or in molecular weight between the dyes was too small to cause on effect on the frequency response.

In a second attempt to alter the spatial frequency response, four different molecular weight PVA binders were examined. It was hoped that the wider range of molecular weights available would change the response significantly but this was not the case.

It became clear that an alternative approach was required. Based on the non-local model presented in Chapter 2 attempts were made to reduce the lengths of the polymer chains. The effects of adding two different retarders to the material were examined. However, once again, there was no significant difference in spatial frequency response. It is possible that the correct concentration of retarder needed to optimally shorten the chains was not determined. It is also possible that a more suitable retarder for this acrylamide based system could give the desired result.

The next chapter will show how the non-local diffusion model derived in Chapter 2 can be applied to the experimental data obtained above.

Chapter 4 Analytic Non-Local Model

In this chapter, the non-local model introduced in Chapter 2 will be refined so that it can be applied to experimental data.

4.1 Introduction

It has been previously shown in Chapter 2 that by introducing a non-local response function into the one-dimensional diffusion equation governing grating formation [Sheri, 00] both the high frequency and low frequency cut-offs in the spatial frequency response of photopolymer materials can be explained. The non-local response is characterised by a non-local length parameter, which quantifies the effects of polymer chain growth initiated at one point in the medium on the polymerisation that takes place some distance away.

In this section, starting with the previously derived results, analytic solutions to the non-local diffusion equation are derived assuming a two harmonic expansion of the monomer concentration. These analytic expressions are compared to the more rigorous four harmonic numerical results, indicating the range of physical parameters for which they are accurate. The model, corrected to allow for Fresnel reflections during recording, is then compared to growth curves produced by measuring the diffraction intensities produced by gratings with different spatial frequencies during recording. The holographic gratings used are all recorded in an acrylamide based photopolymer material. The resulting diffraction efficiencies are calculated allowing for Fresnel boundary losses. By applying Kogelnik's coupled-wave theory [Koge, 69] the corresponding refractive index modulations are calculated. Fitting these curves using the two

harmonic analytic expressions, various physical parameters including R, D and σ (see Chapter 2) are estimated and the trends in their behaviour as the spatial frequency is changed are indicated.

4.2 Theory: Analytic Expressions

In this section, a two harmonic approximation of the non-local theory introduced previously in Chapter 2 and [Sheri, 00] is presented. This approximation leads to closed form analytic solutions for the zeroth and first harmonics of the monomer and polymer concentrations and thus refractive index modulation. These solutions are applied to provide a convenient form for use in comparing theoretical predictions with experimental results. In all the following sections the notation and definitions introduced in Chapter 2 are used.

From Chapter 2 the two first-order non-local coupled concentration equations are given by

$$\frac{du_0(\xi)}{d\xi} = -u_0(\xi) - \frac{V}{2}u_1(\xi) \tag{4.1}$$

And

$$\frac{du_1(\xi)}{d\xi} = -V\,S\,u_0(\xi) - \left(S + R\,\exp[-\alpha\xi]\cosh[\alpha V\xi]\right)u_1(\xi) - \left(\frac{V}{2}S + R\exp[-\alpha\xi]\sinh[\alpha V\xi]\right)u_2(\xi) \tag{4.2}$$

Where u_0, u_1, and u_2 are the first three monomer concentration harmonics. σ is the non-local variance. α is a constant that characterises the rate of decrease of the diffusion coefficients, see [Zhao, 94], $R = DK^2/F_0$ is the ratio of the diffusion rate and the polymerisation rate. V is the visibility, $K = 2\pi/\Lambda$, $\xi = F_0 t = \kappa I_0 t$ is the illumination time, t, multiplied by irradiance and S is defined as

$$S = \exp[-K^2\sigma/2] \tag{4.3}$$

For the two harmonic approximation we assume that all higher harmonics are negligible, $u_2 = u_3 = u_4 = 0$. In this case Equations (4.1) and (4.2) are expressed in terms of u_0 and u_1 only to become:

$$\frac{du_0(\xi)}{d\xi} = -u_0(\xi) - \frac{V}{2}u_1(\xi) \tag{4.3}$$

$$\frac{du_1(\xi)}{d\xi} = -V\,S\,u_0(\xi) - \left(S + R\exp[-\alpha\xi]\cosh\left[\alpha V\xi\right]\right)u_1(\xi) \tag{4.4}$$

It is now assumed that $\exp[-\alpha\xi]\cosh(\alpha V\xi) \approx 1$. This would occur when $\alpha\xi$ (which represents the change of the product of the diffusion coefficients times the exposure energy) is negligible. Such a situation would occur (i) near the start of the polymerisation process, $\xi = 0$ or (ii) if $\alpha = 0$, which can be assumed since changing α is equivalent to varying R (see Chapter 2, [Zhao, 94]).

In this case Equation (4.4) simplifies to,

$$\frac{du_1(\xi)}{d\xi} = -V\,S\,u_0(\xi) - (S+R)u_1(\xi) \tag{4.5}$$

The first-order coupled differential equations (4.3) and (4.5) can then be solved to give

$$u_0(\xi) = \frac{100\exp[-W\xi/2]}{B}\left(B\cosh[B\xi/2] + (R+S-1)\sinh[B\xi/2]\right) \tag{4.6}$$

and

$$u_1(\xi) = \frac{100\,SV}{B}\left\{-\exp\left[(B-W)\xi/2\right] + \exp\left[(B+W)\xi/2\right]\right\} \tag{4.7}$$

Where for brevity, we introduce W = 1+R+S and B = $\sqrt{1+R^2+2R(S-1)+S^2}$.

Following Chapter 2 the resulting concentration of polymerised monomer, after an exposure of duration t seconds, is given by Equation (4.8).

$$N(x,t) = \int_0^t \int_{-\infty}^{+\infty} R(x-x')F(x',t')u(x',t')dx'dt' \tag{4.8}$$

Giving the following polymerisation concentration spatial harmonic components:

$$N_0(\xi) = \int_0^{\xi} \left[u_0(\xi') + (V/2) u_1(\xi') \right] d\xi'$$

(4.9)

$$N_1(\xi) = S \int_0^{\xi} \left[V u_0(\xi') + u_1(\xi') \right] d\xi'$$

(4.10)

Substituting for u_0 and u_1 gives that

$$N_0(\xi) = 100 \exp\left[-W\xi/2\right] \left\{ \cosh\left[W\xi/2\right] - \cosh\left[B\xi/2\right] + \sinh\left[W\xi/2\right] - \frac{(-1+R+S)\sinh\left[B\xi/2\right]}{B} \right\}$$

(4.11)

And

$$N_1(\xi) = \frac{400SV}{4(R+S) - 2SV^2} \left\{ R + \exp\left[W\xi/2\right] \left(-R\cosh\left[B\xi/2\right] - \frac{\left(-2S + R(-1+R+S) + SV^2\right)\sinh\left[B\xi/2\right]}{B} \right) \right\}$$

(4.12)

It is once again assumed that the modulation of the refractive index induced during recording is linearly related to the polymer concentration.

$$n_m(\xi) = C \times N_m(\xi) \qquad (4.13)$$

Substituting for N_0 and N_1 (Equations 4.11 and 4.12) into Equation (4.13) gives that

$$n_0(\xi) = 100\ \mathrm{C}\ \exp\left[-\mathrm{W}\xi/2\right]\left\{\cosh\left[\mathrm{W}\xi/2\right]-\cosh\left[\mathrm{B}\xi/2\right]+\sinh\left[\mathrm{W}\xi/2\right]-\frac{(-1+\mathrm{R}+\mathrm{S})\sinh\left[\mathrm{B}\xi/2\right]}{\mathrm{B}}\right\} \tag{4.14}$$

And,

$$\mathrm{n}_1(\xi)=\frac{400\mathrm{SVC}}{4(\mathrm{R}+\mathrm{S})-2\mathrm{SV}^2}\left\{R+\exp\left[\mathrm{W}\xi/2\right]\left(-\mathrm{R}\cosh\left[\mathrm{B}\xi/2\right]-\frac{\left(-2\mathrm{S}+\mathrm{R}(-1+\mathrm{R}+\mathrm{S})+\mathrm{SV}^2\right)\sinh\left[\mathrm{B}\xi/2\right]}{\mathrm{B}}\right)\right\} \tag{4.15}$$

To calculate the refractive index modulation of a grating recorded in the material, Equations (4.14) and (4.15) are substituted into Equation (4.16) shown below

$$n(x,\xi) = n_0(\xi) + n_1(\xi)\cos(Kx) \tag{4.16}$$

In the next section, the accuracy of the analytic model must be assessed.

4.3 Comparison of Numerical Non-local and Analytic Non-local Models

The predictions of the numerical four harmonic non-local model presented previously in Chapter 2 and [Sheri, 00] are now compared with the analytic two harmonic approximation derived above. This is achieved by plotting (i) monomer and (ii) polymer concentration amplitudes along with (iii) grating profiles for various values of R and σ. For each of the three types of graph the predictions of the analytic and numerical model were examined for the same sets of values of R and σ. Once again the values of R chosen were 0.05, 5 and 50 while the normalised values of σ used were 0, 1/32 and 1/64, which correspond with those used previously in Chapter 2.

For many of the cases mentioned above the predictions of the two models were so similar that the plotted lines overlapped and no difference could be seen. In this section only the cases where there was a visible difference in the predictions of the two models will be examined. A complete set of graphs can be found in Appendix B. Figure 4.1 below shows the greatest difference in the predictions of the two models for the first two harmonics of monomer concentration for the R and σ values mentioned above. It shows u_0 and u_1 for both cases.

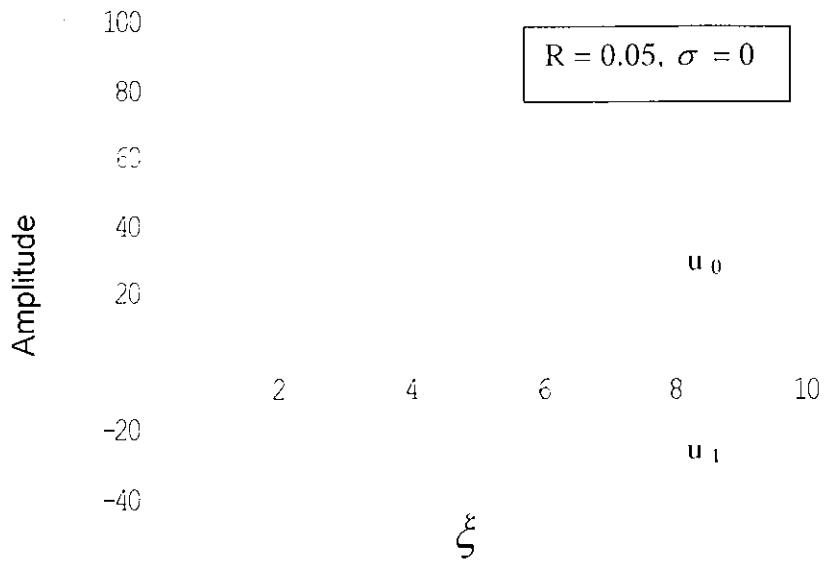

Figure 4.1 Monomer concentration amplitudes u_0 and u_1, R = 0.05, σ = 0. Solid line is the numerical four harmonic predictions, dashed line is the analytic two harmonic predictions.

In the case of the monomer concentration it was observed that the higher the value of R the more similar the predictions of the two and four harmonic models became. For each value of R the same trend was noted as σ increased. From Fig. 4.1 it can be seen that the two harmonic prediction of the final value of u_0 is approximately 10% lower than the four harmonic while for u_1 it is about 25 % higher.

Figure 4.2 below shows the polymer concentration amplitudes n_0 and n_1 when the difference in predictions is greatest, i.e. when R = 0.05 and σ = 0.

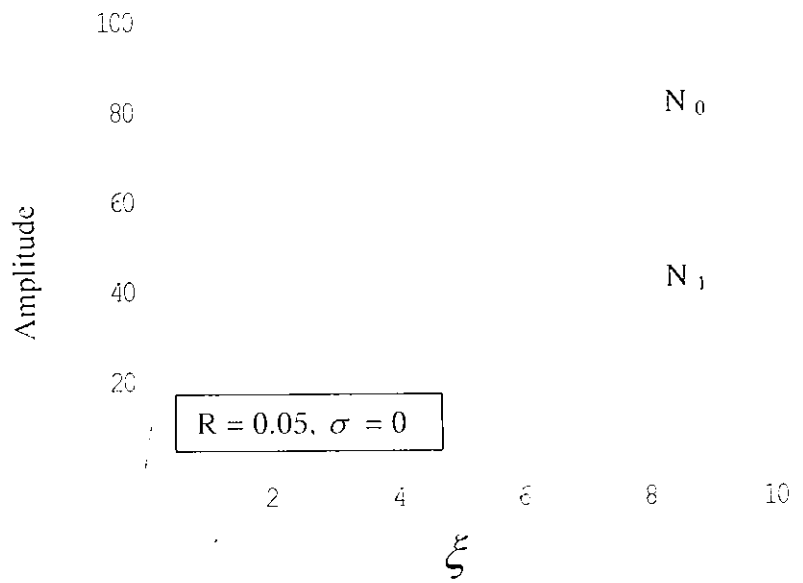

Figure.4.2 Polymer concentration amplitudes N_0 and N_1, with R = 0.05 and σ = 0. The solid line is numerical four harmonic predictions, dashed line is analytic two harmonic predictions.

In the case of polymer concentration profiles the same trend is observable. The higher the value of R (and σ) the closer the predictions match. From Figure 4.2 it can be seen that the predicted values of N_0 differ by about 5% while the maximum difference in the N_1 values is approximately 15%.

These differences in the predicted concentrations give rise to differences in the polymer distribution profiles. The following figure shows the polymer profiles for the four harmonic (Figure 4.3) and two harmonic (Figure 4.4) expansions. In all cases σ = 0 and R takes the value 0.05, 1 and finally 50.

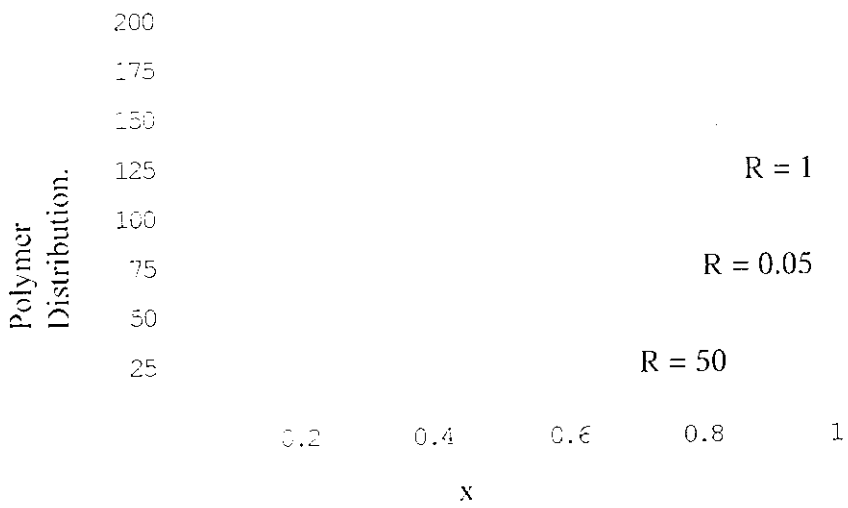

Figure 4.3 *Polymer distribution profiles: Numerical four harmonic model, R = 0.05, 1, 50 and σ =0.*

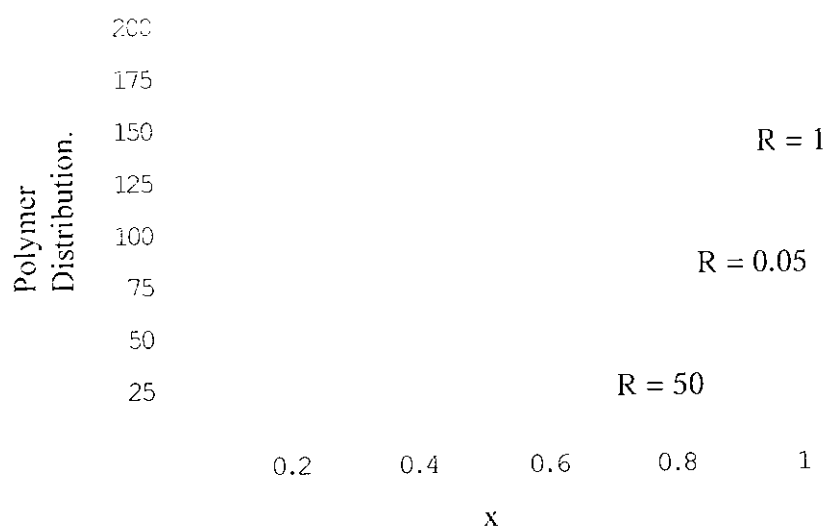

Figure 4.4 *Polymer distribution profiles: Analytic two harmonic model, R = 0.05, 1, 50 and σ =0.*

It can be seen that as expected the existence of non-negligible higher harmonics lead to distortions of the sinusoidal shape in the four harmonic profiles. Because of the approximate nature of the two-harmonic model, this distortion is totally absent from the sinusoidal two harmonic predictions. The two models agree most closely for the case were $R = 50$.

4.4 Experimental Work

The equipment and procedure used for obtaining the data fitted in this section are described in section 3.2.1. The sets of growth curves used were from a set of unslanted transmission gratings with spatial frequencies of 1000, 1250, 2000 and 2250 lines per mm.

The original experimental growth curves show the variation of the on-Bragg diffraction efficiency with time during exposure. The diffraction efficiency data collected, $\eta(t)$, is corrected for Fresnel boundary reflection losses [Born, 80] and converted into refractive index modulation, n_1, using to Kogelnik's two-wave coupled wave theory (Equation 1.9) [Koge, 69]. Time is converted to material exposure energy by multiplying it by the constant recording intensity, which is also corrected for Fresnel losses. The growth curves presented are therefore graphs of corrected refractive index modulation, n_1, as a function of corrected exposure energy, $I_0 \times t$.

Each growth curve consisted of approximately 50 points, the first of which had a zero value of diffraction efficiency. The number of points used in the curve fitting (40) is chosen to ensure that each set of data examined was similar in size and that each growth curve showed the full rise and

levelling-out of the diffraction efficiency. Following capture and conversion of the diffraction efficiency into refractive index modulation, it was found that the difference in refractive index modulation between the zero point and the first non-zero point was approximately $1x10^{-3}$. This could be caused by the low resolution of the LabVIEW program used to capture the data. This step behaviour of the data leads to a lower quality fit at low exposures energies compared to higher energies where this step behaviour is not so significant, see Appendix C for an example. A further difficulty was encountered as even though data capture and exposure of the layer were begun simultaneously, there was a short period of time ($\approx$0.8 seconds) before any diffraction efficiency was recorded. This necessitated further manipulation of the experimental data, which is also discussed in Appendix C.

4.5 Estimation of Material Parameters from Experimental Data.

In this section the parameters for the non-local model will be estimated by fitting experimental growth curves. Such a fit could be achieved by using multivariative least squares techniques [Wolf, 96]. In the case examined here, the variables $S(\sigma,K)$, $R(D, \kappa)$, $\xi(\kappa; I)$ are unknown since σ, the non-local variance, D, the diffusion coefficient and α, which relates the polymerisation to the exposure intensity, are unknown. Furthermore C which relates the amount of polymer to refractive index modulation is also unknown. Given the complexity of using a multivariate technique with four unknowns, such a general numerical approach is not taken here. Instead using the previously derived analytic formulae a simpler, more intuitive manual approach is followed.

4.5.1 Polynomial Fits

The approach which was initially used in this study was to carry out a least squares polynomial fit to the experimental data close to the point $\xi = \kappa It = 0$. Such a n[th] order polynomial fit to the experimental data is of the form

$$a_1^n \xi + a_2^n \xi^2 + a_3^n \xi^3 \ldots\ldots\ldots\ldots + a_n^n \xi^n$$
$$= \left[a_1^n \kappa^1\right](It) + \left[a_2^n \kappa^2\right](It)^2 + \left[a_3^n \kappa^3\right](It)^3 \ldots\ldots\ldots\ldots + \left[a_n^n \kappa^n\right](It)^n \tag{4.17}$$

Starting with the two harmonic analytic solution Equation (4.16) we find the Taylor series approximation to $n_1(\xi)$ expanded Equation (4.15) close to $\xi = 0$ as shown below.

$$100\,C\,S\,V\xi - 50\left[C\,S\,(V+S)\right]\xi^2 + \frac{25}{3}C\,S\left[2S\left(1+R+S\right)+\left(2+S\right)V\right]\xi^3$$
$$+\frac{25}{12}C\,S\left\{-S\left[2+3S+2\left(R+R^2+2RS+S^2\right)\right]-\left[2+S\left(2+R+S\right)\right]V\right\}\xi^4+\ldots$$
$$= a_1^{\infty}\xi + a_2^{\infty}\xi^2 + a_3^{\infty}\xi^3 + a_4^{\infty}\xi^4 + \ldots. \tag{4.18}$$

The Taylor series expansion coefficients (Equation 4.18) are then equated to the values of the coefficients of the corresponding nth order polynomial fit to the experimental data (Equation 4.17). As stated in Section 4.4, the growth curves are grating refractive index modulation (corrected for Fresnel reflections) plotted as a function of $I \times t$, the exposure energy. ξ in

Equation (4.18) can be replaced with $\kappa \times (It)$. Therefore the coefficients of Equation (4.18) become,

$$\left[a_1^n \kappa\right] \cong a_1^{\infty} \kappa = 100 C V \kappa \tag{4.19}$$

$$\left[a_2^n \kappa^2\right] \cong a_2^{\infty} \kappa^2 = -50\left[C S (V + S)\right]\kappa^2 \tag{4.20}$$

$$\left[a_3^n \kappa^3\right] \cong a_3^{\infty} \kappa^3 = \frac{25}{3} C S \left[2S(1 + R + S) + (2 + S)V\right]\kappa^3 \tag{4.21}$$

$$\left[a_4^n \kappa^4\right] \cong a_4^{\infty} \kappa^4 = -\frac{25}{12} C S \left\{-S\left[2 + 3S + 2\left(R + R^2 + 2RS + S^2\right)\right]V\right\}\kappa^4 \tag{4.22}$$

Now it is assumed that the material response is local $\sigma \to 0$, therefore S→1 and also that the visibility, V = 1. From Equation (4.19 and 4.20) it can been seen that

$$\frac{\left[a_2^n \kappa^2\right]}{\left[a_1^n \kappa\right]} \cong \frac{a_2^{\infty} \kappa^2}{a_1^{\infty} \kappa} = -\kappa \tag{4.23}$$

Therefore it is possible to determine a value for κ given the experimentally extracted values of $[a_1^n \kappa]$ and $[a_2^n \kappa^2]$. The second parameter of interest is C, which relates the polymerised material

concentration and the refractive index as shown in Equation (4.13). This can be found from Equation (4.19) given the estimated value of κ from Equation (4.23) and that $V = 1$.

$$C = -\frac{\left[a_2^n \kappa^2\right]}{100\kappa^2} \tag{4.24}$$

The next parameter to be determined is R, the ratio of the rate of diffusion to the rate of polymerisation. A value for R can be found by substituting the values of κ, C and $V=1$ into Equation (4.21).

$$R = -\frac{-3\left[a_3^n \kappa^3\right] + 175\, C\, \kappa^3}{50 C \kappa^3} \tag{4.25}$$

For each spatial frequency growth curve, six different polynomials of increasing order were fitted. From the coefficients of each of these fits, a number of values for R, C and α could be calculated (see Appendix C).. Table 4.1 summarises the average estimated values predicted for R, C and α assuming a local response. The averages were calculated as shown below.

$$\overline{\kappa} = \frac{\kappa^{n=1} + \kappa^{n=2} + \kappa^{n=3} + \kappa^{n=4} + \kappa^{n=5} + \kappa^{n=6}}{6} \tag{4.26}$$

Where $\kappa^{n=m}$ is the value calculated using the m^{th} order polynomial coefficient. Tables listing all the estimated material parameter values for each spatial frequency and for each order polynomial can be found in Appendix C.

Spatial Frequency lines mm^{-1}	$\varkappa$ $m^2/W/s$	C l/mol	R
1000	0.594	1.09E-05	0.424
1250	0.461	9.81E-06	0.218
2000	0.481	7.10E-06	-0.242
2250	0.507	7.52E-06	-0.311
Mean Values	**0.5108**	**8.8235E-06**	**0.0223**

Table 4.1 Estimated values of R, C and $\varkappa$ extracted from experimental data using polynomial fits.

Even though this procedure enabled us to obtain a first estimation of the values of R, C and $\varkappa$ it poses a number of problems. Recall that $R = DK^2/F_0$, and as K^2 is a function of the spatial frequency, the value of R should increase as the spatial frequency increases. On the other hand C and $\varkappa$ are not functions of spatial frequency so should remain constant as the grating period changes. From Table 4.1 it can be seen that this does not appear to be the case. In particular we note the unphysical negative values predicted for R.

Therefore it is obvious that a different approach must be taken. We note that the values for these parameters were estimated by assuming a local response, i.e. $\sigma \to 0$. The next section introduces and examines an alternative experimental curve fitting procedure in which non-local effects are included.

4.5.2 Analytic Curve Fitting Technique

An alternative method of fitting the experimental data was developed in an attempt to overcome the previous problems. Instead of fitting the data with various polynomials, the analytic two harmonic expression for n_1 (Equation 4.15) was used. Initially it was assumed that S =1 (local medium case). Attempts were then made to fit the experimental data by varying R, C and $\varkappa$. All fits were carried out manually and were judged visually as to how well the theoretical predictions were matched to the experimental points. However, it was not found possible to get good results. It was then decided to allow the value of S to vary (non-local medium case).

By varying the values of R and S while keeping C and $\varkappa$ constant good agreement between experimental and theoretical curves could be obtained. The values estimated for $\varkappa$ and C (0.06 $m^2/W/s$ and $2.1x10^{-5}$ l/mol) and assumed fixed for the material used to produce all the sets of experimental data.

The fitted curves are shown below in Figures 4.5 to 4.8. The error bars on the fitted curve correspond to the value of the first non-zero point and represent the limit of resolution of the software used to capture the data, as described in Section 4.4. The theoretical curves were fitted to the full set of forty experimental data points. However for clarity when plotting error bars only ten experimental points are shown instead of forty.

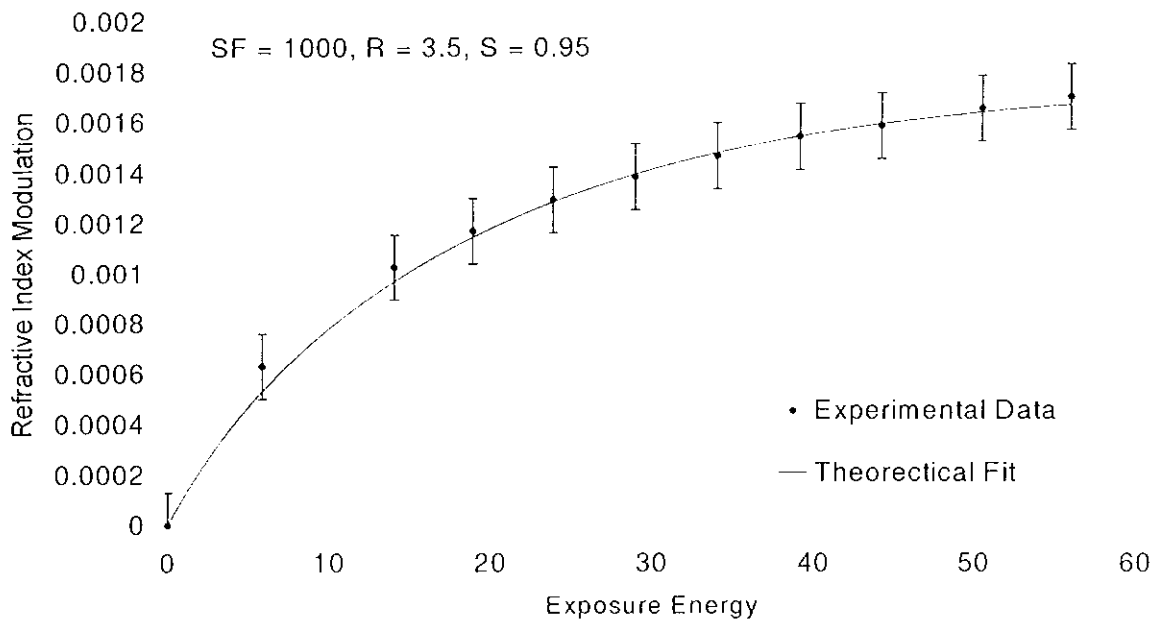

Figure 4.5 *Spatial frequency 1000 lines per millimetre. The solid line is the theoretical fit, the points are experimental data. Error bars* $\approx \pm 10^{-3}$.

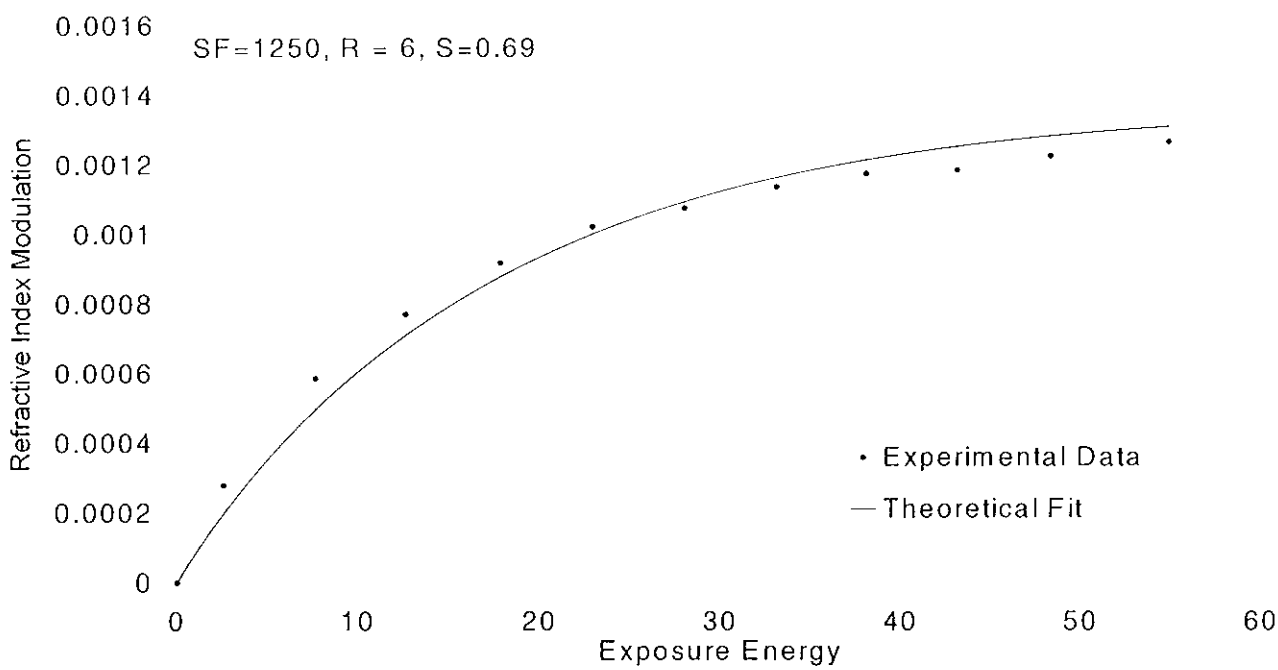

Figure 4.6 *Spatial frequency 1250 lines per millimetre. The solid line is the theoretical fit, the points are experimental data. Error bars* $\approx \pm 10^{-3}$.

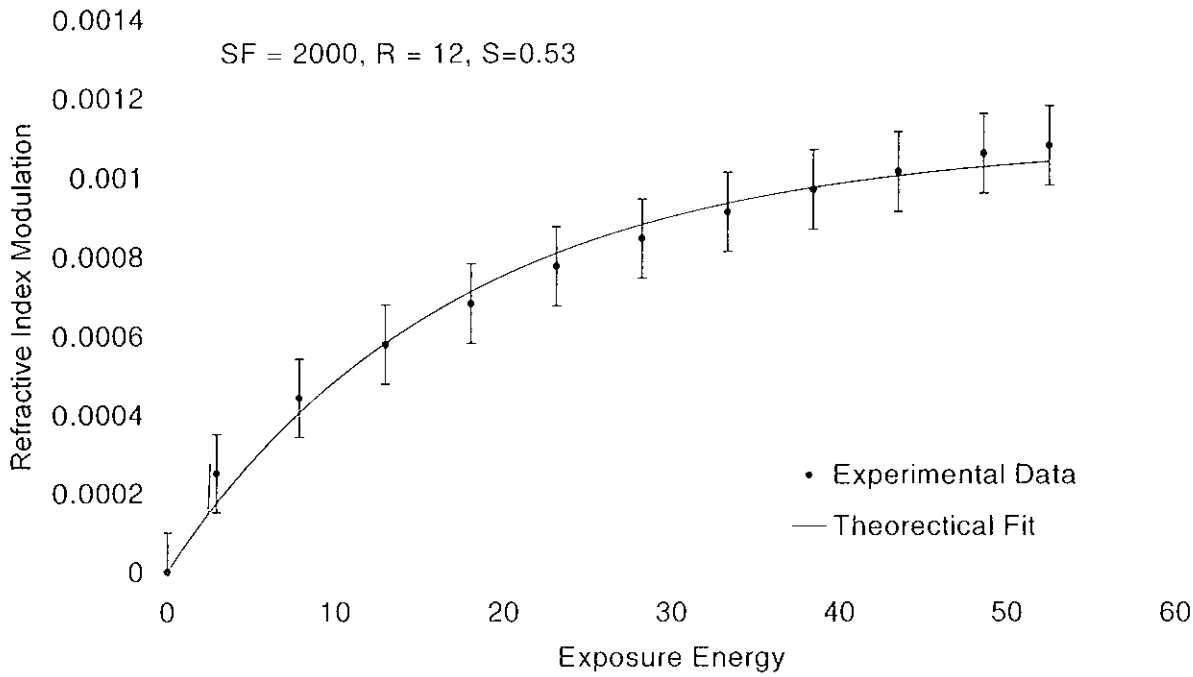

Figure 4.7 *Spatial frequency 2000 lines per millimetre. The solid line is the theoretical fit, the points are experimental data. Error bars* $\approx \pm 10^{-3}$.

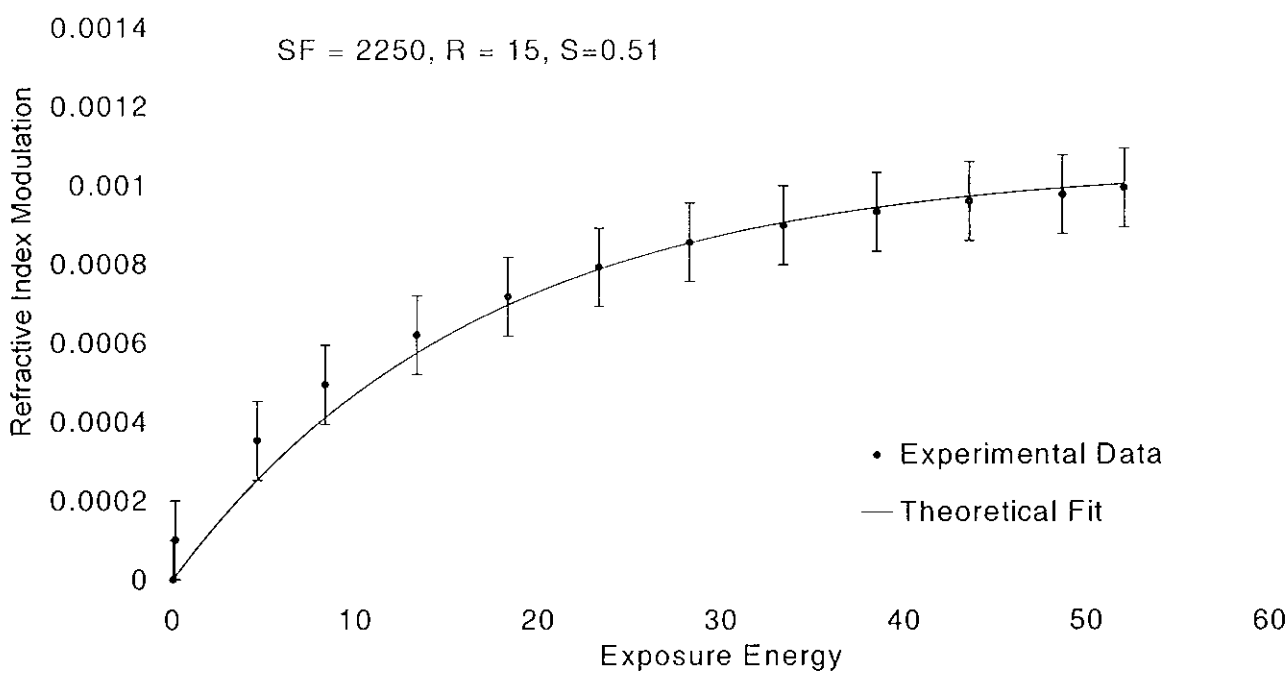

Figure 4.8 *Spatial frequency 2250 lines per millimetre. The solid line is the theoretical fit, the points are experimental data. Error bars* $\approx \pm 10^{-3}$.

Table 4.2 below shows the values of S and R, which gave the best fits using the two harmonic curve fitting procedure. It is noted that the value of R increases as the spatial frequency is increased while the value of C and α are fixed. It can also be seen that S decreases as the spatial frequency increases.

SF Lines mm^{-1}	Λ nm	R	S	$\sqrt{\sigma}$ nm
1000	100	3.5	0.95	51
1250	80	6	0.69	110
2000	50	12	0.53	89.7
2250	44	15	0.51	82.1

Table 4.2 Values of S, R and $\sqrt{\sigma}$ obtained from the two-harmonic curve fitting procedure.

The values of R are within the ranges predicted by Zhao & Mouroulis and Colvin et. al. [Zhao, 94; Colv, 97]. The non-local variance predicts chain lengths of typically between 50 to 110 nm. It is known that the length of a C-C bond is 0.15 nm and the carbon atom is 0.1 nm long. [Solo, 96]. Therefore, the repeat unit in a polyacrylamide chain is typically 0.5 nm long. Given that coiled polymer chains may contain from hundreds to tens of thousands of repeat units [Odia, 70], the lengths predicted by this model seem physically reasonable.

Table 4.3 below outlines the trend in the value of R as the spatial frequency increases. Recall that $R = DK^2/F_0$ where $F_0 = \kappa I_0$ and $K = 2\pi / \Lambda$. It should be noted that D and κ are material constants, I_0 is the illumination intensity and Λ which is equal to inverse spatial frequency, is the grating period. This implies that $R \propto 1/(I_0 \Lambda^2)$. When this relationship is examined for spatial

frequencies of 1000 and 2250 lines/mm, it can be seen that the R value for 2250 lines/mm should be five times the value for R at 1000 lines/mm. As can be seen from Table 4.3, the actual ratio of R at 2250 and R at 1000 lines/mm is 4.286. This shows that the R values predicted by the two-harmonic curve fitting technique follow the $R = DK^2/F_0$ [Zhao, 94].

SF Lines mm^{-1}	Io $mW\ m^{-1}$	$1/(I_0 \times \Lambda^2)$ $mW^{-1}mm^{-1}$	R/R_{1000} Experimental	$\frac{I_0 \times \Lambda_{1000}^2}{I_0 \times \Lambda_{SF}^2}$ Theoretical Prediction
1000	3.825	2.61E+11	1.000	1.00
1250	3.815	4.10E+11	1.714	1.57
2000	3.763	1.06E+12	3.429	4.07
2250	3.733	1.36E+12	4.286	5.19

Table 4.3 Demonstrating the changes in R with increasing spatial frequency.

The two-harmonic curve fitting technique also allows D, the diffusion coefficient, to be calculated. Given that $R = DK^2/F_0$ where $F_0 = \kappa I_0$ and $K = 2\pi / \Lambda$ it can be seen that D can be calculated using Equation (4.27) below.

$$D = \frac{I_0 R \kappa \Lambda^2}{4\pi^2} \tag{4.27}$$

Table 4.4 below shows the values of D, the diffusion coefficient calculated using the values given below and with $\kappa = 2.1 \times 10^{-5}\ m^2/W/s$ as determined by the curve fitting procedure.

SF lines mm^{-1}	Λ mm	R	Io mW	D cm^2/s
1000	$1.0x10^{-06}$	3.5	3.825	$7.12x10^{-14}$
1250	$8.0x10^{-07}$	6	3.815	$7.79x10^{-14}$
2000	$5.0x10^{-07}$	12	3.763	$6.01x10^{-14}$
2250	$4.4x10^{-07}$	15	3.733	$5.88x10^{-14}$
			Mean D=	**$6.70x10^{-14}$**

Table 4.3 Estimated values of D, the diffusion coefficient calculated using Equation 4.27.

Zhao et. al. [Zhao, 94] assumed that by ignoring the effects of α the diffusion coefficient is a constant. As can be seen in Table 4.3, the value of D does not vary significantly. Normally monomer diffusion coefficients range from 10^{-7} to 10^{-9} cm^2/s [Kron, 94]. However, Engin et al. [Engi, 99] has experimentally obtained diffusion coefficients of 10^{-12} cm^2/s with a mixture of an acrylate monomer (TMPTA) and Irgacure 369 as a photo-initaitor. As this system is liquid and contains no binder, the value of D should be higher than that of the acrylamide based photopolymer examined in this study. This is because, unlike the Engin system, the photopolymer contains a polymer matrix through which the monomers must diffuse. Along with this the acrylamide is crosslinked which would cause a further decrease in the diffusion coefficient.

Although the analytic curve fitting technique provides quite encouraging results, serious limitations of the method must be noted. The resolution of the experimental data has already been mentioned in Section (4.4) and Appendix C. It was found that R could be varied by up to 15% and a good fit to experimental data still obtained. The quality of the fit is much more

sensitive to the choice of values of S, which can be varied up to 5% before the quality of the fit deteriorates. This implies that σ can vary by 32.5%. Outside of the ranges of S and R mentioned above the theoretical predictions do not fit the experimental data curves satisfactorily.

We note that the value for κ estimated from the analytic curve fitting technique is approximately ten times smaller than that estimated from the polynomial fits. Recall that the polynomial fits are carried out close to $\xi=0$ while the analytic technique was used to fit the whole growth curve. As $F_0=\kappa I_0$ this would suggest that the rate of polymerisation, F_0, is greater at the start of the exposure than the end. This seems reasonable as at the beginning of the polymerisation there is more monomer available.

4.6 Conclusion

Simple analytic expressions describing grating formation in a diffusion-governed photopolymer have been presented. Their ranges of validity have been examined in comparison with numerical techniques and they have been showed to be of some practical value. The two models agree most closely for the case were R = 50.

It has been shown that the analytic curve fitting technique with $R \propto 1/(I_0 \times \Lambda^2)$ and $\sqrt{\sigma} = 80 \pm 25nm$ provides satisfactory fits to experimental data with estimated values of $\varkappa$=0.06 $m^2/W/s$ and C = 2.1×10^{-5} l/mol. The diffusion coefficient D, was calculated to be approximately 6.5×10^{-14} cm^2/s. However, the fits are not as good at low exposure energies as at higher energies due to the poor resolution of the experimentally captured data.

Recently, Kwon et. al. [Kwon, 99] have pointed out a problem with the Zhao/Colvin analysis. They show that based on the work by Odian [Odia, 70], the change in monomer concentration depends on the square root of intensity. The Zhao/Colvin model is based on the assumption that the change in monomer concentration depends on the intensity and not on it's square root. In Chapter 5 a coupled harmonic method which incorporates both this square root dependence on intensity and the non-local model will be presented.

Chapter 5 Intensity Dependence.

In a recent paper by Kwon et al. [Kwon, 99] an apparent difficulty with the Zhao / Colvin [Zhao, 94: Colv, 97] models was pointed out. Starting with the analysis of Odian [Odia, 70], Kwon assumes the change in monomer concentration depends on the square root of intensity. The Zhao/Colvin model is based on the assumption that the change in monomer concentration depends on the intensity, Equation (2.25), and not it's square root. In this chapter the square root dependence on exposing intensity will be examined and incorporated into the coupled harmonic non-local model. A comparison between the corrected non-local and the uncorrected model will be undertaken.

5.1 Introduction

In this section a review of light induced polymerisation will be carried out. This will demonstrate how the monomer concentration depends on the square root of the intensity. For this analysis the notations used in [Odia, 70] and [Kwon, 99] are followed and are summarised below.

Photopolymerisation is usually initiated in one of two ways. The light can excite a monomer molecule causing it to split into a pair of free radicals, which initiate polymerisation. However in most photopolymer systems a sensitiser Z is used. The sensitiser absorbs light and moves into an excited state, Z*, as shown below.

$$Z + h\nu \rightarrow Z^{*} \tag{5.1}$$

The excited state then transfers its energy to another compound C, which also becomes excited.

$$Z^{*} + C \rightarrow Z + C^{*}$$

(5.2)

Free radicals $R^{\bullet}$, are then formed by the decomposition of the excited state of C.

$$C^{*} \rightarrow 2R^{\bullet}$$

(5.3)

As stated in Chapter 1, the free radical polymerisation mechanism has three stages namely *initiation*, *propagation* and *termination*. Initiation involves the production of free radicals, which bind to a monomer to form the chain-initiation species $M_1^{\bullet}$.

$$R^{\bullet} + M \xrightarrow{k_i} M_1^{\bullet}$$

(5.4)

Where k_i is the initiation rate constant. The radical $M_1^{\bullet}$ then propagates by bonding with other monomer molecules to form a long polymer chain.

$$M_1^{\bullet} + M \xrightarrow{k_p} M_2^{\bullet}$$

$$M_2^{\bullet} + M \xrightarrow{k_p} M_3^{\bullet}$$

And overall

$$M_n^{\bullet} + M \xrightarrow{k_p} M_{n+1}^{\bullet}$$

(5.5)

Where k_p is the propagation rate constant. The growth of the polymer chain is stopped by termination. Termination occurs when the radical attached to the end of the growing polymer chain bonds with a free radical. This reaction produces a 'dead polymer', i.e. a chain with no radical attached to one end, and which is therefore incapable of growing further.

$$M_n^{\bullet} + M_m^{\bullet} \xrightarrow{k_t} dead\ polymer \tag{5.6}$$

Where k_t is the termination rate constant. Normally the rate of termination is higher than the rate of propagation. However the concentration of free radicals is much lower than the concentration of monomer so the polymer chain can grow for some time before it is terminated.

The rate of disappearance of monomer can be given by

$$-\frac{\partial c}{\partial t} = R_i + R_p \tag{5.7}$$

Where c is the monomer concentration, R_i is the initiation rate and R_p is the rate of propagation. It should be noted that the rate of disappearance of monomer is the same as the rate of polymerisation. Due to the large number of monomers compared to free radicals it can be assumed that $R_p >> R_i$ [Odia, 70]. Therefore Equation (5.7) can be written as

$$-\frac{\partial c}{\partial t} = R_p \tag{5.8}$$

The rate of polymerisation can be given by

$$R_p = k_p c c_r \tag{5.9}$$

Where c_r is the total concentration of chain radicals. It should be noted that the chain radical concentration is much lower than the monomer concentration [Odia, 70]. The radical concentration rises exponentially at first, reaching a steady state which is maintained during the polymerisation. This steady state implies that the rate of initiation R_i and the rate of termination R_t are equal giving

$$R_p = 2k_t C_r^2 \tag{5.10}$$

The expression obtained for c_r in Equation (5.10) is now substituted into Equation (5.9) to give the rate of polymerisation

$$R_p = k_p C \left(R_i / 2k_t\right)^{1/2} \propto R_i^{1/2} \tag{5.11}$$

From the above equation it can be seen that the rate of propagation is proportional to the square root of the initiation rate. The initiation rate can be given by

$$R_i = 2\Phi I_a \tag{5.12}$$

Where Φ is the quantum yield of radical production, which can be defined as the number of pairs of radicals formed per quantum of light absorbed [Kwon, 99]. I_a is the intensity of light

absorbed in moles of light quanta per litre per second. $I(x)$ is the spatially modulated illumination. Therefore I_a can be given as

$$I_a(x)=I(x)\left[1-\exp\left(-\varepsilon Z d\right)\right]=I(x)\ (1-T)$$

(5.13)

Where ε is the molar absorptivity, Z is the concentration of the photosensitisers, d is the photopolymer thickness and T is the transmittance of the layer.

When the initiation step is started by the photosensitisers, the concentration of the radicals can be given by

$$C_r=\left[\frac{\Phi I(x)\ (1-T)}{k_t}\right]^{1/2}$$

(5.14)

and the polymerisation rate, Equation (5.9), is given by

$$R_p=k_p C\left[\frac{\Phi I(x)\ (1-T)}{k_t}\right]^{1/2}$$

(5.15)

Combining Equations (5.8) and (5.15) the rate of disappearance of monomer is therefore

$$-\frac{\partial C}{\partial t}=k_p C\left[\frac{\Phi I(x)\ (1-T)}{k_t}\right]^{1/2}$$

(5.16)

As previously discussed, the intensity distribution produced by the interference of the two recording beams can be written as

$$I(x) = I_0\left[1 + V\cos(Kx)\right] \tag{5.17}$$

Where V is the visibility and K is the grating vector magnitude $2\pi/\Lambda$. As stated previously, monomers diffuse from dark regions to bright regions as the monomer concentration is modulated by the illumination. The diffusion equation can be combined with Equation (5.16) to give the monomer concentration.

$$-\frac{\partial c}{\partial t} = D\frac{\partial^2 c}{\partial x^2} + Q\sqrt{1 + V\cos(Kx)}\,c \tag{5.18}$$

Where

$$Q = k_p\left[\frac{\Phi I_0\,(1-T)}{k_t}\right]^{1/2} \tag{5.19}$$

From Equation (5.18), it can be seen why Kwon et al. [Kwon, 99] predicted the square root dependence of monomer concentration. We can see that Q is analogous to F_0 in the Zhao/Colvin model. The parameters κ in Chapter 4 and $k_p\sqrt{[\Phi(1-T)]/k_t}$ are also analogous but have different units. This square root dependence will be incorporated into the non-local model in the next section.

5.2 Non-local Kwon Model

Recall from Chapter 2 that the one-dimensional diffusion equation assuming non-local response was written

$$\frac{\partial u(x,t)}{\partial t} = \frac{\partial}{\partial x}\left[D(x,t)\frac{\partial u(x,t)}{\partial x}\right] - \int_{-\infty}^{+\infty} R(x,x')F(x',t)u(x',t)dx' \tag{5.20}$$

Where

$$u(x',t') = \sum_{i=0}^{M-3} u_i(t)\cos(iKx') \tag{5.21}$$

$$R(x-x') = \frac{e^{-(x-x')^2/2\sigma}}{\sqrt{2\pi\sigma}} \tag{5.22}$$

$$F(x',t) = F_0[1 + V\cos(Kx')] \tag{5.23}$$

Now Equation (5.23) must be adjusted to take account of the square root dependence on intensity therefore instead of Equation (5.23), we write that

$$F(x',t) = F_0\sqrt{1 + V\cos(Kx')} \tag{5.24}$$

Where based on our definition of Q in Equation (5.19) we now define that $F_0 = \kappa I_0^{1/2}$. Figure 5.1 below illustrates the two different rates of polymerisation proportional to $1+V\cos(Kx')$ (solid line) and $\sqrt{1+V\cos(Kx')}$ (dashed line).

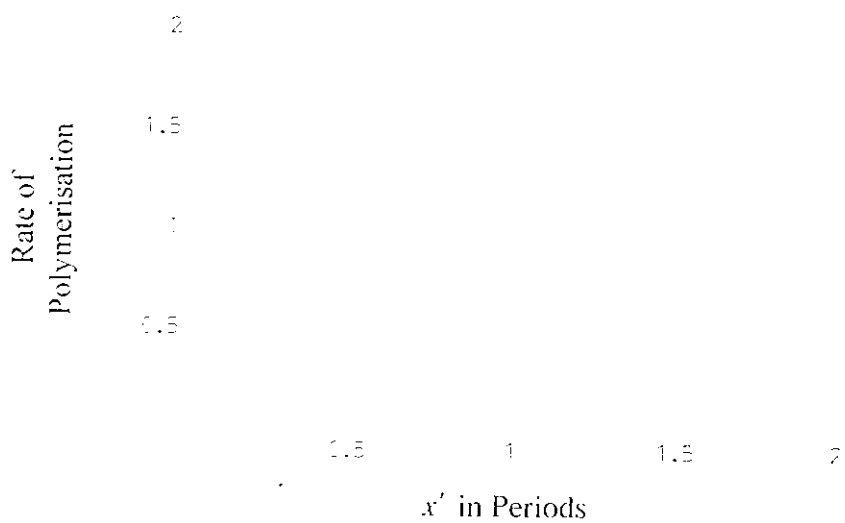

Figure 5.1 *Intensity dependence of the rate of polymerisation. Solid line is* $1+\cos(Kx')$. *Dashed line is* $\sqrt{1+\cos(Kx')}$.

However a general formula for *F(x,t)* can be derived for any intensity distribution which can be represented as a Fourier series.

$$F(x',t)=F_0\sum f_i\cos(iKx') \tag{5.25}$$

Equations (5.21), (5.22) and (5.25) are now substituted into Equation (5.20) to give

$$\frac{\partial u(x,t)}{\partial t}=\frac{\partial}{\partial x}\left[D(x,t)\frac{\partial u(x,t)}{\partial x}\right]-\int_{-\infty}^{+\infty}\frac{\exp[-(x-x')/2\sigma]}{\sqrt{2\pi\sigma}}\times F_0\sum f_i\cos(iKx')\times\sum_{i=0}u_i\cos(iKx')\,dx' \tag{5.26}$$

In the case where the intensity is of the square root form predicted by Kwon et al. [Kwon, 99], Equation (5.26) becomes

$$\frac{\partial u(x,t)}{\partial t} = \frac{\partial}{\partial x}\left[D(x,t)\frac{\partial u(x,t)}{\partial x}\right] - \int_{-\infty}^{\infty} \frac{\exp\left[-(x-x')/2\sigma\right]}{\sqrt{2\pi\sigma}} \times F_0 \sqrt{1+V\cos(iKx')} \times \sum_{i=0} u_i \cos(iKx')\, dx' \tag{5.27}$$

In this next section this equation will be solved following the procedures of Chapter 4 to give analytic expressions for monomer and polymer concentration. The full set of calculations can be found in Appendix E.

5.3 Analytic Formulae with Adjusted Intensity Dependence

Equation (5.26) is now solved following the method used in Chapter 4 to give the first two harmonics of monomer concentration u_0 and u_1

$$\frac{du_0(\xi)}{d\xi} = -f_0 u_0(\xi) + f_1 u_1(\xi)/2 \tag{5.24}$$

$$\frac{du_1(\xi)}{d\xi} = -S f_1 u_0(\xi) - \left[S(f_0 + f_2/2) + R\right] u_1(\xi) \tag{5.25}$$

When V=1, the first three coefficients for the expansion of the square root are: $f_0 = 2\sqrt{2}/\pi$ and $f_1 = 4\sqrt{2}/(3\pi)$ and $f_2 = -4\sqrt{2}/(15\pi)$.

The first order coupled differential equations (5.24) and (5.25) are solved with $u_0(0)$=100 and $u_1(0)$=0, to give

$$u_0(\xi) = \frac{100\exp\left[(B+W)\xi/4\right]}{B}\left\{B\cosh\left[B\xi/4\right]+\left(2R+2f_0(S-1)+f_2S\right)\sinh\left[B\xi/4\right]\right\}$$

(5.26)

And

$$u_1(\xi) = \frac{200 f_1 S}{B}\left\{\exp\left[-(B+f_2S+W)\xi/4\right]-\exp\left[-(B+W)\xi/4\right]\right\}$$

(5.27)

Where, for brevity, we introduce the dimensionless parameters $W = 2f_0 + 2R + 2f_0S + f_2S$ and $B = \sqrt{(2f_0 + 2R + 2f_0S + f_2S)^2 - 8(2f_0R + 2f_0^2S - f_1^2S + f_0f_2S)}$.

Following Chapter 2 the resulting concentration of polymerised monomer, after an exposure of duration t seconds, is given by Equation (5.28).

$$N(x,t) = \int_0^t \int_{-\infty}^{\infty} \mathrm{R}(x-x')F(x',t')u(x',t')dx'dt'$$

(5.28)

Giving the following polymerisation concentration spatial harmonic components:

$$N_0(\xi) = \int_0^{\xi} \left[u_0(\xi') + (V/2)u_1(\xi')\right]d\xi'$$

(5.29)

$$N_1(\xi) = S\int_0^{\xi} \left[V u_0(\xi') + u_1(\xi')\right]d\xi'$$

(5.30)

Substituting for u_0 and u_1 gives that

$$N_0(\xi)=\frac{200}{B}\left\{\frac{(A+B)\exp[(B-W)\xi/4]}{B-W}+\frac{A+B}{W-B}+\frac{B-A}{W+B}+\frac{(A-B)\exp[-(B+W)\xi/4]}{B+W}\right\}$$

(5.31)

And

$$N_1(\xi)=\frac{200S}{B(B-W)(B+W)}\left\{-2B(L+VW)+\exp[-(B+W)\xi/4]\right.$$

$$\left.\times[(L-BV)(B-W)+\exp[B\xi/2](L+BV)(B+W)]\right\}$$

(5.32)

Where in these equations, we introduce the dimensionless parameters $A=-2f_0+2R+2f_0S+f_2S-2f_1SV$ and $L=-4f_1S-2f_0V+2RV+2f_0SV+f_2SV$.

It should be noted that if the intensity is assumed to be sinusoidal, as in Chapter 2 and 4, the parameters $f_0=1$, $f_1=V$ and $f_2=0$. In this case u_0, u_1, N_0, N_1, B and W reduce to the forms given in Chapter 4.

It is now assumed that the modulation of the refractive index induced during recording is linearly related to the polymer concentration.

$$n_m(\xi)=C\times N_m(\xi)$$

(5.33)

Substituting for N_0 and N_1, Equations (5.31) and (5.32) into Equation (5.33) gives that

$$n_0(\xi)=\frac{200C}{B}\left\{\frac{(A+B)\exp[(B-W)\xi/4]}{B-W}+\frac{A+B}{W-B}+\frac{B-A}{W+B}+\frac{(A-B)\exp[-(B+W)\xi/4]}{B+W}\right\}$$

(5.34)

And

$$n_1(\xi)=\frac{200SC}{B(B-W)(B+W)}\left\{-2B(L+VW)+\exp[-(B+W)\xi/4]\right.$$

$$\left.\times[(L-BV)(B-W)+\exp[B\xi/2](L+BV)(B+W)]\right\}$$

(5.35)

To calculate the refractive index modulation of a grating recorded in the material, Equations (5.34) and (5.35) are substituted into Equation (5.36) shown below

$$n(x,\xi)=n_0(\xi)+n_1(\xi)\cos(Kx)$$

(5.36)

5.4 Comparison of the Non-local Kwon and the Non-local Zhao Models.

In this section a comparison of the non-local Kwon model derived above will be made with the analytic non-local Zhao model derived in Chapter 4. This is achieved by examining (i) monomer, (ii) polymer concentration amplitudes and (iii) the resulting grating profiles for various values of R and σ. Essentially we wish to plot $u_i^{Zhao}\left(R=DK^2/\kappa I_0;\xi=\kappa I_0 t\right)$ against $u_i^{Kwon}\left(R'=DK^2/\kappa' I_0^{1/2};\xi'=\kappa' I_0^{1/2}t\right)$. To do this we assume that $R'=R$, i.e. that $\kappa I_0=\kappa' I_0^{1/2}$. In this case $\xi=\xi'$. Once again the values of R chosen were 0.05, 5 and 50 while the normalised values of σ used were 0, 1/64 and1/32. These correspond with the values used previously in Chapter 2 and 4. We note that for convenience we will ot use the primed notation further in this Chapter.

Figure 5.2 below, shows the differences in the values of the zeroth harmonic (u_0) and first harmonic (u_1) of monomer concentration predicted by the analytic Non-local Kwon model (dashed line) and the analytic Non-local Zhao model (solid line). Figure 5.2 (a) shows the largest difference between the predictions while (b) shows the predictions when they most closely match for the values of R and σ given above.

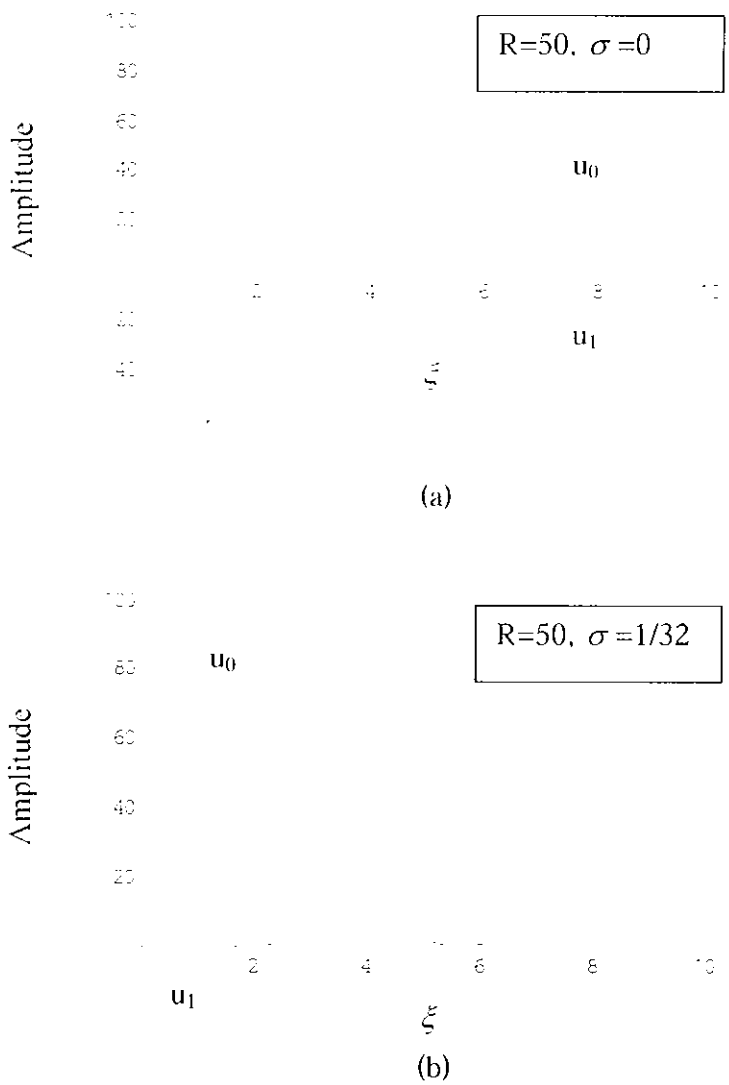

Figure 5.2 Zeroth harmonic (u_0) and first harmonic (u_1) of monomer concentration predicted by the adjusted two-harmonic model (dashed line) and the standard two-harmonic model (solid line). (a) Largest difference between the predictions when R=0.05 and σ=0. (b) shows the predictions when they most closely match R=50 and σ=1/32.

It was found that as R and σ increased the two predictions became more closely matched. The values of u_0 and u_1 also followed the same general trends as were observed in Chapter 2. As σ increased, the monomer concentration falls off more rapidly and the amplitude of the higher harmonics is reduced.

Figure 5.3 below shows an example of the differences in the zeroth, (N_0) and first (N_1) harmonic of polymer concentration as predicted by the anayltic Non-local Zhao model (solid line) and the Non-local Kwon model (dashed line).

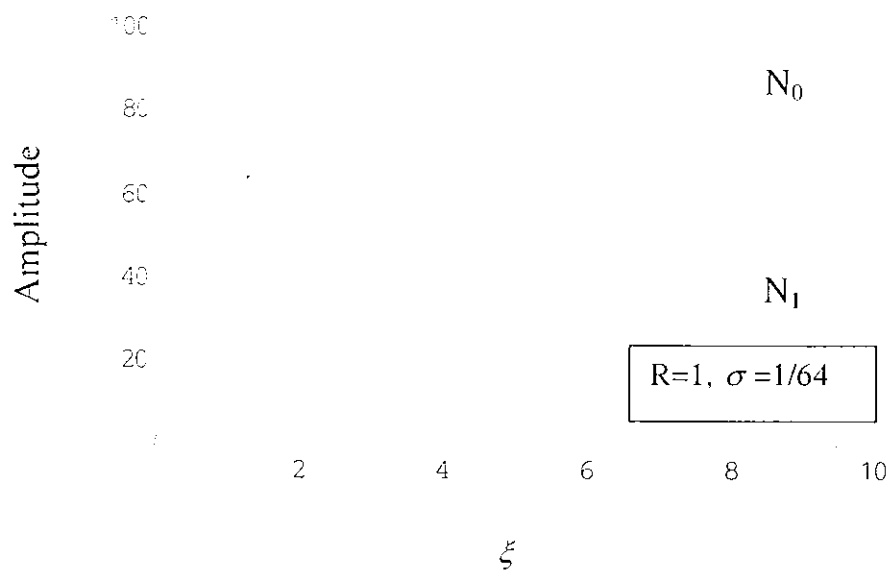

Figure 5.3 Differences in the zeroth and first harmonic of polymer concentration as predicted by the standard two-harmonic model (solid line)and the adjusted two-harmonic model (dashed line).

In Table 5.1, the percentage differences between N_0 as predicted by the Non-local Kwon model and N_0 as predicted by the analytic Non-local Zhao model are given. The percentage differences are calculated by the formula below.

$$\Delta N_0\,\% = \frac{N_0(Kwon) - N_0(Zhao)}{N_0(Zhao)} \times 100 \tag{5.37}$$

All values of N_0 are taken at $\xi = 10$.

	σ =0	σ =l/64	σ =l/32
R=0.05	-3.2	-2.3	-1.2
R=1	4.4	5.6	6.7
R=50	10.8	10.9	10.9

Table 5.1 The percentage difference between N_0 as predicted by the non-local Kwon model and N_0 as predicted by the analytic non-local Zhao model at $x=1$

From Table 5.1 it can be clearly seen that as the value of R increases the difference between the two models becomes greater.

Table 5.2 below shows the percentage difference between N_1 as predicted by the non-local Kwon model and N_1 as predicted by the analytic non-local Zhao model. Again, the difference is calculated using Equation (5.37).

	σ =0	σ =l/64	σ =l/32
R=0.05	36.3	25.0	16.9
R=1	17.4	11.6	7.8
R=50	11.2	8.2	6.0

Table 5.2 The percentage difference between N_1 as predicted by the non-local Kwon model and N_1 as predicted by the analytic non-local Zhao model at $x=1$.

From the table, it can be seen that the higher the value of R and the higher the value of σ, the closer the predictions match.

Following on from the monomer and polymer harmonic amplitudes, the polymer concentration profiles are examined for V=1 and ξ=10. To fully illustrate the effect of the new Kwon intensity dependence, a four-harmonic model incorporating the new intensity dependence, is compared with the standard four-harmonic model derived in Chapter 2. This is done to examine the effects on the higher harmonics, which are neglected by the two-harmonic analytic approach that had been up to this point.

Figure 5.4 shows (a) the largest and (b) smallest differences between the polymer concentration profiles predicted by the four harmonic non-local Kwon model (dashed line) and the four-harmonic non-local Zhao model (solid line) from Chapter 2.

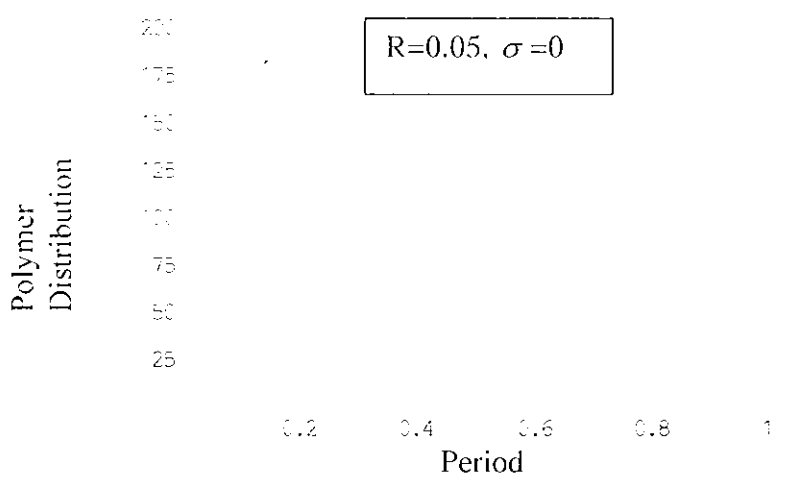

(a)

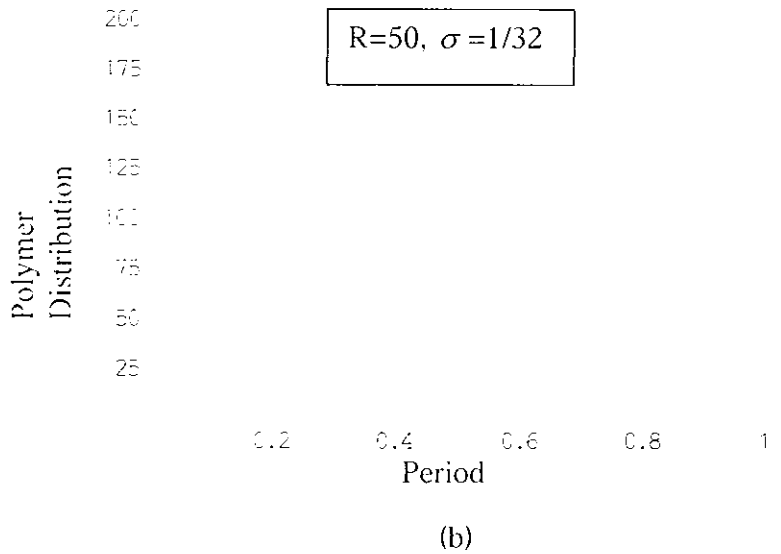

(b)

Figure 5.4 (a) Largest differences in predictions, R=0.05 and σ =0. (b) Smallest difference in predictions: R=50 and σ =1/32. Solid line is four harmonic non-local Zhao and dashed line is four-harmonic non-local Kwon model

It can been seen from Figure 5.4, that the adjusted model follows the same overall trend as the four-harmonic non-local Zhao model presented in Chapter 2. As R increases, the profiles become more sinusoidal in shape. Increasing σ smoothes the profile and its visibility decreases. For all values of R and σ the visibility of the adjusted model profiles is always greater than that of the standard four-harmonic model profiles. The difference decreases as R and σ increase. This is shown in Table 5.3 below where the percentage differences at a single point along the profile, $x/\Lambda = 1$, are calculated using Equation (5.37).

	σ =0	σ =1/64	σ =1/32
R=0.05	73.82	32.39	17.82
R=1	28.44	15.07	11.15
R=50	11.40	11.11	11.04

Table 5.3 Percentage difference between the polymer concentration as predicted by the four-harmonic non-local Kwon model and the four-harmonic non-local Zhao model. Values calculated at $x/\Lambda = 1$.

From the table it can be seen that the predictions match closest when R = 50 and σ = 1/32.

5.5 Application to Experimental Data.

In this section the parameters for the non-local model will be estimated by fitting experimental growth curves using the techniques as shown in Chapter 4. The curve fits will be carried out using the intensity dependence adjusted analytic equations derived in section (5.3).

5.5.1 Polynomial Fits.

We now follow the form of presentation used in section (4.5.1). Least squares polynomial fit to the experimental data close to the point $\xi = \kappa I^{1/2} t = 0$ is used for this purpose. Such a fit to the experimental data is of the form

$$a_1^n \xi + a_2^n \xi^2 + a_3^n \xi^3 ..... + a_n^n \xi^n \tag{5.38}$$

Starting with the two harmonic analytic solution Equation (5.32) we find the Taylor series approximation to $n_1(\xi)$ close to $\xi = 0$ shown below in Equation (5.35).

$$\begin{aligned} 100\,C\,S\,V\xi - 50\left[CS\,(f_1 S + f_0 V)\right]\xi^2 + \frac{25}{3} C\,S\left[2 f_0 f_1 S(S+1) + 2 f_0^2 V + f_1 S(2R + f_2 + f_1 V)\right]\xi^3 \\ + \frac{25}{24} C\,S\left\{-4 f_0^2 f_1 S\left(1 + S + S^2\right) - 4 f_0^3 V + 2 f_0 f_1 S\left[-(1+2S)(2R + f_2 S) - f_1(2+S)V\right]\right. \\ \left. - f_1 S\left[2 f_1^2 S + (2R + f_2 S)(2R + f_2 S + f_1 V)\right]\right\}\xi^4 + ... \\ = a_1^{\infty}\xi + a_2^{\infty}\xi^2 + a_3^{\infty}\xi^3 + a_4^{\infty}\xi^4 + ... \end{aligned} \tag{5.39}$$

The theoretical n^{th} order expansion coefficients are then equated to the values of the coefficients of the corresponding nth order polynomial fit to the experimental data. As stated earlier, the growth curves are corrected refractive index modulation plotted as a function of $I \times t$, the exposure energy. As $\xi = \kappa I t$ we can replace ξ in Equation (5.39) with κ. Therefore the coefficients of Equation (5.39) become,

$$\left[a_1^n \kappa\right] \times I_0^{1/2} \cong a_1 \kappa = 100 C S V \kappa \tag{5.40}$$

$$\left[a_2^n \kappa^2\right] \times I_0^{1/2} \cong a_2 \kappa^2 = -50\left[C S\left(f_1 S + f_0 V\right)\right]\kappa^2 \tag{5.41}$$

$$\left[a_3^n \kappa^3\right] \times I_0^{1/2} \cong a_3 \kappa^3 = \frac{25}{3} C S\left[2 f_0 f_1 S(S+1) + 2 f_0^2 V + f_1 S(2R + f_2 + f_1 V)\right]\xi^3 \tag{5.42}$$

$$\left[a_4^n \kappa^4\right] \times I_0^{1/2} \cong a_4 \kappa^4 = \frac{25}{24} C S\{-4 f_0^2 f_1 S(1+S+S^2) - 4 f_0^3 V + 2 f_0 f_1 S[-(1+2S)(2R+f_2 S) - f_1(2+S)V] - f_1 S[2 f_1^2 S + (2R+f_2 S)(2R+f_2 S+f_1 V)]\}\kappa^4 \tag{5.43}$$

If it is assumed that the material response is local $\sigma \to 0$, i.e. S→1, and that V=1, then from Equation (5.40) κ can be found.

$$\kappa = -\frac{3\pi\left[a_2^n \kappa^2\right] \times I_0^{1/2}}{5\sqrt{2}} \tag{5.44}$$

Therefore it is possible to determine a value for $\varkappa$ given experimentally extracted values of $[a_1^n \varkappa]$ and $[a_2^n \varkappa^2]$. The second parameter of interest is C, which relates the polymerised material concentration and the refractive index as shown in Equation (5.30). This can be found from Equation (5.41) as $\varkappa$ and the visibility V=1, are already known.

$$C = -\frac{3\left[a_2^n \kappa^{-2}\right] \times I_0^{2/2} \pi}{500\sqrt{2}\kappa^{-2}}$$

(5.45)

The next parameter to be determined is R, the ratio of the rate of diffusion to the rate of polymerisation. A value for R can be found by substituting the values of $\varkappa$, C and V=1 into Equation (5.42).

$$R = \frac{27\left[a_n^3 \kappa^{-3}\right] I_0^{3/2} \pi^2 - 9040 C \kappa^{-3}}{600\sqrt{2}\pi\kappa^{-3}}$$

(5.46)

Table 5.4 summarises the average estimated values predicted for R, C and $\varkappa$. Tables listing all the estimated material parameter values for each spatial frequency and for each order polynomial can be found in Appendix C.

Spatial Frequency lines mm^{-1}	κ m/W$^{1/2}$/s	C l/mol	R
1000	3.028	2.13E-06	-1.510
1250	2.345	1.93E-06	-1.810
2000	2.414	1.42E-06	-1.835
2250	2.522	1.51E-06	-1.843
Mean Value	**2.577**	**1.75E-06**	**-1.750**

Table 5.4 Estimated values of R, C and $\varkappa$ extracted from experimental data using polynomial fits with intensity adjusted formulae.

There was a large variation in the calculated parameters, the averages of which are shown above in Table 5.4. The values of κ were larger by an order of magnitude than those obtained using the unadjusted analytic equations. C values were also smaller by about 25%. The R values were lower for the non-local Kwon model with an average R of 0.0223 for the Zhao model and –1.75 for the Kwon model. Once again we note the unphysical negative values of R.

It can be seen that the parameters do not follow the expected trends as outlined in Chapter 4. As $R = D_0K^2/ F_0$, and as K^2 is a function of the spatial frequency, the value of R should increase as the spatial frequency increases. On the other hand C and κ are not functions of spatial frequency so should remain constant as the grating period changes. From Table 5.4 it can be seen that this does not appear to be the case. In the next section, the analytic curve fitting technique used in Chapter 4 will be applied using the intensity dependence adjusted analytic formulae.

5.5.2 Analytic Curve Fitting Technique.

To fit the growth curves, the adjusted analytic two harmonic Kwon expression for n_1 (Equation 5.32) was used. By varying the values of R and S while keeping C and κ constant good agreement between experimental and theoretical curves could be obtained. The values chosen for κ (0.035 $m^2/W/s$) and C (1.9×10^{-5} l/mol). The error bars and number of points used and displayed are the same as for Figures 4.5 to 4.8. The fitted curves are shown below in Figures 5.5 to 5.8.

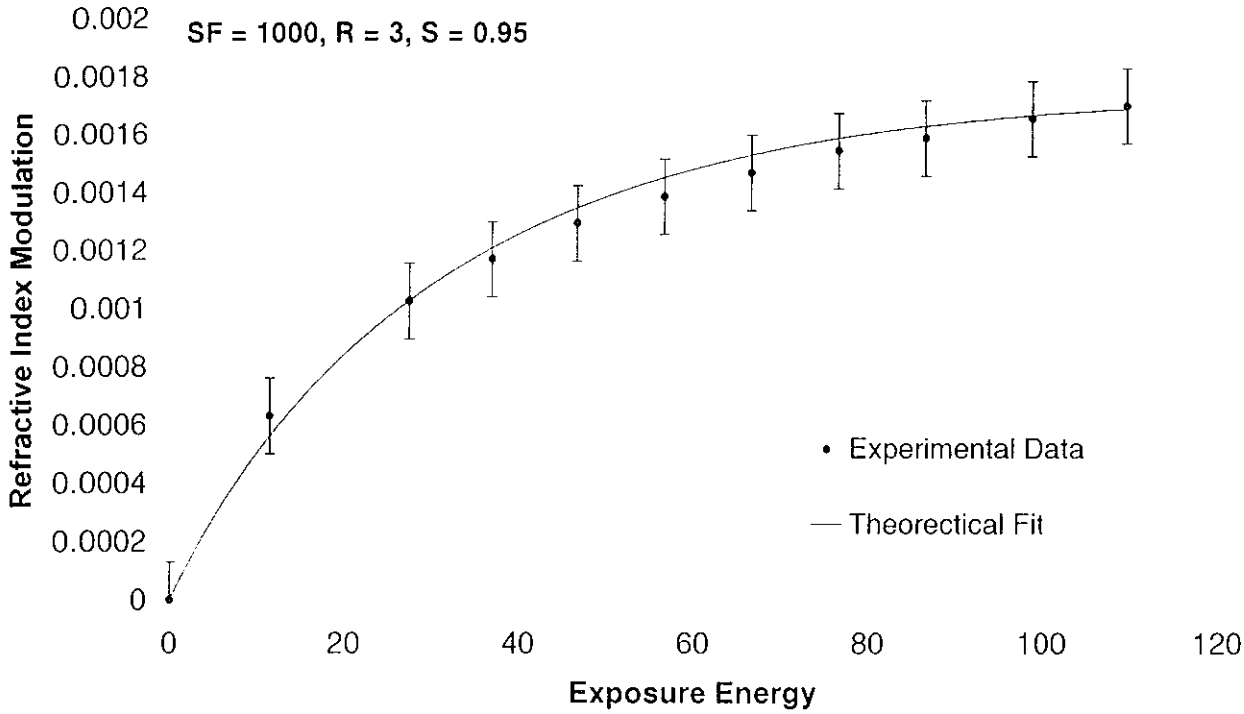

Figure 5.5 *Spatial frequency 1000 lines per millimetre. Solid line is theoretical fit, points are experimental data. Error bars* $\approx \pm 10^{-3}$.

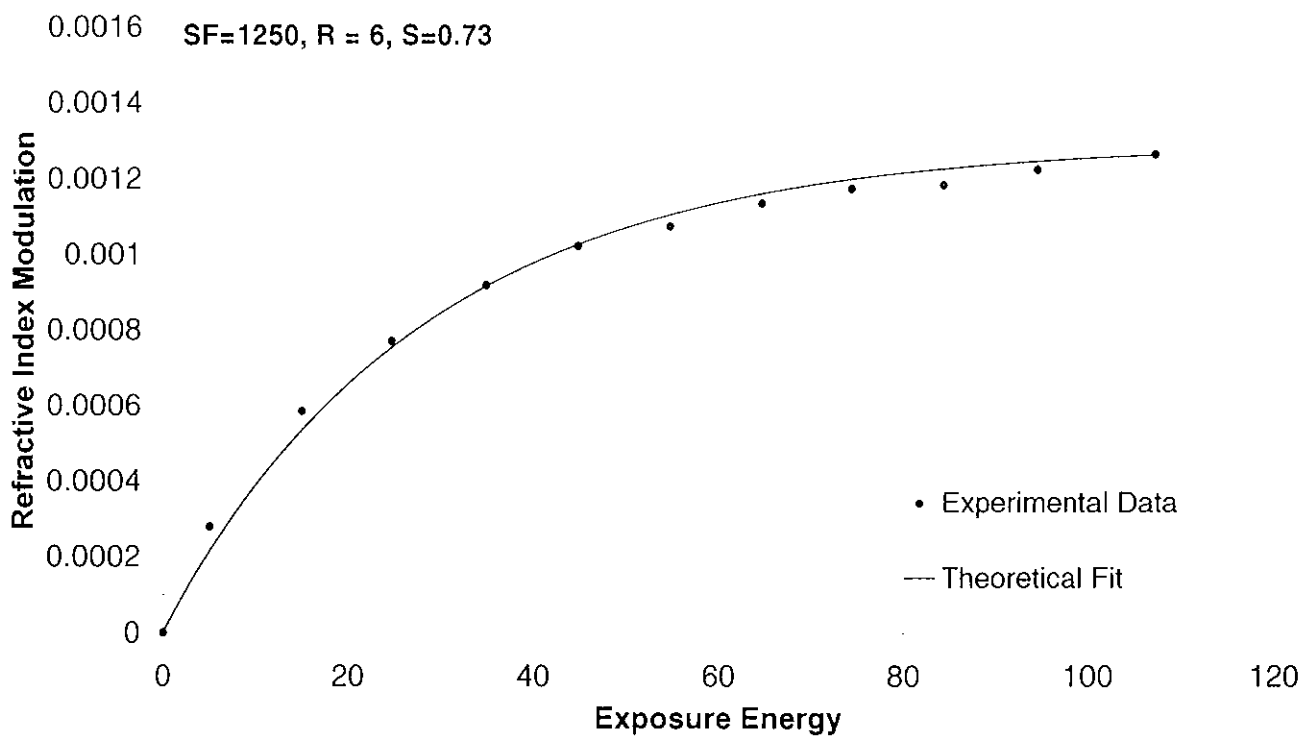

Figure 5.6 *Spatial frequency 1250 lines per millimetre. Solid line is theoretical fit, points are experimental data. Error bars* $\approx \pm 10^{-3}$.

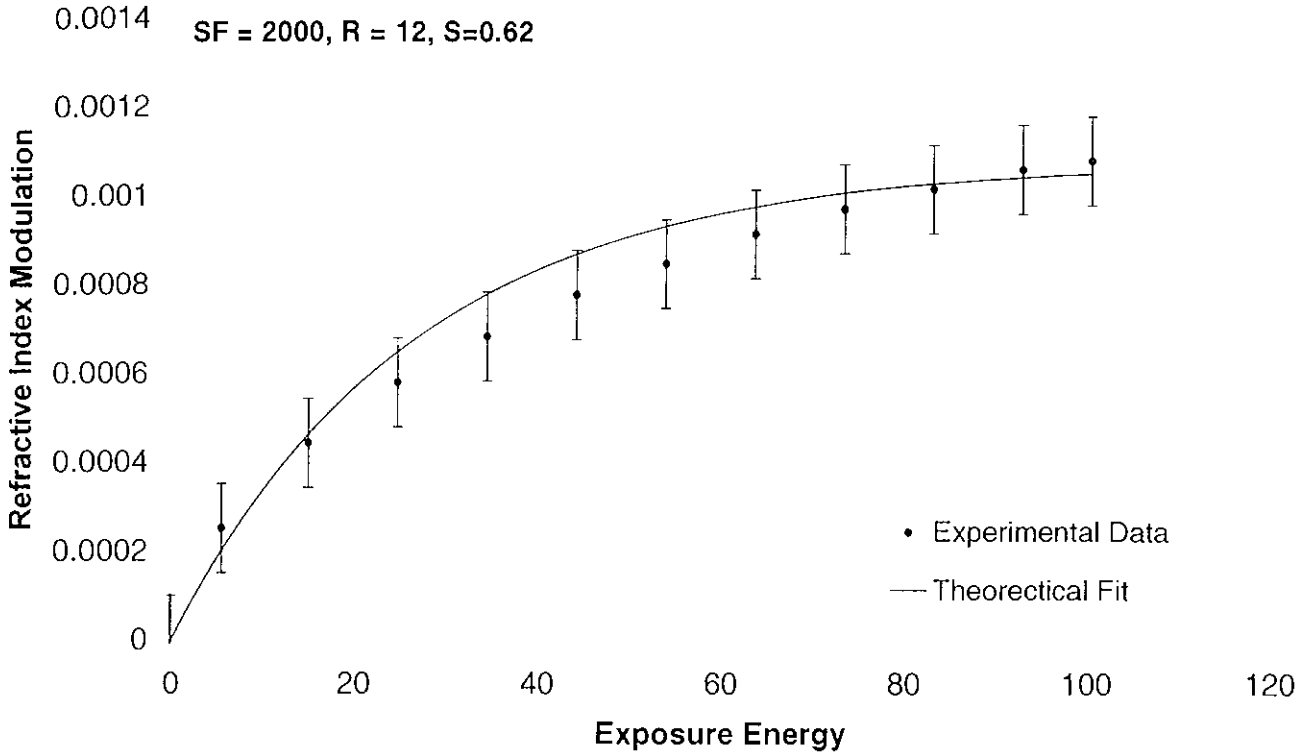

Figure 5.7 *Spatial frequency 2000 lines per millimetre. Solid line is theoretical fit, points are experimental data. Error bars* $\approx \pm 10^{-3}$.

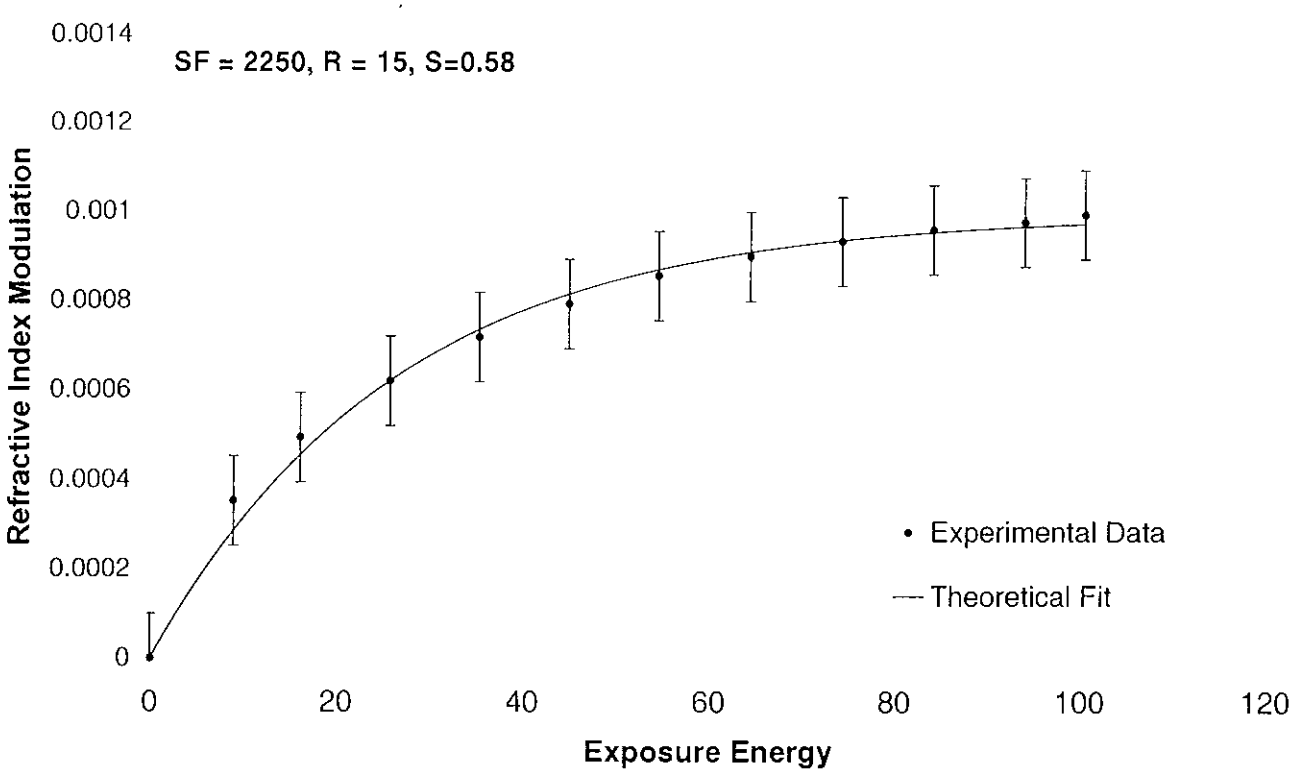

Figure 5.8 *Spatial frequency 2250 lines per millimetre. Solid line is theoretical fit, points are experimental data. Error bars* $\approx \pm 10^{-3}$.

Table 5.5 below shows the values of S and R, which gave the best fits with the two-harmonic curve fitting procedure using the non-local Kwon model. It is noted that similar to Chapter 4 the value of R increases as the spatial frequency is increased while the value of C and $\varkappa$ are fixed. It can also be seen that S decreases as the spatial frequency increases

SF lines mm^{-1}	Λ mm	R	S	$\sqrt{\sigma}$ nm
1000	1.0x10^{-06}	3	0.95	51
1250	8.0x10^{-07}	6	0.73	101
2000	5.0x10^{-07}	12	0.62	77.8
2250	4.4x10^{-07}	15	0.58	73.8
			Mean =	**75.9**

Table 5.5 Values of S, R and $\sqrt{\sigma}$ obtained from the adjusted two-harmonic curve fitting procedure.

Table 5.6 below outlines the trend in the value of R as the spatial frequency increases. As in Chapter 4, the R values follow the $R \propto 1/\left(I^{1/2}\Lambda^2\right)$ relationship predicted by Zhao [Zhao, 94].

SF lines mm-1	Io mW	$1/\left(I_0^{1/2}\times\Lambda^2\right)$ mW^{-1}mm^{-1}	R/R$_{1000}$ Experimental	$\frac{I_0^{1/2}\times\Lambda_{1000}^2}{I_0^{1/2}\times\Lambda_{SF}^2}$ Theoretical prediction
1000	3.825	5.11E+11	1.0	1.00
1250	3.815	8.00E+11	2.0	1.56
2000	3.763	2.06E+12	4.0	4.03
2250	3.733	2.62E+12	5.0	5.12

Table 5.6 Demonstrating the changes in R with increasing spatial frequency.

It should be noted that the experimental R values non-local Kwon model follows the theoretical predictions more closely than the non-local Zhao model. The diffusion coefficient is also calculated using Equation 4.27. Using the non-local Kwon model D is 3.31x10^{-14} cm^2/s, which is almost the same as the value predicted by the non-local Zhao model. As in

Chapter 4, it was found that R could be varied by up to 15% and a good fit to experimental data still obtained. The quality of the fit is much more sensitive to the choice of values of S, which can be varied up to 5% before the quality of the fit deteriorates. This implies that σ can vary by 32.5%. Outside of the ranges of S and R mentioned above the theoretical predictions do not fit the experimental data curves satisfactorily.

5.6 Conclusion

In this chapter, the non-local Zhao model was adjusted to take into account any form of dependence of monomer concentration on intensity. Analytic expressions were derived taking into account a square root dependence of monomer concentration on intensity. This adjustment was shown to be necessary by Kwon et al. [Kwon, 99] and was related to fundamental physical parameters such as the quantum yield Φ.

A comparison of the non-local Kwon expression with the non-local Zhao model has been carried out. The two models agree most closely for the case were $R = 50$ and $\sigma = 1/32$.

It has been shown that by using a two-harmonic curve fitting technique with $R \propto 1/\left(I^{1/2}\Lambda^2\right)$and $\sqrt{\sigma} = 75.9 \pm 25nm$ provide excellent fits to experimental data with estimated values of κ=0.035 m/W$^{1/2}$/s and C = 1.9x10^{-5} l/mol. The diffusion coefficient D, was calculated to be approximately 3.31x10-^{14} cm^3/s. It should be noted that the experimental R values non-local Kwon model follows the theoretical predictions more closely than the non-local Zhao model

In the next chapter, applications of the DuPont photopolymer material will be discussed.

Chapter 6 Holographic Optical Elements: Applications

In this chapter the use of the commercially available DuPont holographic recording material will be introduced. The preparation of the material for holographic recording is discussed. The theory, fabrication and testing of substrate mode and polarisation selective holograms in DuPont material are discussed. An application of these specialised holograms is shown. The chapter concludes with a general comparison of the DuPont material with an acrylamide based system.

6.1 DuPont Photopolymer Material.

In this section the DuPont material is discussed and the experimental procedures for its use are outlined.

6.1.1 Introduction

One of the few commercially available photopolymers is the acrylate based system developed by E.I. DuPont Nemours and Co. [Boot, 72; Boot, 75]. It consists of an acrylate based monomer, an initiator system and a cellulose binder. The exact composition is proprietary and therefore unknown to us. Diffraction efficiencies of up to 90 % can be obtained and the material has a resolution of 3000 lines/mm. The diffraction efficiencies can be improved by post exposure with a fluorescent lamp. However the material is essentially self-developing.

Because of its limited resolution this material can not be used for reflection holograms. To rectify this DuPont developed the Omnidex photopolymer system [Monr, 91]. This material has

a resolution of about 6000 lines /mm and efficiencies of 99 % have been obtained. These results can be achieved with exposure energies of 50–100 mJ/cm^2. The material is a dry layer consisting of an acrylic monomer, a photosensitising dye, an initiator, a chain transfer agent, a plasticizer and a polymer binder coated onto a polyethyleneterephtalate film substrate. The material is capable of producing a large refractive index modulation (n_1 = 0.07) relative to other systems. This is thought to be due to the large difference in refractive index between the aromatic binder and the aliphatic monomer [Monr, 91b]. As with the earlier DuPont material the efficiencies of the Omnidex system can be increased with post exposure to a uniform beam and simple heat treatment. Because of their high diffraction efficiency, high sensitivity and good resolution the DuPont Omnidex material is generally considered to be the best commercially available photopolymer holographic recording material available at this time.

6.1.2 Experimental Use of DuPont Photpolymer

In this section the procedures used to record holograms in the DuPont HRF-700X001-20 material are described. The material is supplied sandwiched between two A5 sized sheets of Mylar stored in a light-proof wrapping. For use it is normally cut into thin strips and laminated onto a glass microscope slide. To prepare the holographic plates for exposure the following procedure must be followed [Dupo, 94]:

1. The photopolymer material should only be handled under red safety lights.
2. The glass microscope slides should be cleaned thoroughly with glass cleaner and then acetone.
3. Strips of photopolymer layer are cut from the sheet and one of the Mylar layers is peeled off.

4. The strip is laminated to the slide by placing the edge of the tacky photopolymer on the slide and carefully rolling it down until it is perfectly flat on the surface of the glass.
5. The prepared plates are then stored in a sealed box until needed for use.

The recommended exposure and post processing conditions for the DuPont HRF 700 materials are as follows [Dupo, 94]

1. Exposure requirements: 15 mJ/cm^2 by simple mirrors at normal incidence.
2. Sensitised at 514 nm wavelength.
3. Curing conditions: Overall UV and / or visible light exposure of 50–100 mJ/cm^2.
4. Baking conditions after curing: 120° for 2 hours.

The apparatus required to for holographic recording is shown below.

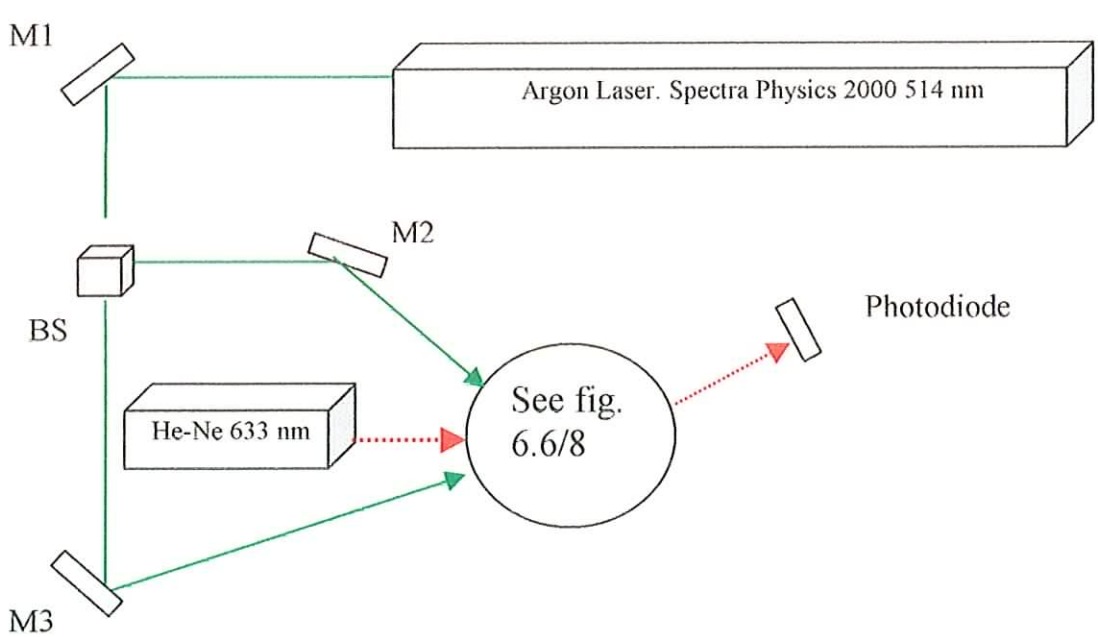

Figure 6.1 Set-up for holographic recording/testing.

The two spatially filtered and collimated beams were set up as shown in Figure 6.1. Two prisms were used to couple the beams into the layer. The exact arrangement of the prisms depends on the specification of hologram required. The prism arrangements for both substrate mode and polarisation selective holograms are discussed in the following sections. The prisms and holographic plate were indexed matched using xylene.

6.2 Polarisation Selective Holograms (PSH)

Polarisation selective holograms are optical elements that separate the Transverse Electric (TE) and Transverse Magnetic (TM) polarisation modes of inputted light. These elements can be used as a polarising beam-splitters or as part of an optical switching system [Huan, 94; Habr, 95].

6.2.1 PSH Background Theory

Transverse Electric (TE) mode is when the electric vector is perpendicular to the plane of incidence and Transverse Magnetic (TM) is when the magnetic vector is perpendicular to the plane of incidence. These two modes are illustrated in Figure 6.2 below.

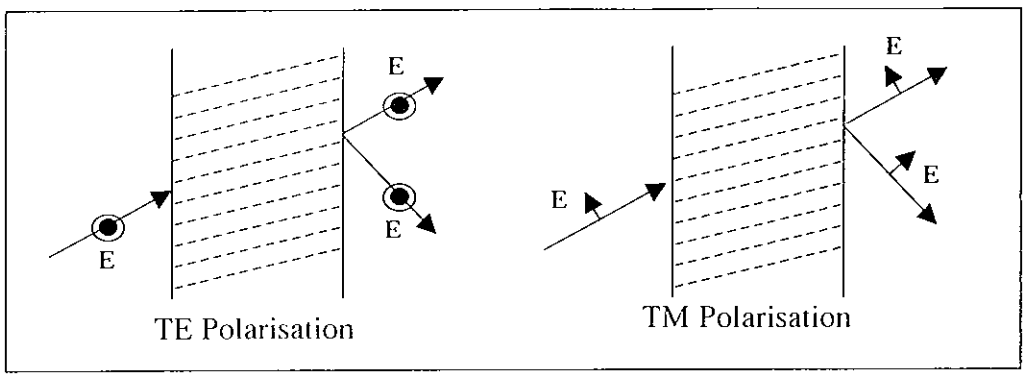

Figure 6.2 TE and TM polarisation.

According to Kogelnik's coupled wave theory [Koge. 69] the diffraction efficiency of a thick phase transmission hologram replayed under the Bragg conditions is given by:

$$\eta = \sin^2 \nu \tag{6.1}$$

and for reflection holograms by:

$$\eta = \tanh^2 \nu \tag{6.2}$$

Where ν is the 'grating strength' or 'modulation constant'. For a replay beam which is TE polarised, ν is defined as

$$\nu_{TE} = \frac{\pi n_1 d}{\lambda \sqrt{\cos\theta_1 \cos\theta_2}} \tag{6.3}$$

Where n_1 is the refractive index modulation, d is the thickness of the photopolymer layer, λ is the replay wavelength inside the material and θ_1 and θ_2 are the angles of incidence and diffraction inside the recording medium respectively. The grating strength for a TM polarised replay beam is defined as

$$\nu_{TM} = \nu_{TE}\cos(\theta_1 - \theta_2) \tag{6.4}$$

Where θ_1 and θ_2 are the incident and diffracted angles respectively. From these equations it can be seen that if the angle θ_1-θ_2 is equal to 90° and $\nu_{TE} = \pi/2$ only the TE component of the replay beam will undergo diffraction while the TM mode will be undiffracted. A growth curve shown in Figure 6.3 below, where $\nu_{TE} = \pi/2$ for refractive index modulation values of 0.018 and higher.

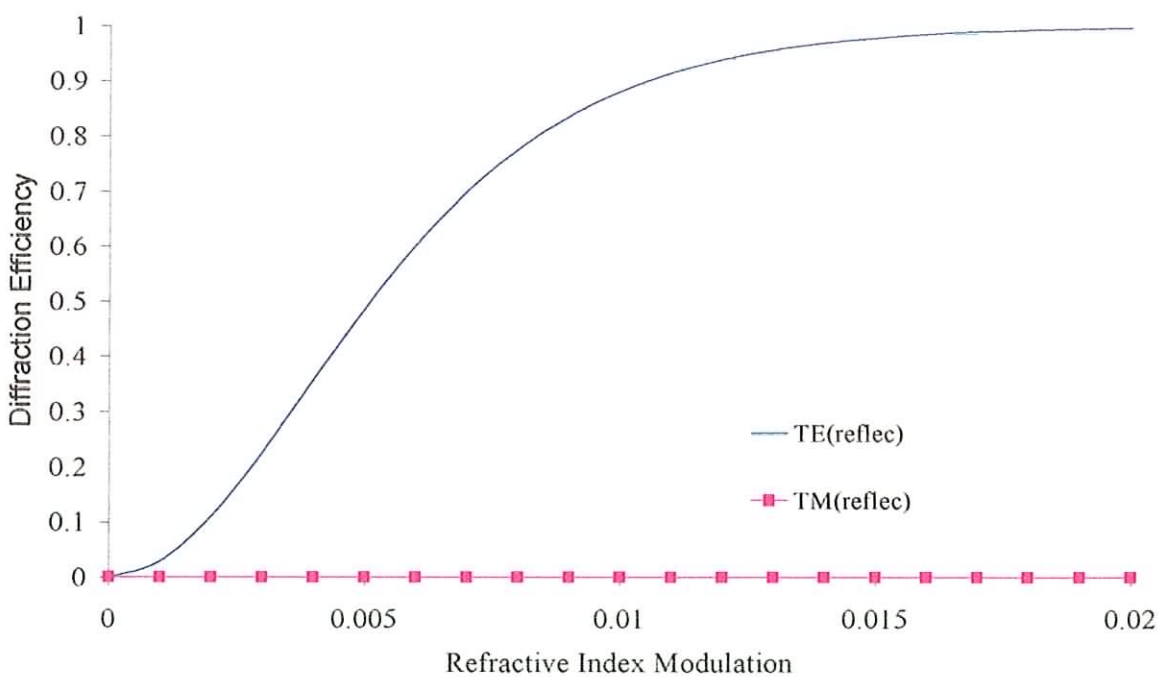

Figure 6.3 Reflection and transmission of TE and TM components of a replay beam for a Polarisation Selective Hologram, PSH.

The geometry of a 100% efficient unslanted reflection, polarisation selective hologram is show, below in Figure 6.4. All angles shown are inside the material.

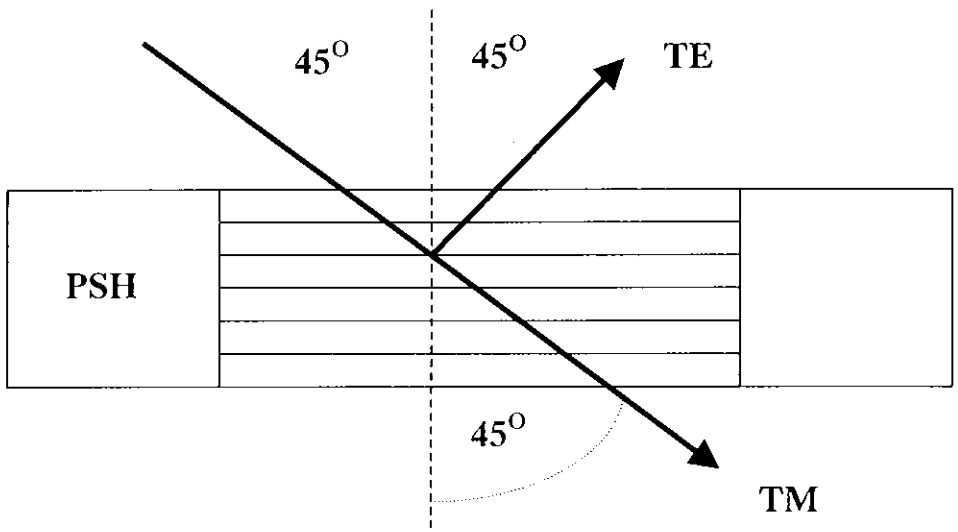

Fig. 6.4 Polarisation Selective Hologram, PSH.

6.2.2 PSH Experimental Work.

The procedure used to record holograms has already been described in Section 6.2. The following diagram (Figure 6.5) shows the prism arrangement necessary to record the polarisation selective elements.

1. The beam is incident on one face of a prism as shown in Figure 6.5 below. The photopolymer layer and the absorption filter are index matched to the prism using ortho-xylene.

2. The prism is arranged so that the laser beam is normal to the surface of the prism. Prior to recording the prism is then rotated through an angle of 17° to obtain convenient Bragg conditions (90°) for replay with a HeNe laser (633 nm).

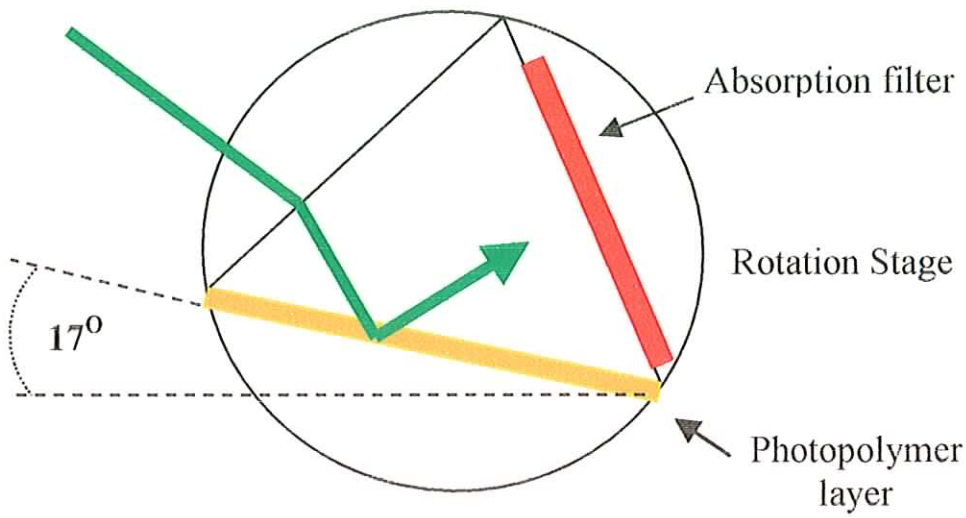

Figure 6.5 Recording geometry for Polarisation Selective Holograms, PSH.

6.3 Substrate Mode Hologram (SMH)

The SMH is an optical element that couples incident light into a substrate. These can be used as free-space optical interconnects [Huan, 90; Zhou, 95].

6.3.1 SMH Background Theory

The grating geometry needed to couple an incident beam into a substrate is shown below in Figure 6.6. All angles are inside the medium

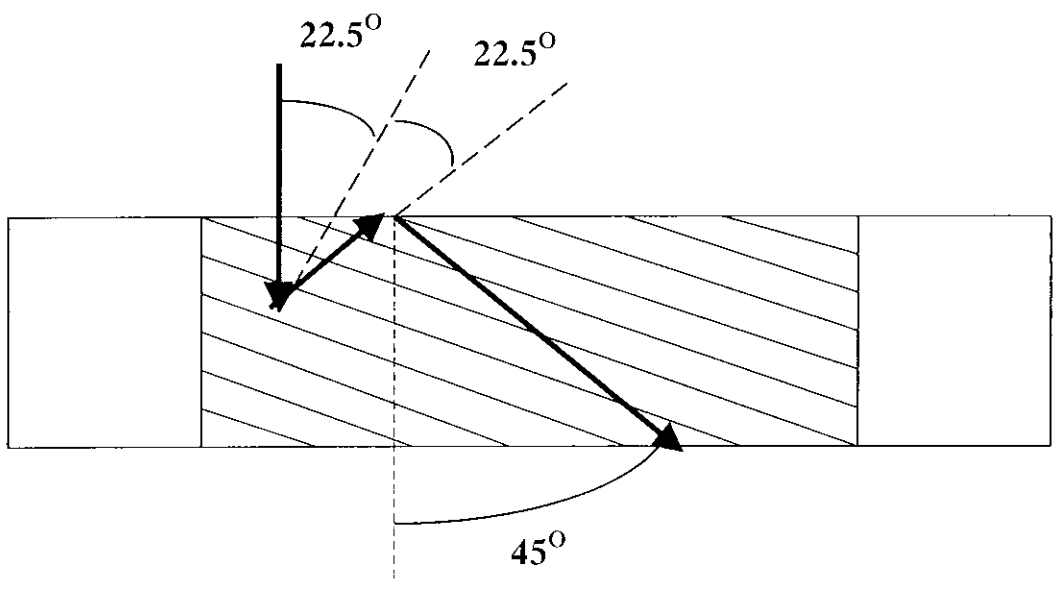

Figure 6.6 Substrate Mode Hologram, SMH.

This element has a grating slant angle of 22.5° which means an incident beam normal to the surface of the hologram is diffracted at an angle of 45° inside the material. When such gratings are recorded in reflection mode they are not perfectly polarisation selective.

6.3.3 SMH Experimental Work.

The experimental procedures for recording and post processing of holograms in DuPont photopolymer have been described in section 6.1.2. In this section the set-up for recording the substrate mode hologram is described.

1. The beam is incident on one face of a prism as shown in the diagram below (Figure 6.7). The photopolymer layer and the absorption filter are index matched to the prism using ortho-xylene.
2. The prism is arranged so that the laser beam is normal to the surface of the prism. Prior to recording the prism is then rotated through an angle of 31° to obtain convenient Bragg conditions for replay (90°) with a HeNe laser (633 nm).

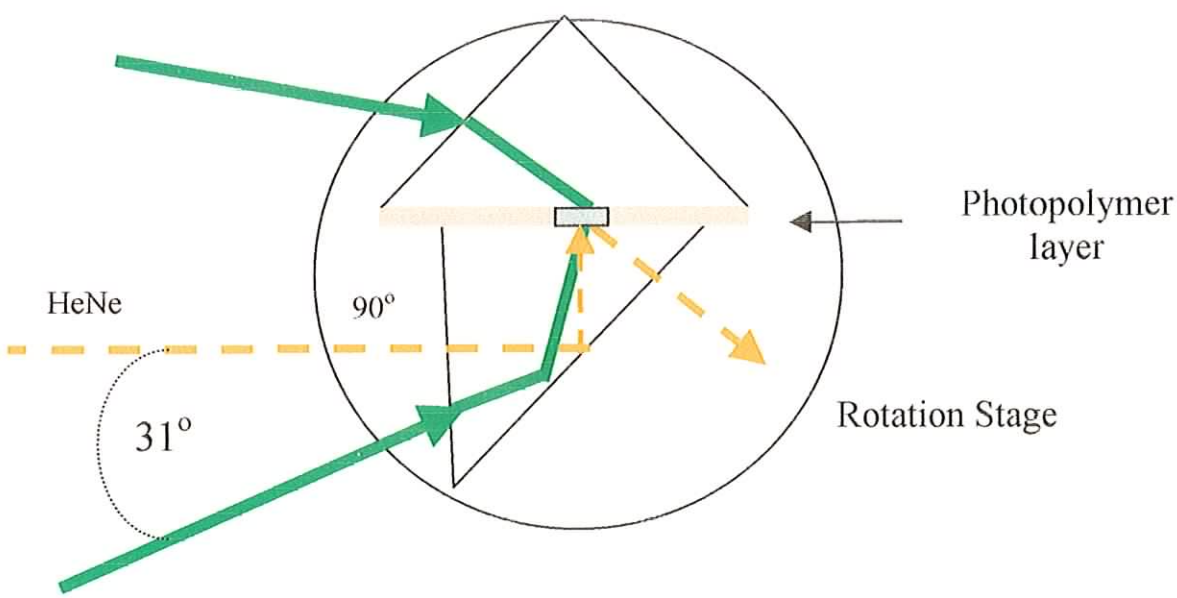

Figure 6.7 Recording geometry for Substrate Mode Hologram, SMH.

6.4 Applications

Substrate Mode and Polarisation Selective Holograms have many applications. SMH can be used in optical interconnects, edge illumination method holography and in beam forming [Huan, 90; Zhou, 95]. PSH can be used in optical switching or as compact polarising beam splitters. During this study, an interferometric sensor based on these two optical elements has been developed [Sain, 99; More, 00]. A diagram outlining the sensor is shown below (Figure 6.8). For clarity the operation of the sensor is split into two parts. Figure 6.8(a) shows the beams leaving the sensor while Figure 6.9(b) shows the beams re-entering the sensor.

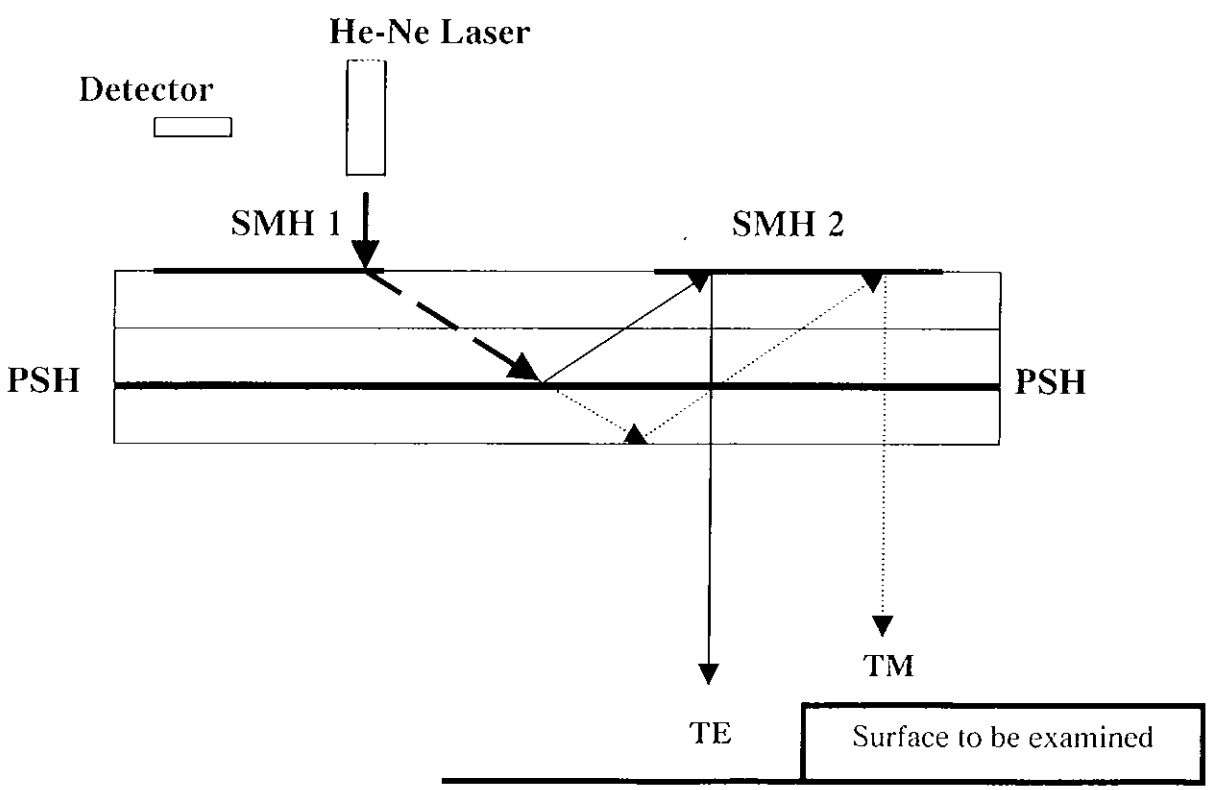

(a)

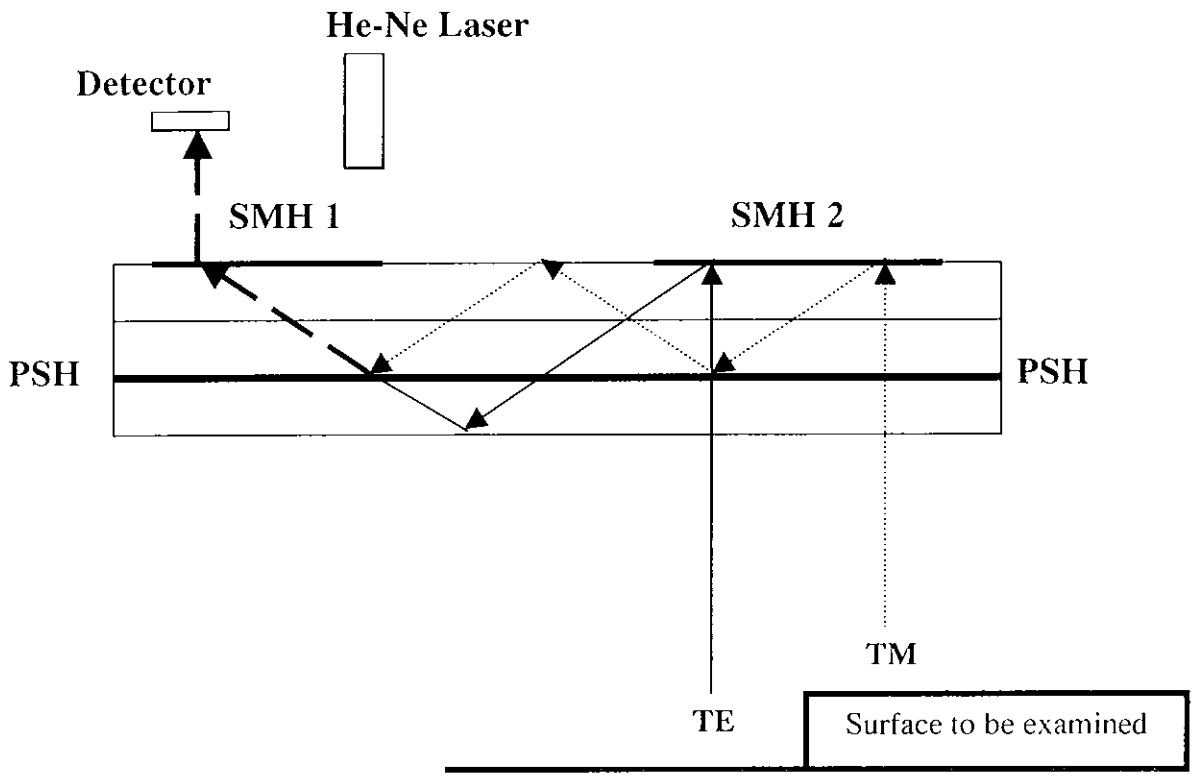

(b)

Figure 6.8 Layout of the interferometric sensor.

The sensor operates by splitting a input He-Ne laser beam (heavy dashed line) into its TE (solid line) and TM (light dashed line) components and coupling the two resultant beams out of the sensor. The two beams reflect off the surface to be tested and are then coupled back into the sensor along the same paths. The two beams are recombined and coupled out to a detector. If the object being tested moves, it will cause a change in the path lengths of the TE and TM beams. This results in a change of the interference pattern of the recombined beams at the detector. This

change of the interference pattern can be seen as a fading and brightening of the output beam which can be displayed on a PC or digital oscilloscope.

This system was used to detect a slight shrinking/swelling of the DuPont photopolymer material during recording [More, 99; More, 00].

6.5 Exposure Characteristics of DuPont Omnidex Photopolymer

In this section the exposure characteristics for Substrate Mode Holograms recorded in DuPont HRF 700X001-20 are discussed.

The holograms are recorded using the set-up and procedures already outlined. For this analysis the gratings were probed during recording using a He-Ne laser (633 nm). The diffracted beam was measured using a photodiode and a digital oscilloscope. The data was then stored on a PC. The Substrate Mode Holograms were recorded using intensities at the prism faces of 0.5 mW, 1.0 mW, 2.0 mW, 2.5 mW, 3.0 mW and 3.3 mW.

Figure 6.9 below shows the growth curves for the holograms at various recording intensities.

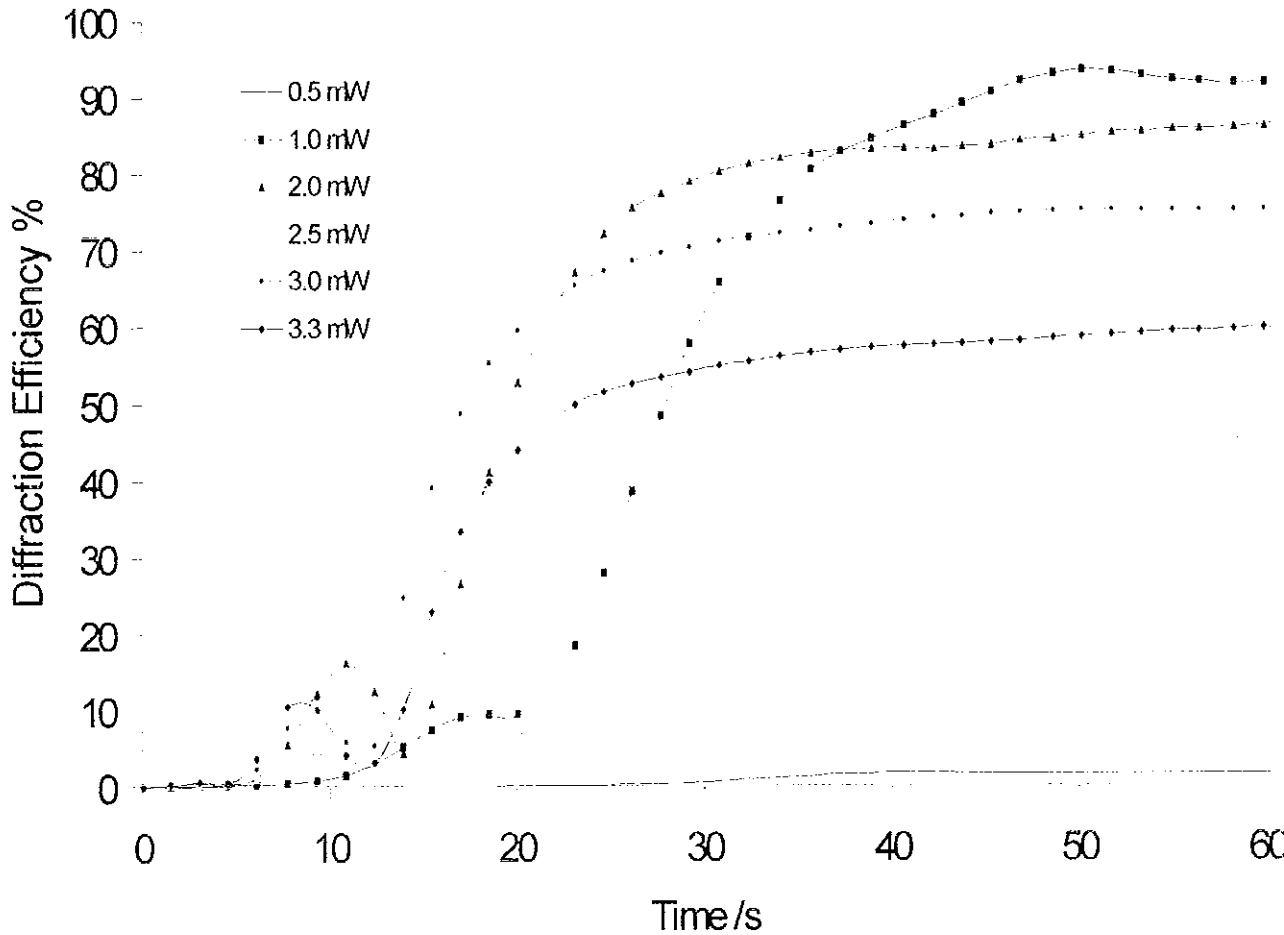

Figure 6.9 DuPont HRF 700 growth curves for different exposure intensities.

From the graph it can be seen that for the range of recording intensities 1 and 2 mW seem to give the largest diffracted power while 0.5 mW gives the lowest.

An unusual feature of the growth curves of the DuPont material compared to the acrylamide based photopolymer is the peak in diffracted power between 10 and 20 seconds. Such a peak has not been reported in the literature for acrylamide photopolymer growth curves. However, such peaks in acrylamide photopolymers were observed by Feely [Feel, 99]. An example of typical acrylamide based material growth curves presented in Figure 6.10 below.

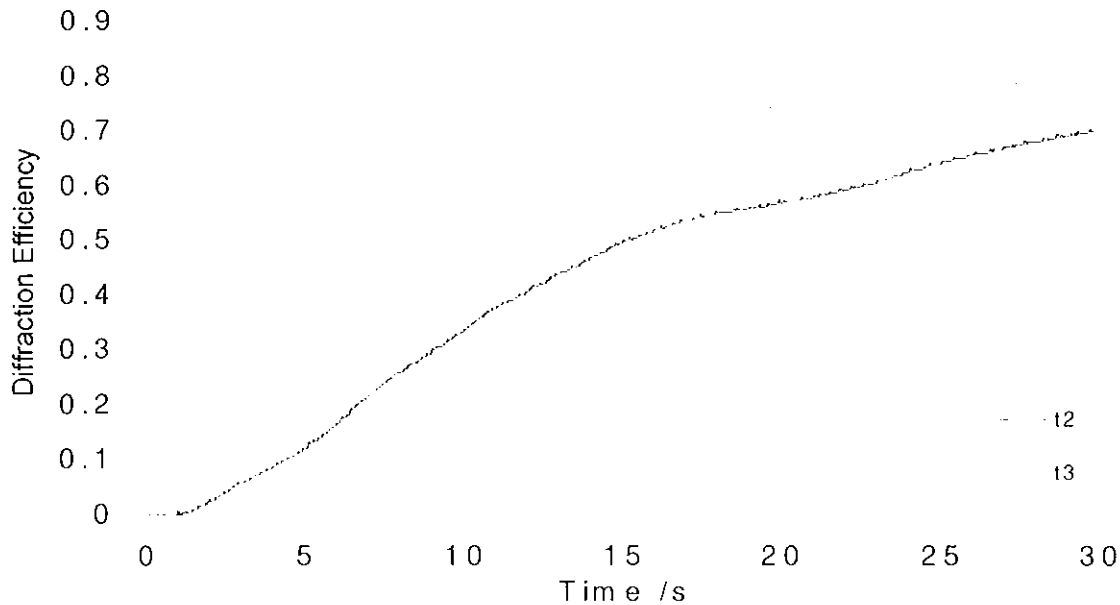

Figure 6.10 Typical acrylamide based photopolymer growth curves.

It should be noted that this type of behaviour is not predicted by the models presented in this study or by any other models. The exact cause of these peaks in DuPont photopolymer is not fully understood but a possible explanation has been but forward by Booth [Boot, 75]. He observes that such growth curves occur when the rate of polymerisation was greater than the rate of diffusion, i.e. $R<<1$. This condition can be met when: (i) recording intensities are high, or (ii) there is a low monomer concentration or (iii) when low spatial frequencies are recorded. Booth explains that on exposure to the interference pattern the regions of highest intensity begin to polymerise. If the polymerisation rate is higher than the rate of diffusion then the initial increase in diffraction efficiency will be followed by a decrease as material begins to diffuse into the exposed regions, lowering the refractive index modulation and therefore the diffraction efficiency. If the polymerisation rate is not higher than the diffusion rate then the diffraction efficiency will rise continuously.

However, these gratings were recorded at a relatively low intensity and at high spatial frequency so, according to Booth, they should not show such a rise and fall in efficiency. It is known that the DuPont material used in this study is an improved version of the one examined by Booth [Boot, 75]. It is possible that the characteristics of the Omnidex material are different from the older version. For example it is known that the older version had a spatial frequency limit of about 3000 lines per mm while Omnidex has a limit of 6000 lines/mm [Monr, 91].

6.6 General Comparison of DuPont and Acrylamide based Photopolymers.

In this section a general comparison between the DuPont material and the acrylamide based photopolymer used earlier will be carried out.

- *Cost*: The DuPont HRF 700 material used in this study cost $75 per 30 cm x 20 cm sheet. As this is an experimental version of the Omnidex material, it is cheaper than the full commercial system. The acrylamide material cannot be bought commercially so must be made in the laboratory. The chemicals used for the acrylamide material are not expensive. Therefore the acrylamide material is cheaper.
- *Ease of use*: The DuPont material must be peeled from its Mylar substrate and laminated onto a glass slide. It is then ready for immediate use. The liquid acrylamide material must be dropped onto a glass plate and allowed to dry for 24 to 48 hours before use. Once the DuPont lamination procedure is mastered, the DuPont material is ready for immediate use.
- *Flexibility*: There are four types of DuPont material, which are shown in Table 6.1 below. If the users wish to record at a different wavelength, they must purchase a different material.

The basic acrylamide material can record at either 514 nm or 633 nm. This can be achieved by changing the dye used while preparing the material. The DuPont material is proprietary so the users cannot change the chemical composition or thickness of the material to suit their individual needs. However workers can change the amount or type of chemicals used in acrylamide materials. Various layer thicknesses can be prepared easily. Therefore the acrylamide material is more flexible than the DuPont photopolymer.

- *Performance*: This is the main reason why the DuPont material is superior to the acrylamide based polymer. The table below shows the various types of commercially available DuPont material compared with acrylamide.

	OmniDex 7061	HRF 800X	HRF 600	HRF 700X	Acrylamide
Layer thickness	20	15	6 to 20	10 to 20	20 to 120
Cover sheet	PVC	PET	PET	PET	None
Spectral sensitivity/nm	476-532	458-532 633-647	476-532	476-532	514 or 633
Sensitivity mJ/cm^2	25	4 to 18	10 to 100	3 to 30	80
Peak diffraction efficiency /%	99.99	98 to 99.9	>95	>99	>80

Table 6.1 Comparison of DuPont and acrylamide based photopolymer materials.

The DuPont materials are capable of recording higher spatial frequencies than the acrylamide photopolymers. This means that they can be used for reflection holography whereas only weak reflection gratings have to date been recorded in acrylamide polymers [Onei, 00a].

In summary, the DuPont material is easier to use and has a superior performance. However it is more expensive than the acrylamide material and the form and chemical composition of the material cannot be changed to suit the users needs.

6.7 Conclusions

In this chapter, the commercial DuPont HRF 700X photopolymer material used was introduced. A brief overview was given of the historical development of these materials. The experimental procedures for holographic recording with the DuPont system was outlined.

The background theory of Polarisation Selective and Substrate Mode holograms were described. The experimental set-ups needed to fabricate these specialised holographic optical elements were outlined. These two elements can be combined for use as an interferometric sensor. The layout and operation of such a sensor was discussed.

The exposure characteristics of the DuPont photopolymer during the recording of Substrate Mode Holograms was examined. It was found that the optimum exposure energy was between 1 and 2 mW. An unusual feature of the DuPont growth curves was a small rise and fall in diffraction efficiency before the efficiency rose to it's final value. This behaviour has not been reported in the literature for acrylamide photopolymers.

Finally, a general comparison between the DuPont material and the acrylamide based system used in this study was carried out. It was found that the DuPont material is easier to use and has a superior performance. However, it is more expensive than the acrylamide material and the form and chemical composition of the material cannot be changed to suit the users needs.

Chapter 7 Conclusions and Future Work

In this chapter the conclusions of this study will be presented along with an outline of future work to be carried out.

7.1 Conclusions

In Chapter 1, the aims of this study were presented along with an outline of the structure of the work carried out.

A general introduction to holography was given and the basic models of light diffraction by gratings, including Fraunhofer and Bragg diffraction, were introduced. Kogelnik's coupled wave theory [Koge, 69] was decribed and its use in the calculation of various parameters was outlined. This theory is later applied to experimental data in Chapter 3. There are a number of other theories used to model holographic gratings such as modal theory, transparency theory and the optical path method. These are not considered further as the coupled wave theory provides all the information necessary here.

The properties of an ideal holographic material were then outlined and the two most common materials silver halide emulsion and dichromated gelatin were introduced. The historical development and properties of various types of photopolymers were given with emphasis on acrylamide based systems. The photochemical and polymerisation process in acrylamide based photpolymer systems was discussed.

Chapter 2 introduced the theory of grating formation by diffusion. An extension of current models by the introduction of a non-local response was presented. The predictions of the local diffusion model, $\sigma = 0$, [Zhao, 94; Colv, 97] might be stated as follows. In general the larger the value of R (the ratio of the rate of polymerisation to the rate of diffusion) the stronger the first order grating and the more closely the resulting grating profile matches the illuminating fringe pattern. These results can be summarised as follows:

(i) As I_0 increases $F_0 = \kappa I_0$ increases and $R \propto 1/F_0$ decreases.

(ii) As Λ increases $K = 2\pi / \Lambda$ decreases and $R \propto K^2$ decreases.

Therefore the lower the illuminating intensity, I_0 (and the longer the exposure time, t), the finer the fringe period, the larger R and so the better the profile.

The concept of non-local response was introduced in Chapter 2. It is proposed to arise when polymer chains initiated in the dark regions grow into adjoining bright regions thereby smearing the exposing sinusoidal pattern recorded. This leads to a decrease in diffraction efficiency and may account for the spatial frequency cut-off observed in photopolymer materials. In the non-local response regime, $\sigma > 0$, a further qualification must be noted. The larger the non-local response variance the lower the visibility of the profile but also the more closely the profile recorded resembles the sinusoidal interference pattern. Therefore two additional results are predicted.

(iii) As Λ decreases, $K^2\sigma$ increases, $n_1 = CN_1$ decreases and the first order grating is suppressed.

(iv) As Λ decreases, $(mK)^2\sigma$ increases more rapidly and so $n_m=CN_m$ decreases and the higher order grating harmonics are even more heavily suppressed.

Where N_m is the m^{th} harmonic of the polymer profile.

Finally a spatial frequency response curve was shown. This clearly shows a drop off in spatial frequency response for the non-local case, which is not predicted by the local diffusion models.

The diffusion model has been extended in a way, which should make it applicable to a wider range of observable phenomena.

In Chapter 3, the procedures used to determine the spatial frequency response of the photopolymer material were presented. The composition of the material and the methods used to prepare it were outlined.

A number of experiments were carried out to establish the effect of changing the material composition on the spatial frequency response. First, the spatial frequency response of the material sensitised with four different xanthene dyes was measured. There was no significant difference in the responses. This is thought to indicate that dye diffusion does not have a major role to play in determining spatial frequency response. However, it is possible that the difference in molecular weight between the dyes was too small to have a significant effect on the frequency response.

In a further attempt to alter the rate of diffusion, four different molecular weight PVA binders were examined. It was hoped that the wider range of molecular weights available would change the spatial frequency response, but this was not the case. It became clear that an alternative approach was required. Based on the non-local model presented in Chapter 2 attempts were made to control the lengths of the polymer chains. The effects of adding two different retarders to the material were examined. Again there was no significant differences in spatial frequency response. It is thought that the correct concentration of retarder needed to shorten chains was not determined. It is also possible that a more suitable retarder for this acrylamide based system could give the desired result.

In Chapter 4 simple analytic expressions describing grating formation in a diffusion-governed photopolymer have been presented. Their ranges of validity have been examined in comparison with numerical techniques and they have been shown to be of some practical value. The two models agree most closely for the case were $R = 50$.

It has been shown, using the analytic curve fitting technique that with $R \propto 1/(I_0 \times \Lambda^2)$ and $\sqrt{\sigma} = 80 \pm 25nm$ satisfactory fits can be made to experimental data with estimated values of κ=0.06 $m^2/W/s$ and $C = 2.1 \times 10^{-5}$ l/mol. The diffusion coefficient D, was calculated to be approximately 6.5×10^{-14} cm^3/s. However, the fits are not as good at low exposure energies as at higher energies due to the poor resolution of the experimentally captured data.

In Chapter 5, the non-local Zhao model was adjusted to take into account any form of dependence of monomer concentration on intensity. Analytic expressions were derived taking into account a square root dependence of monomer concentration on intensity. This

adjustment was shown to be necessary by Kwon et al. [Kwon, 99] and was related to fundamental physical parameters such as the quantum yield Φ.

A comparison of the non-local Kwon expression with the non-local Zhao model has been carried out. The two models agree most closely for the case were $R = 50$ and $\sigma = 1/32$.

It has been shown that, using a two-harmonic curve fitting technique, with $R \propto 1/\left(I^{1/2}\Lambda^2\right)$ and $\sqrt{\sigma} = 75.9 \pm 25nm$ excellent fits to experimental data can be found with estimated values of κ=0.035 m/W$^{1/2}$/s and C = 1.9x10^{-5} l/mol. The diffusion coefficient D, was calculated to be approximately 3.31x10^{-14} cm^3/s. It should be noted that the experimental R values estimated using the non-local Kwon model has been found to follow the predicted theoretical behaviour more closely than the non-local Zhao model

In Chapter 6, the DuPont HRF 700X photopolymer material was introduced and a brief overview was given of the historical development of these materials. The experimental procedures for holographic recording with the DuPont system was outlined.

The background theory of Polarisation Selective Holograms, PSH, and Substrate Mode Holograms, SMH, are described. The experimental set-ups needed to fabricate these specialised holographic optical elements were outlined. These two elements can be combined for use as in interferometric sensor. The layout and operation of such a sensor was discussed.

The exposure characteristics of DuPont photopolymer during the recording of Substrate Mode Holograms were examined. It was found that the optimum exposure energy was between 1 and 2 mW. An unusual feature of the DuPont growth curves was a small rise and fall in

diffraction efficiency before the efficiency rose to its final value. This behaviour has not been reported in the literature for acrylamide photopolymers. It is also not predicted by any model and only a unsatisfactory explanation has been given by Booth [Boot, 75].

Finally, a general comparison between the DuPont material and the acrylamide based system used in this study was carried out. It was found that the DuPont material is easier to use and has a superior performance. However it is more expensive than the acrylamide material and the form and chemical composition of the material cannot be changed to suit the users needs.

7.2 Future Work

In this section, the future work to be carried out will be outlined.

- *Position dependent non-locality*: Recall that the rate of polymerisation depends on the intensity. As gratings are recorded with a sinusoidal intensity profile some areas of the material are exposed to a higher intensity than others and therefore have more chain initiating radicals. This means that the chains growing in high intensity areas have more competition for monomer than those in the low intensity regions as more chains are being initiated. Therefore the polymer chains in high intensity areas will be shorter than in the low intensity areas giving different values of σ . The models presented in this study assume that the value of σ is constant between all areas of the material.
- As discussed in Chapters 4 and 5, one of the flaws in the curve fitting techniques was the low resolution of the experimental data. To improve resolution, adjustments could be made to the LabVIEW program used to capture the data. A more sensitive optical power

meter could also be used. The curve fitting technique could be further improved and automated

- The techniques described in this study could be applied to other photopolymer materials such as the DuPont material.
- The model could be extended to include the diffusion of other chemical components. At the moment only monomer diffusion is considered.
- In Chapter 3, an attempt was made to shorten polymer chain length by the addition of retarders. Further experiments on different retarders and different concentrations of the retarder used in this study could be carried out.
- It would also be useful to experimentally determine values for the parameters used in this study. Raman spectroscopy could be used to determine F_0 and κ. Techniques such as Gel Permeation Chromotography could be used to determine the lengths of the polymer chains formed during holographic recording. These values could be then compared with those estimated using the models presented in this study.

References

[Adha, 91] R. R. Adhami, D. J. Lanteigne, D. A. Gregory, "Photopolymer hologram formation theory", Microwave and Optical Technology Letters, Vol. 4, No. 3, Pg.106-109, (1991).

[Acdi, 98] Advance Chemistry Development Inc. website: www.acdlabs.com

[Atki, 92] P. W. Atkins, *Physical Chemistry*, 4th edition, Oxford University Press, Oxford, U.K., (1992).

[Birk, 75] J. B. Birk, *Organic Molecular Photophysics* Vol. 2, John Wiley & Son, New York, U.S.A., (1975).

[Blay, 98] S. Blaya, R. Mallavia, L. Carretero, A. Fimia, R. F. Madrigal, "Highly sensitive photopolymerisable dry film for use in real time holography", Applied Physics Letters, Vol. 75, No. 12, Pg.1628-1630, (1998).

[Boot, 72] B.L. Booth, "Photopolymer material for holography",Applied Optics Vol. 11, No. Pg. 2096-2097, (1972).

[Boot, 75] B. L. Booth, "Photopolymer material for holography" Applied Optics, Vol. 14, No. 3, Pg. 593-601, (1975).

[Born, 80] M. Born, E. Wolf, *Principles of Optics: Electromagnetic Theory of Propagation, Interference and Diffraction of Light*, 6th edition, Pergamon Press, Oxford, U.K., (1980).

[Bove, 78] F. A. Bovey, F. H. Winslow, *Macromolecules, an introduction to polymer science*, Acadenic Press, New York, U.S.A., (1978).

[Cali, 87] S. Calixto, "Dry polymer for holographic recording", Applied Optics, Vol. 26, No. 18, Pg. 3904-3909, (1987).

[Carr, 90] C. Carre, D. J. Lougnot, "Photopolymerisable material for recording in the 450-550 nm domain", J. Optics (Paris), Vol. 21, No. 3, pg. 147-152, (1990).

[Carr, 92] C. Carre, D. J. Lougnot, Y. Renotte, P. Leclere, Y. Lion, "Photopolymerisable material for recording in the 450-550 nm domain: Characterisation and Applications Part 2.", J. Optics (Paris), Vol. 23, No. 2, Pg. 73-79, (1992).

[Chan, 79a] B. J. Chang, C. D. Leonard, "Dichromated Gelatin for the fabrication of holographic optical elements", Applied Optics, Vol. 48, No. 9, Pg. 2407-2417, (1979).

[Chan, 79b] B. J. Chang, "Dichromated gelatin as a holographic storage medium", Proc. SPIE, Vol. 177, Pg. 71-81, (1979).

[Chan, 80] B. J. Chang, "Dichromated gelatin holograms and their applications", Opt. Eng., Vol. 19, No. 5, Pg. 642-648, (1980).

[Clos, 69] D. H. Close, A. D. Jacobson, R. C. Magerum, R. G. Brault, F. J. McClung, "Hologram recording on photopolymer materials", Applied Physics Letters, Vol. 14, No. 5, Pg. 159-160, (1969).

[Colb, 71] W.S. Colburn, K.A. Haines, "Volume hologram formation in photopolymer materials", Applied Optics Vol. 10, No. 7, Pg. 1636-1641, (1971).

[Coll, 71] R. J. Collier, C. R. Bruckhardt, L. H. Lin, *Optical Holography*, Academic Press, New York, U.S.A., (1971).

[Colv, 97] V. L. Colvin, R. G. Larson, A. L. Harris, M. L. Schilling, "Quantitative model of volume hologram formation in photopolymers", J. Applied Physics, Vol. 81, No. 9, Pg. 5913-5923, (1997).

[Conr, 67] J. Conrad, *Encyclopedia of Polymer Science and Technology*, Vol. 7, (1967).

[Dave, 99] Dr. A. Davey, University of Dublin, Private communication, (1999).

[Doi, 97] M. Doi, *Introduction to Polymer Physics*, Clarendon Press, Oxford, U.K., (1997).

[Down, 96] J. D. Downie, D. T. Smithey, "Measurements of holographic properties of bacteriorhodopsin films", Applied Optics, Vol. 35, No. 29, Pg. 5780-5789, (1996).

[Dhar, 98] L. Dhar, K. Curtis, M. Tackitt, M. Schilling, S. Campbell, W. Wilson, A. Hill, C. Boyd, N. Levinos, A. Harris, "Holographic storage of multiple high-capacity digital data pages in thick photopolymer systems", Optics Letters, Vol. 23, No. 21, Pg. 1710-1712, (1998).

[Dupo, 94] DuPont holographic recording film product information sheet for Omnidex HRF-700X001-20, (1994).

[Elia, 77] H.-G. Elias, *Macromolecules, Part I. Structures and Properties*, Plenum Press, New York, USA, (1977).

[Engi, 99] D. Engin, A. S. Kewitsch, A. Yariv, "Holographic characterisation of chain photopolymerisation", JOSA B, Vol. 16, No. 8, Pg. 1213-1219, (1999).

[Feel, 98] C. A. Feely, "The development and characterisation of a red-sensitised photopolymer holographic recording material", Doctoral Thesis, University of Dublin, (1998).

[Feel, 99] Dr. C. A. Feely, Dublin Institute of Technology, Private Communication, (1999).

[Fimi, 92] A. Fimia, N. Lopez, F. Mateos, "Acrylamide photopolymers for use in real time holography: Improving energetic sensitivity", Proc. SPIE Vol. 1732, Pg. 105-109, (1992).

[Fimi, 93] A. Fimia, N. Lopez, F. Mateos, R. Sastre, J. Pineda, F. Amat-Guerri, "Elimination of oxygen inhibition in photopolymer systems used as holographic recording materials", J. Modern Optics, Vol. 40, No. 4, Pg. 699-706, (1993).

[Finc, 80] W. H. A. Fincham, M. H. Freeman, *Optics*, 9th edition, Butterworths, London, U.K., (1980).

[Gabo, 48] D. Gabor, "A new microscopic principle", Nature Vol. 161, Pg. 777, (1948).

[Gamb, 94] W. Gambogi, K. Steijn, S. Mackara, T. Duzick, B. Hamzavy, J. Kelly, "HOE imaging in DuPont holographic photopolymers.", Proc. SPIE, Vol. 2152, Pg. 282-293, (1994).

[Gilb, 91] A. Gilbert, J. Baggott, *Essentials of Molecular Photochemistry*, Blackwell Scientific Publications, Oxford, U.K., (1991).

[Habr, 95] S. Habraken, Y. Renotte, St. Roose, E. Stijns, Y. Lion, "Design for polarising holographic optical elements", Applied Optics, Vol. 34, No. 19, (1995).

[Huan, 90] Y. Huan, M. Kato, R. K. Kostuk, "Methods for fabricating substrate- mode holographic optical elements", Proc. SPIE, Vol. 1211, Pg. 166-174, (1990).

[Huan, 94] Y. Huang, "Polarisation-selective volume holograms: general design", Applied Optics, Vol. 33, No. 11, Pg. 2115-2120, (1994).

[Ingw, 89] R. T. Ingwall, M. Troll, "Mechanism of hologram formation in DMP-128 photopolymer", Optical Engineering, Vol. 28, No. 6, Pg. 586-591, (1989).

[Jenn, 70] J. A. Jenney, "Holographic recording in photopolymers", JOSA, Vol. 60, No. 9, Pg. 1155-1161, (1970).

[Jenn, 71] J. A. Jenney, "Nonlinearities of photopolymer holographic recording materials", Applied Optics, Vol. 11, No. 6, Pg. 1371-1381, (1971).

[Jeud, 75] M. J. Jeudy, J. J. Robillard, "Spectral photosensitisation of a variable index material for recording phase holograms with high efficiency", Optics Communications, Vol. 13, No. 1, Pg. 25-28, (1975).

[Koge, 69] H. Kogelnik, "Coupled wave theory for thick holographic gratings", Bell Systems Technical J., Vol. 48, Pg. 2909-2947, (1969).

[Kron, 94] V. W. Krongauz, A. D. Trifunac, *Processes In Photoreactive Photopolymers*, Chapman & Hall, New York, U.S.A., (1994).

[Kwon, 99] J. H. Kwon, H. C. Chang, K. C. Woo, "Analysis of temporal behaviour of beams diffracted by volume gratings formed in photopolymers", JOSA B, Vol. 16, No. 10, Pg. 1651-1657, (1999).

[Lawr, 00a] Justin R. Lawrence, Feidhlim T. O'Neill, John T. Sheridan, "Photopolymer material parameter estimation using diffusion based analytic formula", submitted for publication, Journal of Applied Physics, (2000).

[Lawr, 00b] Justin R. Lawrence, Feidhlim T. O'Neill, John T. Sheridan, "Adjusted intensity dependence non-local diffusion model of holographic grating formation in photopolymer", submitted for publication, JOSA A, (2000).

[Leit, 63] E. N. Leith, J. Upatnieks, "Reconstructed waveforms and communication theory", JOSA, Vol. 52, Pg. 1123, (1962).

[Mani, 94] G. Manivannan, R. A. Lesard, "Trends in holographic recording materials", TRIP Vol. 2, No. 8, Pg. 282-290, (1994).

[Mart, 94] S. Martin, P. Leclere, Y. Renotte, V. Toal, Y. Lion, "Characterisation of an acrylamide-based dry photopolymer holographic recording material", Optical Engineering, Vol. 33, No. 12, Pg. 3942-3946, (1994).

[Monr, 91a] B. M. Monroe, W. K. Smothers, D. E. Keys, R.R Krebs, D. J. Mickish, A. F. Harrington, S. R. Schicker, M. K. Armstrong, D. M. T. Chan, C. I. Weathers, "Improved photopolymers for holographic recording Part 1", J. Imaging Science, Vol. 35, Pg. 19-25, (1991).

[Monr, 91b] B. M. Monroe, "Improved photopolymers for holographic recording Part 2", J. Imaging Science, Vol. 35, Pg. 25-29, (1991).

[More, 99] V. Moreau, Y. Renotte, Y. Lion, "Planar integrated inteferometric sensor with holographic gratings", Proc. SPIE, Vol. 3951, Pg. 108-115, (1999).

[More, 00] V. Moreau, J. R. Lawrence, S. Soler-Hernandez, B. Tilkens, Y. Renotte, Y. Lion, "Optimisation of holograms recorded in DuPont photopolymer", accepted for publication, Proc. SPIE, (2000).

[Odia, 70] G. Odian, *Principles of Polymerisation*, McGraw-Hill Book Company, New York, U.S.A., (1970).

[Ohan, 89] H. C. Ohanian, *Physics*, 2nd edition, W. W Norton & Co. Inc., New York, U.S.A., (1989).

[Onei, 00a] F. T. O'Neill, J. R. Lawrence, J. T. Sheridan, "Thickness variation of a self-processing acrylamide-based photopolymer and reflection holography", accepted for publication, Optical Engineering, (2000).

[Onei, 00b] F. T. O'Neill, J. R. Lawrence, J. T. Sheridan, "Automated recording and testing of holographic optical element arrays", accepted for publication, Optik, (2000).

[Onei, 00c] F. T. O'Neill, J. R. Lawrence, J. T. Sheridan, "Improvement of a holographic recording material using a acrosol sealant", submitted for publication, J. European Optical Society A., (2000).

[Oste, 60] G. K. Oster, G. Oster, "Photochemical modifications of high polymers by visible light", J. of Polymer Science, Vol. 48, Pg. 321-327, (1960).

[Piaz, 96] S. Piazzolla, B. K. Jenkins, "Holographic grating formation in photopolymers", Optics Letters, Vol. 21, No. 14, Pg. 1075-1077, (1996).

[Pitt, 80] T. N. Pitts Jr., G. S. Hammond, K. Gallnick, D. Grosjier, *Advance Photochemistry* 12, John Wiley Interscience, New York, U.S.A., (1980).

[Pont, 98] Dr. S. Ponrathnam, National Chemical Laboratory, India, Private Communication, (1998).

[Ryan, 98] D. P. Ryan, "Optical Experimental Data Processing using LabVIEW", Undergraduate project, Dublin Institute of Technology, (1999).

[Sadl, 75] N. Sadlej, B. Smolinska, "Stable photo-sensitive polymer layers for holography", Optics and Laser Technology, Pg. 175-179, (August, 1975).

[Sain, 99] P. Saint-George, "Composants diffractifs a mode du substrat: application", Undergraduate project, Universite de Liege, (1999).

[Shah, 98] M. S. Shahriar, L. Wong, B. Han, P. R. Hemmer, "Ultra-high density optical data storage", TOPS, Vol. 23, (1998).

[Sheri, 00] John T. Sheridan, Justin R. Lawrence, "Non-local response diffusion model of holographic recording in photopolymer", JOSA A, Vol. 17, No. 6, Pg. 1108-1114, (2000).

[Sigm, 99] Sigma-Aldrich Website, www.sigma-aldrich.com (1999).

[Smot, 90] W.K. Smothers, A. M. Weber, "Photopolymers for Holography", Practical Holography IV, Proc. SPIE Vol. 1212 Pg. 351-360, (1990).

[Solo, 96] T. W. Graham Solomons, *Organic Chemistry*, 6th edition, John Wiley & Sons, New York, U.S.A., (1996).

[Soly, 81] L. Solymar, D. J. Cooke, *Volume Holography and Volume Gratings*, Academic Press, London, U.K., 1981.

[Stec, 98] G. J. Steckman, I. Solomantine, G. Zhou, D. Psaltis, "Characterisation of phenanthrenequinone-doped poly(methyl methacrylate) for holographic memory", Optics Letters, Vol. 23, No. 16, Pg. 1310-1312, (1998).

[Suga, 75] S. Sugawara, K. Murase, T. Kitayama,"Holographic recording by dye-sesnitized photopolymerisation of acrylamide" Applied Optics,Vol. 14, No. 2, Pg. 378-382, (1975)

[Suke, 75] K. Sukegawa, S. Sugawara, K. Murase, "Holographic recording by Fe^{3+} sensitized photopolymerization", Electron. Commun. Jap. Vol. 58-C(11), Pg. 132-138, (1975).

[Suke, 77] K. Sukegawa, S. Sugawara, K. Murase; Rev. Elect. Comm. Labs., Vol. 25, **Pg.** 580, (1977).

[Wang, 88] C. H. Wang, J. L. Xia, "Holographic grating studies of the diffusion process of camphorquinone in polycarbonate above and below Tg", Macromolecules, Vol. 21, No. 12, Pg.3519-3523, (1988).

[Wolf, 96] S. Wolfram, *Mathematica* 3rd edition, Cambridge University Press, Cambridge, U.K., 1996.

[Webe, 90] A. M. Weber, W. K. Smothers, T. J. Trout, D. J. Mickish, "Hologram recording in DuPonts's new photopolymer material", Practical Holography IV, Proc. SPIE Vol. 1212, Pg. 30-39, (1990).

[Weis, 96] V. Weiss, E. Millul, A. A. Friesem, " Photpolymeric holographic recording me in-situ and real-time characterisation.", Proc. SPIE, Vol. 2688, Pg. 11-21, (1996).

[Wops, 72] R. H. Wopschall, T. R. Pampalone, "Dry photopolymer film for recording holograms", Applied Optics, Vol. 10, Pg. 1636-1641, (1971).

[Zakr, 87] A. Zakrzewski, D. C. Neckers, "Bleaching products of Rose Bengal under reducing conditions", Tetrahedron, Vol. 43, No. 20, Pg. 4507-4512, (1987).

[Zhao, 94] G. Zhao, P. Mouroulis, "Diffusion model of hologram formation in dry photopolymer materials", J. Mod. Optics, Vol. 41, No. 10, Pg. 1929-1939, (1994).

[Zhao, 98] F. Zhao, E. E. E. Frietmann, X. Li, "Novel type of red sensitive photopolymer system for optical storage", Proc. SPIE Vol. 3468, Pg. 317-321, (1998).

[Zhou, 95] H. J. Zhou, V. Morozov, J. Neff, "Characterisation of DuPont photoplymers in infrared light for free-space optical interconnects", Applied Optics, Vol. 34, No. 32, Pg.7457-7459, (1995).

Appendix A: Non-local Diffusion Model

In this appendix, the derivation of the set of coupled differential equations for non-local response medium from the standard diffusion equation will be presented.

$$\frac{\partial u(x,t)}{\partial t} = \frac{\partial}{\partial x}\left(D(x,t)\frac{\partial u(x,t)}{\partial x}\right) - \int_{-\infty}^{+\infty} \int_{0}^{t} R(x,x';t,t')F(x',t')u(x',t')dt'dx' \tag{A.1}$$

$$R(x-x') = \frac{e^{-(x-x')^2/2\sigma}}{\sqrt{2\pi\sigma}} \tag{A.2}$$

The diffusion equation (A.1) with the non-local response term R must be solved, given the following initial condition.

$$u(x,0) = U_0 = 100, \text{ for } -\infty < x < +\infty \tag{A.3}$$

In the case of symmetric two beam illumination, an unslanted sinusoidal transmission grating is recorded with the spatial intensity distribution

$$I(x,t) = I_0[1 + V\cos(Kx)] \tag{A.4}$$

I_0 is the average intensity in the medium, V is the fringe visibility, $K=2\pi/\Lambda$ is the grating vector magnitude and Λ is the grating period. It is assumed that the rate of polymerization is directly proportional to the exposing intensity and therefore

$$F(x,t) = F_0[1 + V\cos(Kx)]$$

(A.5)

Where $F_0 = \kappa I_0$, and κ is a fixed constant. The monomer concentration is also assumed to be an even periodic function of x with a fundamental spatial frequency K.

$$u(x,t) = \sum_{i=0}^{\infty} u_i(t)\cos(iKx)$$

(A.6)

Finally, the variation of the diffusion constant is also assumed to vary periodically as a function of the polymer distribution. It is expanded as

$$D(x,t) = \sum_{i=0}^{\infty} D_i(t)\cos(iKx)$$

(A.7)

It is assumed that the variation of the diffusion coefficient can be expressed as a Fourier series. We now truncate this expansion assuming that only the first two terms must be retained.

$$D(x,t) = D_0(t) + D_1(t)\cos(Kx)$$

(A.8)

This assumption has previously been examined for the local response case and was shown to be acceptable, since the first or average term dominates except in cases of high non-linearity [Zhao, 94]. This assumption is re-evaluated in this paper for the case of a non-local response. The diffusion constant is assumed to decay exponentially as a function of the polymerization

rate. The maximum and minimum of the diffusion rate corresponding to the maximum and minimum of the exposing interference pattern are then given by

$$D_{\max}(t) = D_a e^{-\alpha F_0 (1-V)t}$$

(A.9)

$$D_{\min}(t) = D_a e^{-\alpha F_0 (1+V)t}$$

(A.10)

D_a represents the initial diffusion constant. In the exponents the α term is a diffusion constant decay parameter. Comparing the results in Equation (A.9) and (A.10) it can be shown that

$$D_0(t) = \frac{1}{2}\left[D_{\max}(t) + D_{\min}(t)\right] = D_a e^{-\alpha F_0 t} \cosh(\alpha F_0 V t)$$

(A.11)

$$D_1(t) = \frac{1}{2}\left[D_{\max}(t) - D_{\min}(t)\right] = -D_a e^{-\alpha F_0 t} \sinh(\alpha F_0 V t)$$

(A.12)

We now introduce the variable ξ, which is proportional to the exposure energy

$$\xi = F_0 t = \kappa I_0 t$$

(A.13)

We now substitute from Equation (A.2) into Equation (A.1)

$$\frac{\partial u(x,t)}{\partial t} = \frac{\partial D(x,t)}{\partial x}\frac{\partial u(x,t)}{\partial x} + D(x,t)\frac{\partial^2 u(x,t)}{\partial x^2} - \int_{-\infty}^{\infty} \frac{e^{-(x-x')^2/2\sigma}}{\sqrt{2\pi\sigma}} F(x',t) u(x',t) dx'$$

(A.14)

We rewrite the first-order coupled-concentration equations in terms of this variable

$$\frac{du_0(\xi)}{d\xi} = -u_0(\xi) - \frac{V}{2}u_1(\xi)$$

(A.15)

$$\frac{du_1(\xi)}{d\xi} = -V e^{-K^2\sigma^2} u_0(t) - \left[e^{-K^2\sigma^2} + \frac{K^2 D_0(\xi)}{F_0}\right]u_1(\xi) - \left[\frac{V}{2}e^{-K^2\sigma^2} + \frac{K^2 D_1(\xi)}{F_0}\right]u_2(\xi)$$

(A.16)

which can be rewritten:

$$\frac{du_1(\xi)}{d\xi} = -Ve^{-K^2\sigma^2}u_0(t) - \left[e^{-K^2\sigma^2} + \frac{K^2}{F_0}D_a e^{-\alpha\xi}\cosh(\alpha V\xi)\right]u_1(\xi)$$

$$-\left[\frac{V}{2}e^{-K^2\sigma^2} - \frac{K^2}{F_0}D_a e^{-\alpha\xi}\sinh(\alpha V\xi)\right]u_2(\xi)$$

(A.17)

$$\frac{du_2(\xi)}{d\xi} = -\left[e^{-(2K)^2\sigma^2} + \frac{(K2)^2 D_0(\xi)}{F_0}\right]u_2(\xi)$$

$$-\left[\frac{V}{2}e^{-(2K)^2\sigma^2} + \frac{K^2}{F_0}D_1(\xi)\right]u_1(\xi) - \left[\frac{V}{2}e^{-(2K)^2\sigma^2} + \frac{3K^2}{F_0}D_1(\xi)\right]u_3(\xi)$$

(A.18)

which can be rewritten:

$$\frac{du_2(\xi)}{d\xi} = -\left[e^{-(2K)^2\sigma^2} + \frac{(K2)^2}{F_0}D_a e^{-\alpha\xi}\cosh(\alpha V\xi)\right]u_2(\xi)$$

$$-\left[\frac{V}{2}e^{-(2K)^2\sigma^2} - \frac{K^2}{F_0}D_a e^{-\alpha\xi}\sinh(\alpha V\xi)\right]u_1(\xi)$$

$$-\left[\frac{V}{2}e^{-(2K)^2\sigma^2} - \frac{3K^2}{F_0}D_a e^{-\alpha\xi}\sinh(\alpha V\xi)\right]u_3(\xi)$$

(A.19)

$$\frac{du_3(\xi)}{d\xi} = -\left[e^{-(3K)^2\sigma^2} + \frac{(K3)^2 D_0(\xi)}{F_0}\right]u_3(\xi) - \left[\frac{V}{2}e^{-(3K)^2\sigma^2} + \frac{3K^2 D_1(\xi)}{F_0}\right]u_2(\xi)$$

(A.20)

which can be rewritten:

$$\frac{\partial u_3(\xi)}{\partial \xi} = -\left[e^{-(3K)^2\sigma^2} + \frac{(K3)^2}{F_0}D_a e^{-\alpha\xi}\cosh(\alpha V\xi)\right]u_3(\xi)$$

$$-\left[\frac{V}{2}e^{-(3K)^2\sigma^2} + \frac{3K^2}{F_0}D_a e^{-\alpha\xi}\sinh(\alpha V\xi)\right]u_2(\xi)$$

(A.21)

Furthermore we introduced a lumped parameter R, which is the ratio between the diffusion rate, $D_a K^2$, and the polymerization rate, F_0.

$$R = \frac{D_a K^2}{F_0}$$

(A.22)

Using this notation a concise form of the four first-order coupled-concentration equations can be derived:

$$\frac{du_0(\xi)}{d\xi} = -u_0(\xi) - \frac{V}{2}u_1(\xi)$$

(A.23)

$$\frac{du_1(\xi)}{d\xi} = -Ve^{-K^2\sigma^2}u_0(t) - \left[e^{-K^2\sigma^2} + \mathrm{Re}^{-\alpha\xi}\cosh(\alpha V\xi)\right]u_1(\xi)$$

$$-\left[\frac{V}{2}e^{-K^2\sigma^2} + \mathrm{Re}^{-\alpha\xi}\sinh(\alpha V\xi)\right]u_2(\xi)$$

(A.24)

$$\frac{du_2(\xi)}{d\xi} = -\left[e^{-K^2\sigma^2/2} + 4\mathrm{Re}^{-\alpha\xi}\cosh(\alpha V\xi)\right]u_2(\xi)$$
$$-\left[\frac{V}{2}e^{-K^2\sigma^2/2} - \mathrm{Re}^{-\alpha\xi}\sinh(\alpha V\xi)\right]u_1(\xi)$$
$$-\left[\frac{V}{2}e^{-K^2\sigma^2/2} - 3\mathrm{Re}^{-\alpha\xi}\sinh(\alpha V\xi)\right]u_3(\xi)$$

(A.25)

$$\frac{du_3(\xi)}{d\xi} = -\left[e^{-(3K)^2\sigma^2/2} + 9\mathrm{Re}^{-\alpha\xi}\cosh(\alpha V\xi)\right]u_3(\xi)$$
$$-\left[\frac{V}{2}e^{-(3K)^2\sigma^2/2} + 3\mathrm{Re}^{-\alpha\xi}\sinh(\alpha V\xi)\right]u_2(\xi)$$

(A.26)

These first-order coupled-concentration equations must now be solved under the boundary conditions given in Equation (A.3).

The resulting concentration of polymerized monomer, after an exposure of duration t seconds, is given by

$$N(x,t) = \int_0^t \int_{-\infty}^{\infty} R(x-x')F(x',t'')u(x',t'')dx'dt''$$

(A.27)

This is can be shown to be equal to

$$N(x,t) = F_0 \sum_{i=0}^{+\infty} \left\{ \int_0^t u_i(t'')dt'' \right\} \left\{ e^{-(iK)^2\sigma^2/2} \cos(iKx) \right.$$

$$\left. + (V/2)\left[e^{-K^2(1-i)^2\sigma^2/2} \cos((1-i)Kx) + e^{-K^2(1+i)^2\sigma^2/2} \cos((1+i)Kx) \right] \right\}$$

(A.28)

This resulting distribution of polymerised material is of the form

$$N(x,t) = N_0(t) + N_1(t)\cos(Kx) + N_2(t)\cos(2Kx) + ...$$

(A.29)

Using the parameter ξ, the individual lower harmonic coefficients of the concentration of monomer, can be equated to expressions in terms of the monomer concentration

$$N_0(\xi) = \int_0^{\xi} \left[u_0(\xi'') + (V/2)u_1(\xi'') \right] d\xi''$$

(A.30)

$$N_1(\xi) = e^{-K^2\sigma^2/2} \int_0^{\xi} \left[Vu_0(\xi'') + u_1(\xi'') + (V/2)u_2(\xi'') \right] d\xi''$$

(A.31)

$$N_2(\xi) = e^{-2K^2\sigma} \int_0^{\xi} \left[(V/2)u_1(\xi'') + u_2(\xi'') + (V/2)u_3(\xi'') \right] d\xi''$$

(A.32)

$$N_3(\xi) = e^{-9K^2\sigma^2/2} \int_0^{\xi} \left[(V/2)u_2(\xi'') + u_3(\xi'') \right] d\xi''$$

(A.33)

It is now assumed that the modulation of the refractive index induced during recording is approximately linearly related to the polymer concentration. Therefore each of the above terms corresponds to a change in the size of a spatial frequency component of a grating pattern recorded in the volume.

$$n(x,\xi) = n_{av} + C\sum_{i=0}^{+\infty} N_i(\xi)\cos(iKx) \tag{A.34}$$

It is now assumed that the modulation of the refractive index induced during recording is approximately linearly related to the polymer concentration. Therefore each of the above terms corresponds to a change in the size of a spatial frequency component of a grating pattern recorded in the volume.

$$n(x,\xi) = n_{av} + C\sum_{i=0}^{\infty} N_i(\xi)\cos(iKx) \tag{A.34}$$

Appendix B: Comparison of Numerical and Analytic Non-local Zhao Models

This appendix contains a more complete set of graphs plotted when comparing the numerical four harmonic and the analytic two harmonic models from Chapter 4.

In all figures R is the ratio of the rate of polymerisation to the rate of diffusion, σ is the non-local variance which is normalised with respect to the period, u_0 and u_1 are the zeroth and first harmonics of monomer concentration respectively. N_0 and N_1 are the zeroth and first harmonics of polymer concentration, x is the grating period and $\xi = \kappa I t$ which is the exposure energy.

In all cases, (a) shows the monomer concentrations, u_0 and u_1, plotted against ξ, (b) shows the polymer concentrations, N_0 and N_1, against ξ and (c) shows the saturated polymer concentrations at $\xi = 10$ against the grating period. It should be noted that the saturated polymer concentration is proportional to refractive index modulation.

Figure B.1 R= 0.05, σ = 0 Numerical solid line, Analytic dashed line

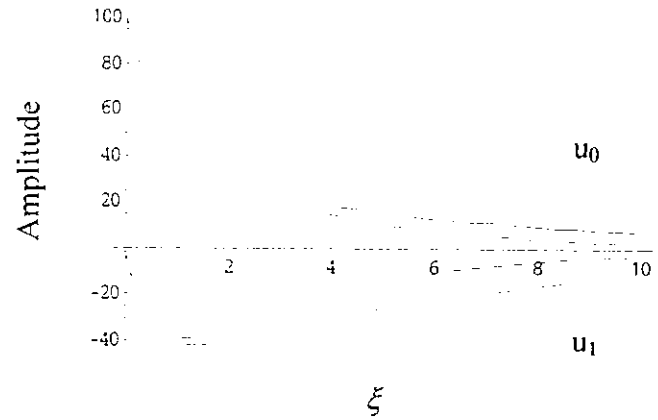

(a)

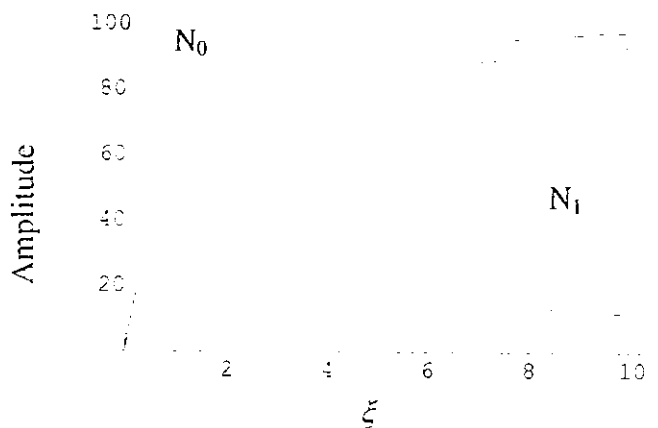

(b)

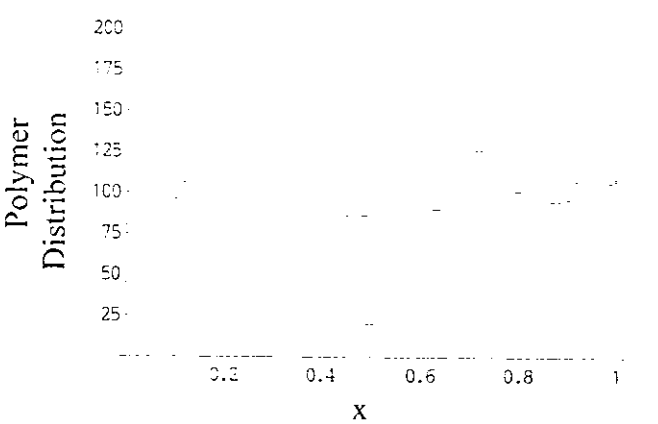

(c)

Figure B.2 R = 0.05, σ = 1/64 Numerical solid line, Analytic dashed line

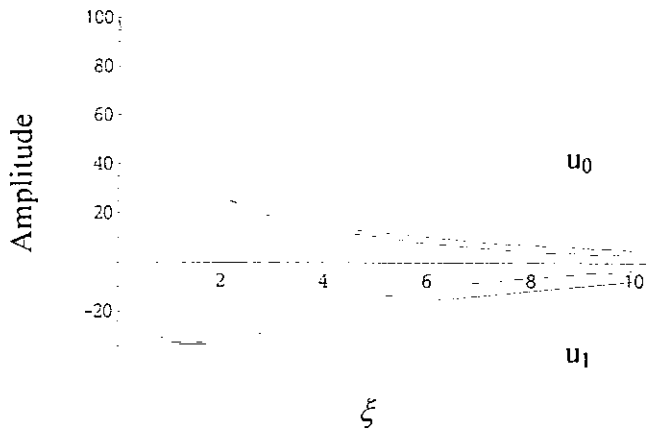

(a)

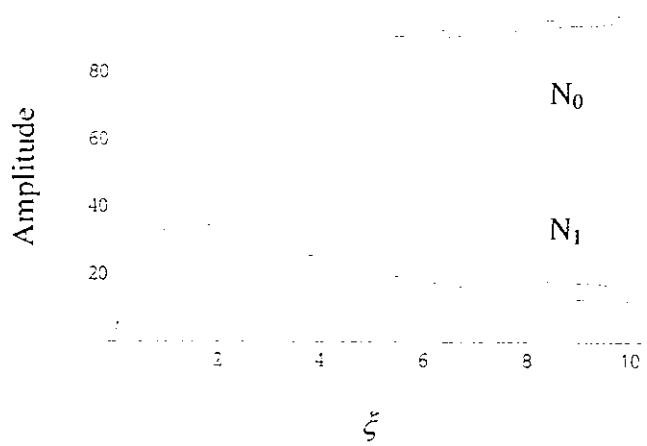

(b)

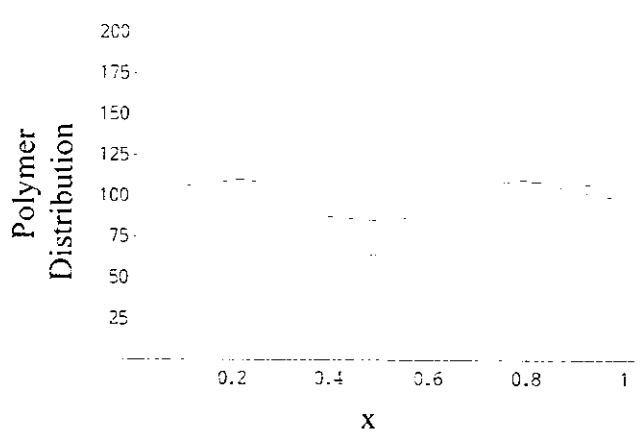

(c)

Figure B.3 R = 0.05, σ = 1/32 Numerical solid line, Analytic dashed line

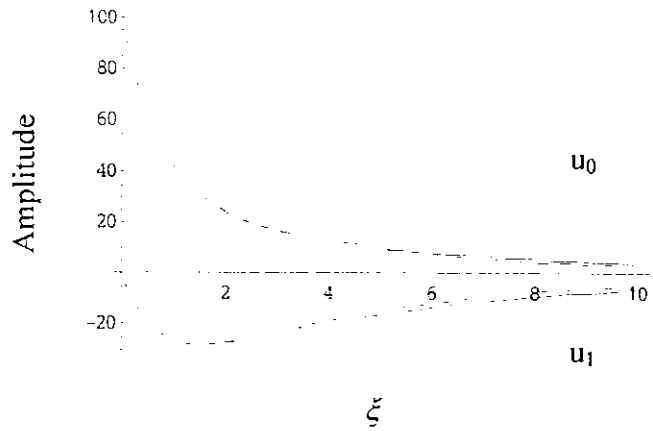

(a)

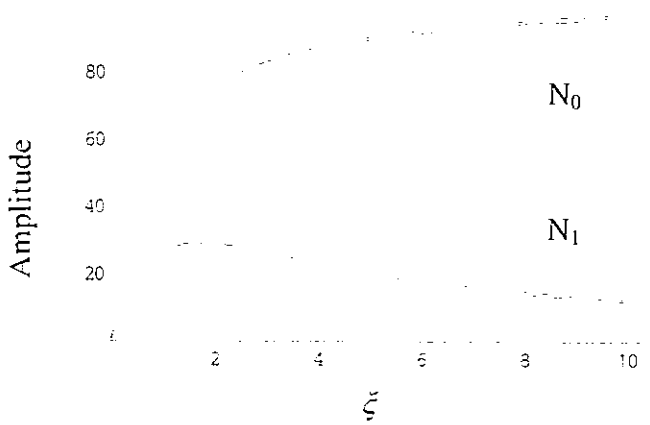

(b)

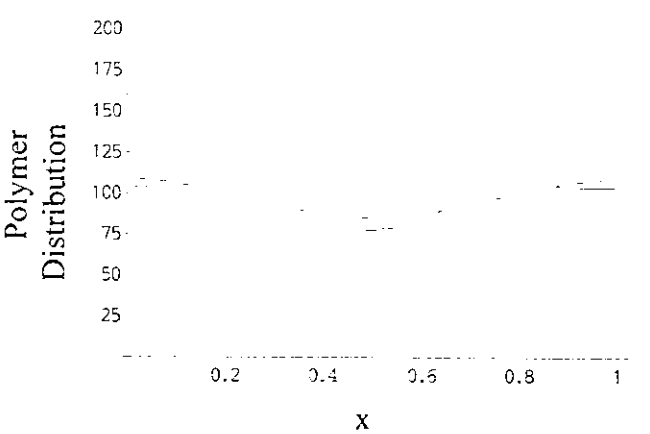

(c)

Figure B.4 R = 1, σ = 0, Numerical solid line, Analytic dashed line

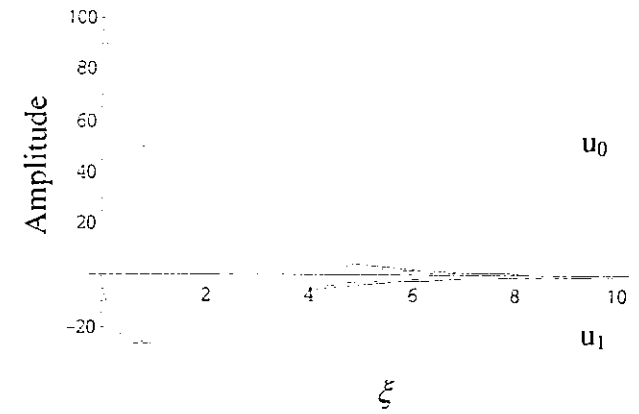

(a)

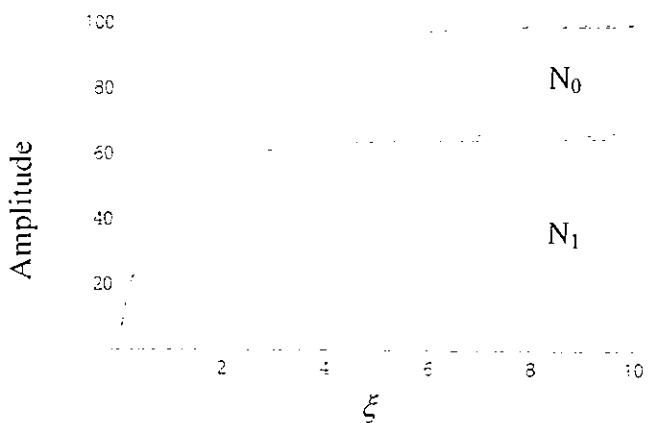

(b)

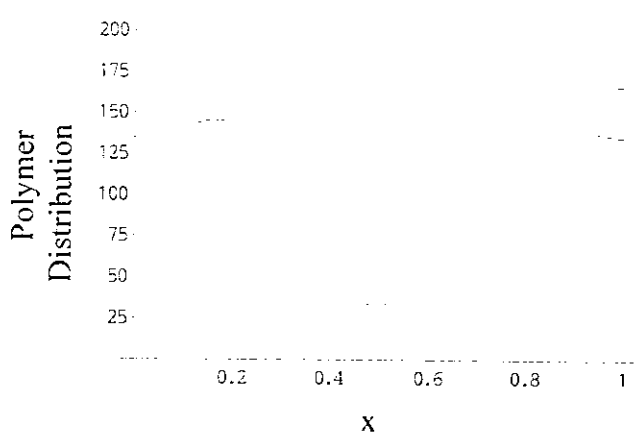

(c)

Figure B.5 R = 1, σ = 1/64, Numerical solid line, Analytic dashed line

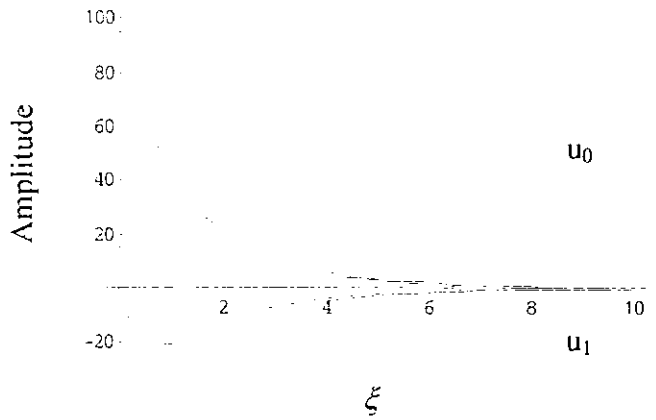

(a)

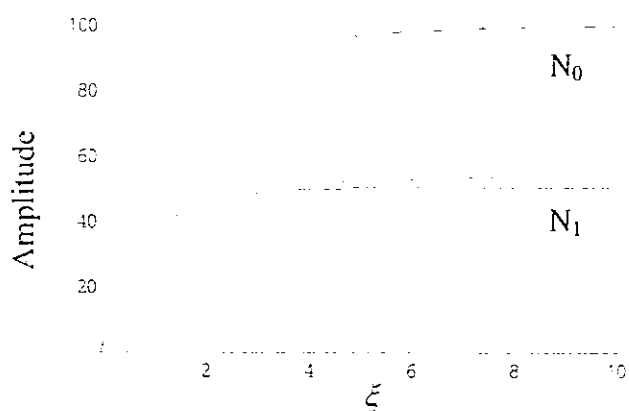

(b)

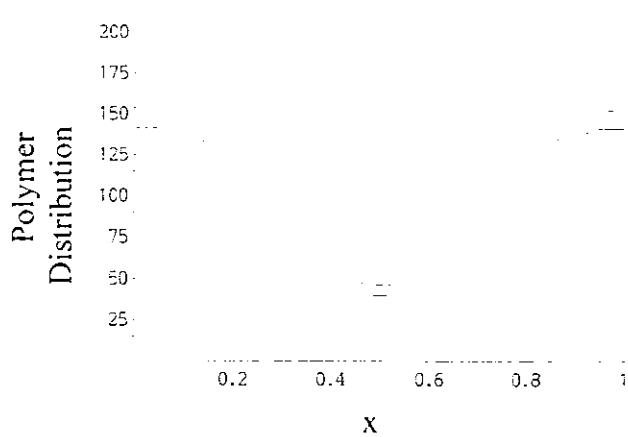

(c)

Figure B.6 R = 1, σ = 1/32, Numerical solid line, Analytic dashed line

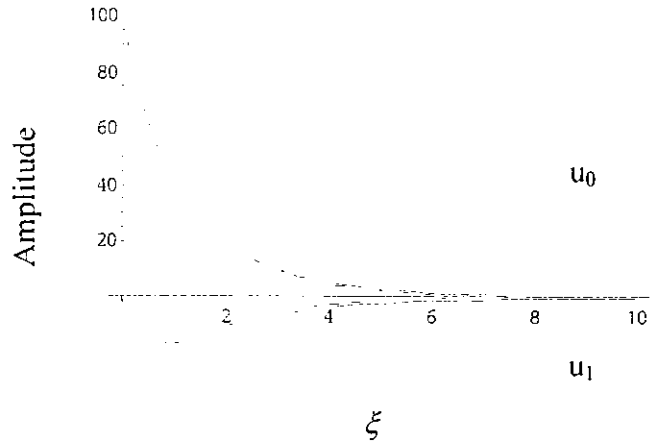

(a)

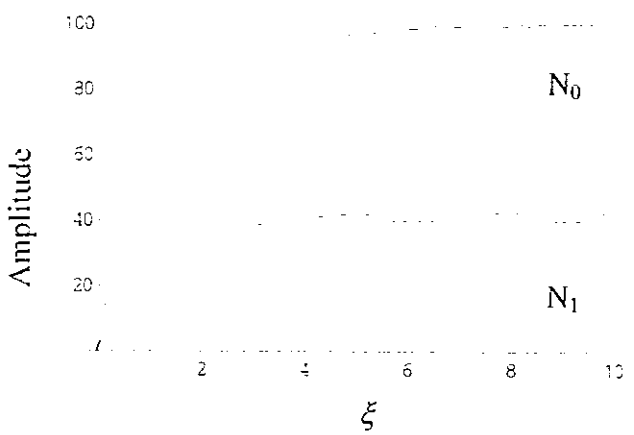

(b)

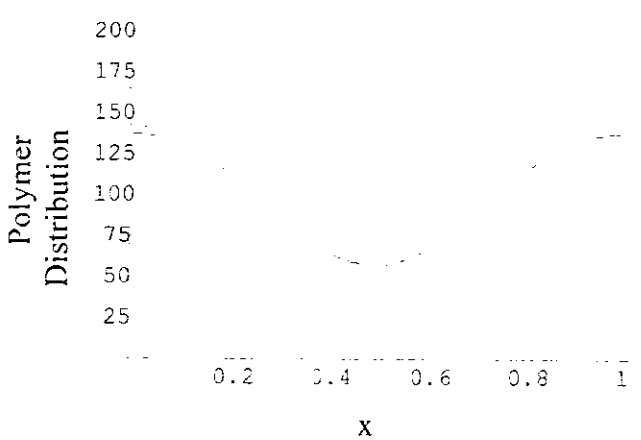

(c)

Figure B.7 R = 50, σ = 0, Numerical solid line, Analytic dashed line

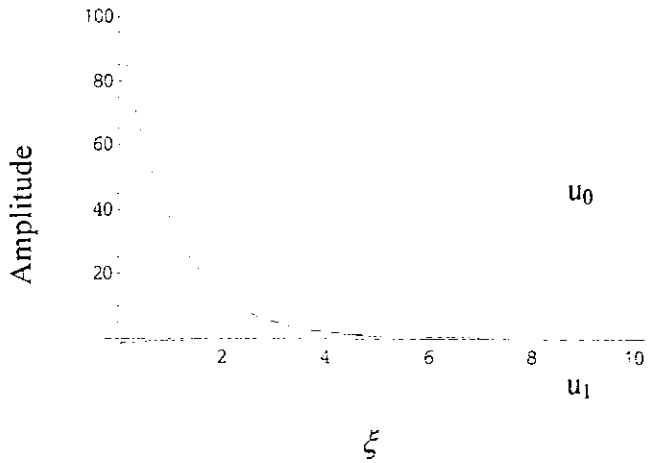

(a)

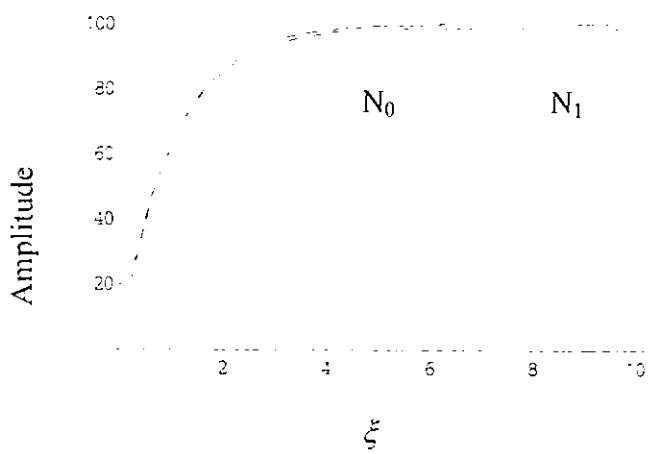

(b)

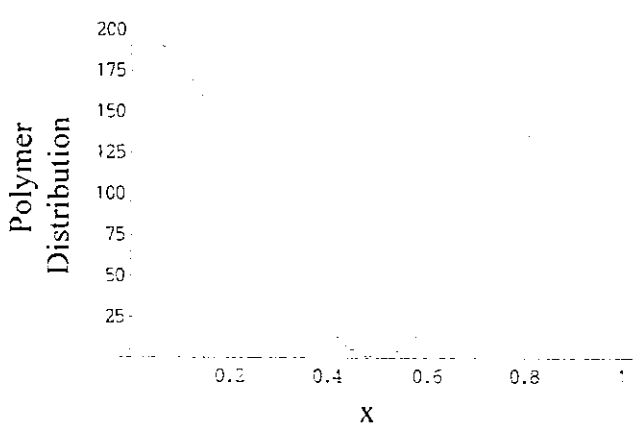

(c)

Figure B.8 R = 50, σ = 1/64, Numerical solid line, Analytic dashed line

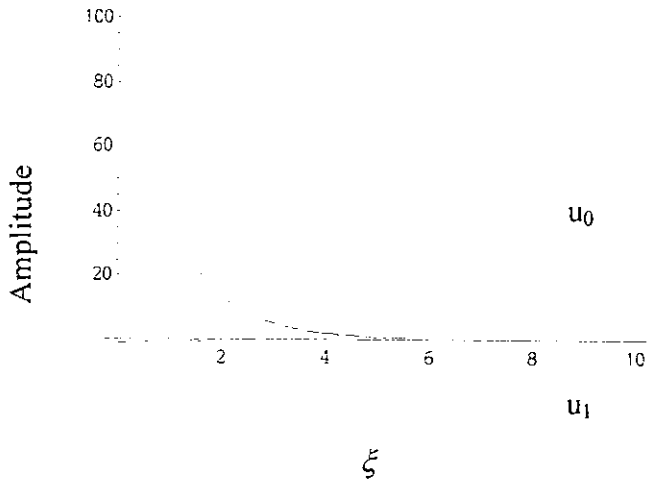

(a)

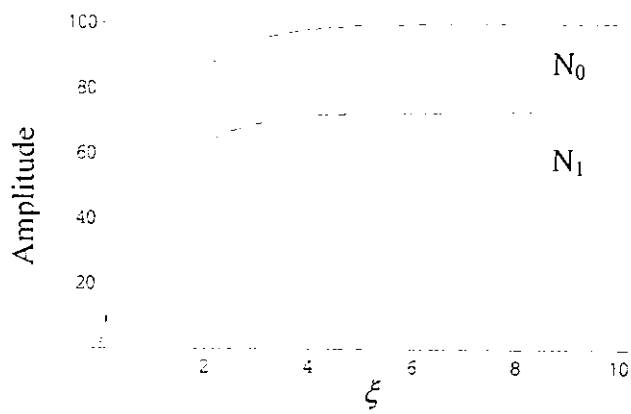

(b)

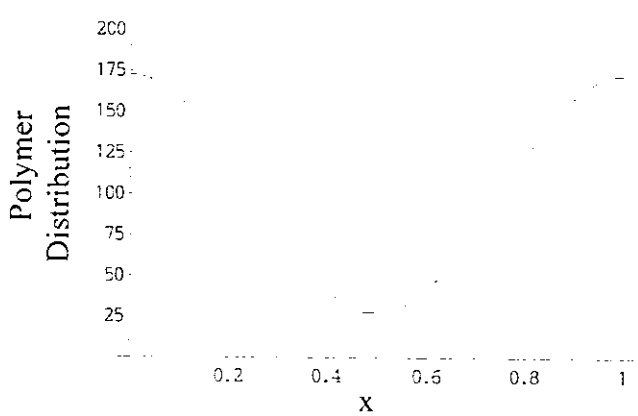

(c)

Figure B.9 R = 50, σ = 1/32, Numerical solid line, Analytic dashed line

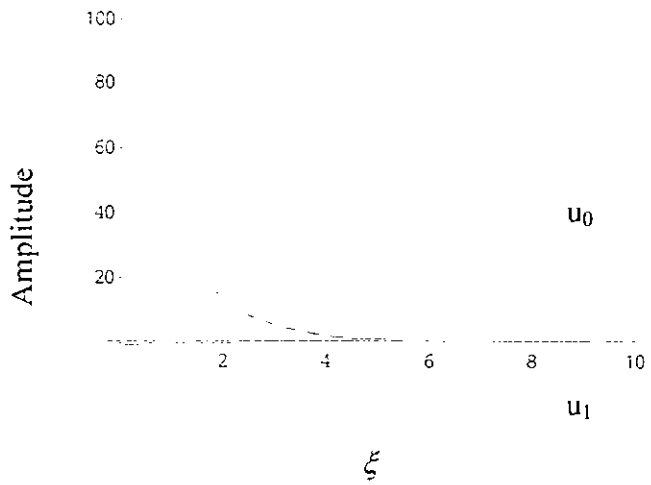

(a)

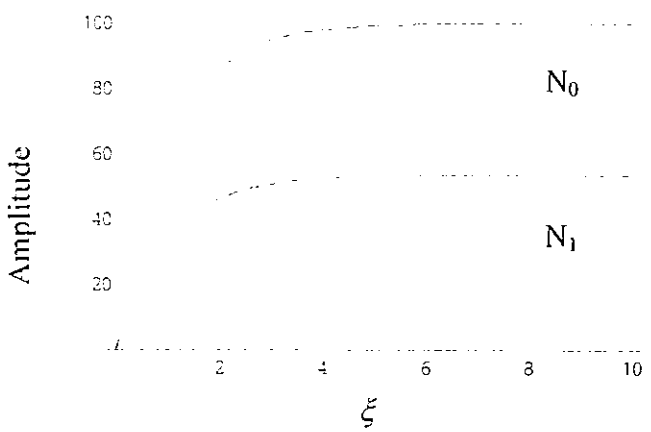

(b)

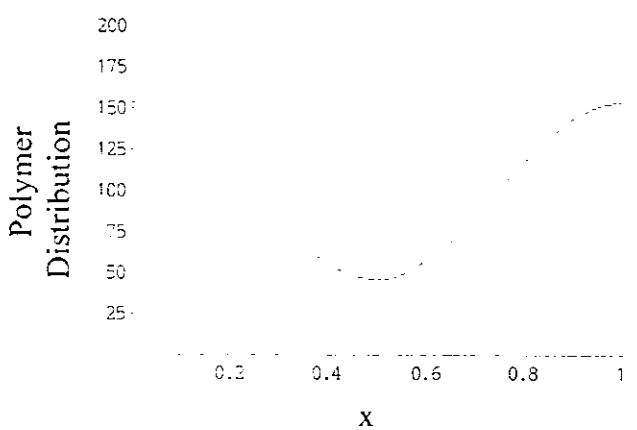

(c)

Appendix C: Polynomial Curve Fitting

In this section, the procedures used to manipulate and fit the data will be outlined.

1. The data is captured by the software as intensity versus time. The software then converts the intensity to diffraction efficiency. An example of this data was shown in Figure (6.10).
2. The diffraction efficiency is adjusted for Fresnel losses using the equations from Born and Wolf [Born, 80].
3. The corrected diffraction efficiency data is converted to refractive index modulation by applying Kogelnik's coupled wave theory as discussed in Section (1.1.3). The time data is converted to exposure intensity by multiplying by Fresnel corrected I_0. This data is shown in Figure B.1 below

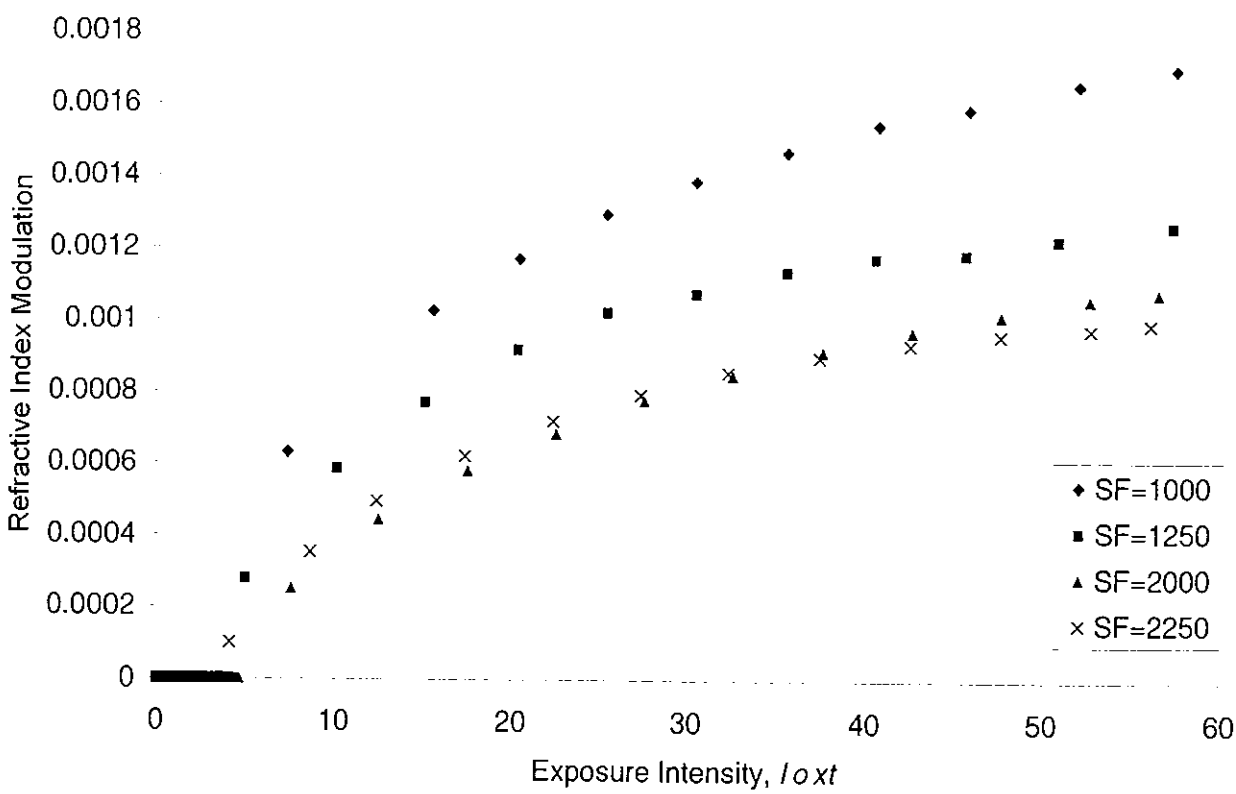

Figure B.1 Experimental data, corrected for Fresnel losses and converted to refractive index modulation and exposure intensity I_0xt.

4. For the polynomial fits only data close to $I_0 \times t$ is fitted.

As mentioned in Chapter 4, the resolution of the gathered data was low. It can been seen from Figure B.2 below, that each set of data has a number points at zero.

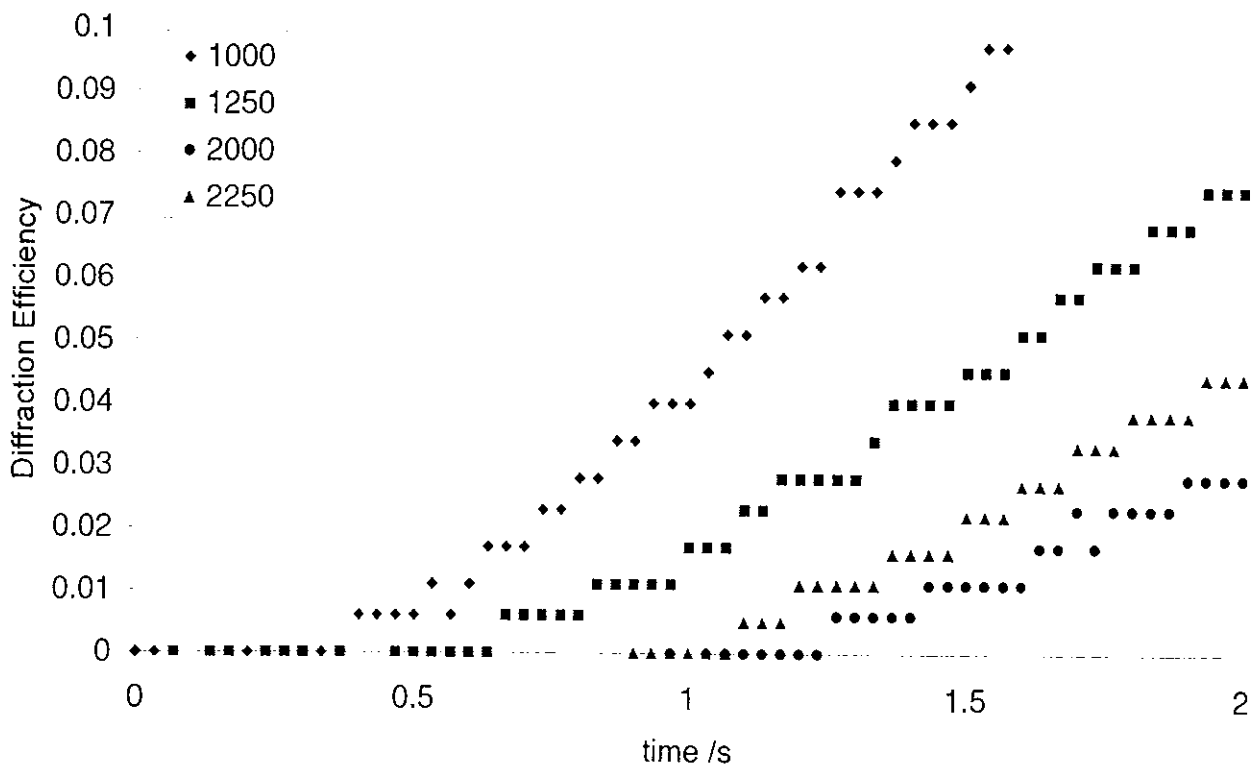

Figure B.2 Step behaviour of experimental data close to zero for different spatial frequencies.

When the graphs are converted to refractive index modulation against corrected exposure energy, $I_0 \times t$ this caused problems when fitting polynomial curves. To overcome this, a constant energy value was subtracted from each point so that the first coefficient of each polynomial (the D.C. term) was as close to zero as possible. This resulted in the curves given in Chapters 4 and 5.

This section contains the full set of coefficients obtained from polynomial fits of increasing order to experimental growth curves. See section 4.2.

SF=1000

x0	$[a_1^{(n)}K]$	$[a_2^{(n)}K]$	$[a_3^{(n)}K]$	$[a_4^{(n)}K]$	$[a_5^{(n)}K]$	$[a_6^{(n)}K]$
4.844410E-13	1.071600E-04					
8.688820E-13	1.450680E-04	-7.679460E-06				
4.497350E-13	1.858910E-04	-2.962290E-05	3.151270E-06			
1.919180E-13	2.351610E-04	-7.891220E-05	2.014380E-05	-1.903240E-06		
2.203450E-12	3.667540E-04	-3.015050E-04	1.598100E-04	-3.890780E-05	3.497520E-06	
2.520100E-12	6.119020E-04	-9.786280E-04	8.495670E-04	-3.611280E-04	7.353610E-05	-5.742630E-06

SF=1250

x0	$[a_1^{(n)}K]$	$[a_2^{(n)}K]$	$[a_3^{(n)}K]$	$[a_4^{(n)}K]$	$[a_5^{(n)}K]$	$[a_6^{(n)}K]$
2.687970E-13	7.448450E-05					
2.548350E-13	1.077500E-04	-5.061820E-06				
7.966190E-13	1.338670E-04	-1.554700E-05	1.126020E-06			
1.717230E-12	1.910470E-04	-5.884830E-05	1.251180E-05	-9.790320E-07		
1.673250E-13	2.854670E-04	-1.812680E-04	7.140660E-05	-1.295390E-05	8.688010E-07	
1.120660E-12	4.665740E-04	-5.595640E-04	3.654110E-04	-1.182540E-04	1.847020E-05	-1.112180E-06

SF=2000

x0	$[a_1^{(n)}K]$	$[a_2^{(n)}K]$	$[a_3^{(n)}K]$	$[a_4^{(n)}K]$	$[a_5^{(n)}K]$	$[a_6^{(n)}K]$
3.935367E-14	5.208151E-05					
8.176969E-14	9.082422E-05	-5.617744E-06				
7.400539E-13	1.329480E-04	-2.303929E-05	1.876807E-06			
3.902516E-14	1.713345E-04	-5.294710E-05	9.710031E-06	-6.638766E-07		
8.705924E-13	2.789282E-04	-1.944654E-04	7.769672E-05	-1.444694E-05	9.978996E-07	
2.371816E-12	4.182660E-04	-4.873121E-04	3.040786E-04	-9.487352E-05	1.431459E-05	-8.326159E-07

SF=2250

x0	$[a_1^{(n)}K]$	$[a_2^{(n)}K]$	$[a_3^{(n)}K]$	$[a_4^{(n)}K]$	$[a_5^{(n)}K]$	$[a_6^{(n)}K]$
1.130930E-13	5.757930E-05					
9.387670E-13	9.875080E-05	-6.174110E-06				
6.499860E-13	1.503790E-04	-2.854000E-05	2.510930E-06			
4.199030E-13	1.966480E-04	-6.696760E-05	1.308060E-05	-9.329830E-07		
2.692480E-12	3.179360E-04	-2.373890E-04	9.885940E-05	-1.898430E+00	1.349820E-06	
3.127160E-12	4.575300E-04	-5.464770E-04	3.465150E-04	-1.095510E-04	1.673040E-05	-9.842570E-07

Table B.1 Coefficients of the linear, first, second, third, fourth, fifth and sixth order polynomials to each spatial frequency growth curve.

SF=1000	r^2	κ $m^2/W/s$	C l/mol	R
Linear	0.971602			
1st order	0.977117	0.052937	2.7404E-05	
2nd order	0.978102	0.159356	1.1665E-05	0.50535
3rd order	0.978475	0.335567	7.0079E-06	1.06425
4th order	0.979766	0.822091	4.4612E-06	0.36849
5th order	0.983276	1.599321	3.8260E-06	-0.24317
	Mean	**0.593854**	**1.0873E-05**	**0.42373**

SF=1250	r^2	κ $m^2/W/s$	C l/mol	R
Linear	0.968987			
1st order	0.977079	0.046977	2.2937E-05	
2nd order	0.977776	0.116138	1.1527E-05	0.24178
3rd order	0.978677	0.308030	6.2022E-06	0.64136
4th order	0.979879	0.634988	4.4956E-06	0.22223
5th order	0.983184	1.199304	3.8904E-06	-0.23296
	Mean	**0.461087**	**9.8103E-06**	**0.21810**

SF=2000	r^2	κ $m^2/W/s$	C l/mol	R
Linear	0.939539			
1st order	0.959723	0.061853	1.4684E-05	
2nd order	0.963723	0.173295	7.6718E-06	-0.67958
3rd order	0.964598	0.309028	5.5443E-06	0.06067
4th order	0.968015	0.697188	4.0008E-06	-0.06156
5th order	0.972089	1.165077	3.5900E-06	-0.28652
	Mean	**0.481288**	**7.0981E-06**	**-0.24175**

SF=2250	r^2	κ $m^2/W/s$	C l/mol	R
Linear	0.951184			
1st order	0.971046	0.062522	1.5795E-05	
2nd order	0.976780	0.189787	7.9236E-06	-0.71859
3rd order	0.978138	0.340546	5.7745E-06	-0.05857
4th order	0.982964	0.746657	4.2581E-06	-0.15352
5th order	0.987274	1.194407	3.8306E-06	-0.31471
	Mean	**0.506784**	**7.5163E-06**	**-0.31135**

Table B.2 The correlation coefficient r^2 for each order polynomial along with the calculated values of κ, C and R. for the non-local Zhao model.

SF=1000	r^2	κ m/W^{-2}/s	C l/mol	R
Linear	0.971602			
1st order	0.977117	0.269884	5.3752E-06	
2nd order	0.978102	0.812432	2.28808E-06	-1.47054
3rd order	0.978475	1.710789	1.37458E-06	-1.20253
4th order	0.979766	4.191189	8.7506E-07	-1.53617
5th order	0.983276	8.153674	7.50462E-07	-1.82947
	Mean	**3.027593**	**2.133E-06**	**-1.50968**

SF=1250	r^2	κ m/W^{-2}/s	C l/mol	R
Linear	0.968987			
1st order	0.977079	0.238875	4.51073E-06	
2nd order	0.977776	0.590546	2.26683E-06	-1.80024
3rd order	0.978677	1.566298	1.21974E-06	-1.63034
4th order	0.979879	3.228835	8.84118E-07	-1.80855
5th order	0.983184	6.098316	7.65087E-07	-2.00209
	Mean	**2.344574**	**1.929E-06**	**-1.81031**

SF=2000	r^2	κ m/W^{-2}/s	C l/mol	R
Linear	0.939539			
1st order	0.959723	0.310228	2.92766E-06	
2nd order	0.963723	0.869176	1.52959E-06	-2.04391
3rd order	0.964598	1.549950	1.10542E-06	-1.69031
4th order	0.968015	3.496796	7.97668E-07	-1.74870
5th order	0.972089	5.843526	7.15777E-07	-1.85616
	Mean	**2.413935**	**1.415E-06**	**-1.83477**

SF=2250	r^2	κ m/W^{-2}/s	C l/mol	R
Linear	0.951184			
1st order	0.971046	0.311084	3.17441E-06	
2nd order	0.976780	0.944302	1.59249E-06	-2.04111
3rd order	0.978138	1.694413	1.16057E-06	-1.72074
4th order	0.982964	3.715053	8.55805E-07	-1.76683
5th order	0.987274	5.942873	7.6988E-07	-1.84507
	Mean	**2.521545**	**1.511E-06**	**-1.84344**

Table B.3 The correlation coefficient r^2 for each order polynomial along with the calculated values of κ, C and R using the analytic non-local Kwon model, see section 5.5.

Appendix D: General Intensity Non-local Model.

In this appendix, the derivation of the set of coupled differential equations for non-local response medium from the standard diffusion equation with a general form of intensity dependence will be presented. It should be noted that we are not following Kwon et. al. [Kwon, 99] numerical method as they do not present an analytic solution.

$$\frac{\partial u(x,t)}{\partial t} = \frac{\partial}{\partial x}\left(D(x,t)\frac{\partial u(x,t)}{\partial x}\right) - \int_{-\infty}^{+\infty}\int_{0}^{t} R(x,x';t,t')F(x',t')u(x',t')dt'dx' \tag{D.1}$$

$$R(x-x') = \frac{e^{-(x-x')^2/2\sigma}}{\sqrt{2\pi\sigma}} \tag{D.2}$$

The diffusion equation (D.1) with the non-local response term R must be solved, given the following initial condition.

$$u(x,0) = U_0 = 100, \text{ for } -\infty < x < +\infty \tag{D.3}$$

In the case of symmetric two beam illumination, an unslanted sinusoidal transmission grating is recorded with the spatial intensity distribution

$$I(x,t) = \{I_0[1+V\cos(Kx)]\}^{1/2} \tag{D.4}$$

I_0 is the average intensity in the medium, V is the fringe visibility, $K=2\pi/\Lambda$ is the grating vector magnitude and Λ is the grating period. We assume that the rate of polymerisation is directly proportional to the exposing intensity and therefore

$$F(x,t) = F_0[1 + V\cos(Kx)]^{1/2} \tag{D.5}$$

$F'_0 = \kappa'(I_0)^{1/2} = Q = k_p\left[\frac{\phi I_0(1-T)}{k_t}\right]^{1/2}$, κ a fixed constant. The monomer concentration is also assumed to be an even periodic function of x with a fundamental spatial frequency K.

$$u(x,t) = \sum_{i=0}^{-\infty} u_i(t)\cos(iKx) \tag{D.6}$$

Finally, the variation of the diffusion constant is also assumed to vary periodically as a function of the polymer distribution. It is expanded as

$$D(x,t) = \sum_{i=0}^{+\infty} D_i(t)\cos(iKx) \tag{D.7}$$

We also expand the rate of polymerisation F(x, t) as a Fourier series assuming V = 1.

$$F(x,t) = F_0[1+\cos(Kx)]^{1/2} = F_0\left[f_0 + \sum_{m=1}^{+\infty} f_m(t)\cos(mKx)\right] \tag{D.8}$$

where

$$f_0 = \frac{2\sqrt{2}}{\pi}, \quad f_m(t) = \frac{16\sqrt{2}m\cos(m\pi)[-1+2m\sin(m\pi)]}{(-1+2m)(1+2m)[4m\pi+\sin(4m\pi)]}$$

We now substitute from Equation (D.2) into Equation (D.1)

$$\frac{\partial u(x,t)}{\partial t} = \frac{\partial D(x,t)}{\partial x}\frac{\partial u(x,t)}{\partial x} + D(x,t)\frac{\partial^2 u(x,t)}{\partial x^2} - \int_{-\infty}^{+\infty} \frac{e^{-(x-x')^2/2\sigma}}{\sqrt{2\pi\sigma}} F(x',t)u(x',t)dx'$$

(D.9)

and then substituting into Equation (D.9) from Equations (D.4), (D.7) and (D.8) gives that

$$\sum_{i=0}^{+\infty} \frac{du_i(t)}{dt}\cos(iKx) = \left(-\sum_{i=0}^{+\infty} iKD_i(t)\sin(iKx)\right)\left(-\sum_{i=0}^{+\infty} iKu_i(t)\sin(iKx)\right)$$

$$+\left(\sum_{i=0}^{+\infty} D_i(t)\cos(iKx)\right)\left(-\sum_{i=0}^{+\infty} (iK)^2 u_i(t)\cos(iKx)\right)$$

$$-\int_{-\infty}^{+\infty} \frac{e^{-(x-x')^2/2\sigma}}{\sqrt{2\pi\sigma}} F_0\left[f_0 + \sum_{m=1}^{+\infty} f_m(t)\cos(mKx)\right]\sum_{i=0}^{+\infty} u_i(t)\cos(iKx')dx'$$

(D.10)

The final term in equation (D.10) can be rewritten as follows

$$-\frac{F_0}{\sqrt{2\pi\sigma}}\sum_{i=0}^{+\infty} u_i(t)\int_{-\infty}^{+\infty}\left[f_0 + \sum_{m=1}^{+\infty} f_m(t)\cos(mKx')\right]\cos(iKx')e^{-(x-x')^2/2\sigma}dx'$$

which is equal to

$$-F_0\sum_{i=0}^{+\infty} u_i(t)\left\{ f_0 e^{-(iK)^2\sigma^2/2}\cos(iKx)\right.$$

$$\left.+\sum_{m=1}^{\infty}\frac{f_m}{2}\left[e^{-K^2(m-i)^2\sigma^2/2}\cos((m-i)Kx) + e^{-K^2(m+i)^2\sigma^2/2}\cos((m+i)Kx)\right]\right\}$$

(D.11)

Returning to equation (D.9) we now have the equation

$$\sum_{i=0}^{+\infty} \frac{du_i(t)}{dt}\cos(iKx) = \left(-\sum_{m=0}^{+\infty} mKD_m(t)\sin(mKx)\right)\left(-\sum_{n=0}^{+\infty} nKu_n(t)\sin(nKx)\right)$$

$$+\left(\sum_{p=0}^{+\infty} D_p(t)\cos(pKx)\right)\left(-\sum_{q=0}^{+\infty} (qK)^2 u_q(t)\cos(qKx)\right)$$

$$-F_0\sum_{i=0}^{+\infty} u_i(t)\Bigg\{ f_0 e^{-(iK)^2\sigma^2}\cos(iKx) + \sum_{m=1}^{\infty} \frac{f_m}{2}\left[e^{-K^2(m-i)^2\sigma^2}\cos\left((m-i)Kx\right)+e^{-K^2(m+i)^2\sigma^2/2}\cos\left((m+i)Kx\right)\right]\Bigg\}$$

(D.12)

Carrying out some algebraic manipulation we get that

$$\sum_{i=0}^{+\infty}\frac{du_i(t)}{dt}\cos(iKx)=\sum_{m=0}^{+\infty}\sum_{n=0}^{+\infty}\left(mnK^2D_m(t)u_n(t)\sin(nKx)\sin(mKx)\right) -\sum_{p=0}^{+\infty}\sum_{q=0}^{+\infty}\left((qK)^2D_p(t)u_q(t)\cos(pKx)\cos(qKx)\right)$$

$$-F_0\sum_{i=0}^{+\infty} u_i(t)\Bigg\{ f_0 e^{-(iK)^2\sigma^2}\cos(iKx) + \sum_{m=1}^{\infty} \frac{f_m}{2}\left[e^{-K^2(m-i)^2\sigma^2}\cos\left((m-i)Kx\right)+e^{-K^2(m-i)^2\sigma^2}\cos\left((m+i)Kx\right)\right]\Bigg\}$$

(D.13)

Now using the trigonometric identities:

$$\sin(mKx)\sin(nKx)=\frac{1}{2}\{\cos[(m-n)Kx]-\cos[(m+n)Kx]\}$$

$$\cos(pKx)\cos(qKx)=\frac{1}{2}\{\cos[(p-q)Kx]+\cos[(p+q)Kx]\}$$

Equation (D.13) can be rewritten as

$$\sum_{i=0}^{+\infty}\frac{du_i(t)}{dt}\cos(iKx)=\sum_{m=0}^{+\infty}\sum_{n=0}^{+\infty}\left(mnK^2D_m(t)u_n(t)\frac{1}{2}\{\cos[(m-n)Kx]-\cos[(m+n)Kx]\}\right)$$

$$-\sum_{p=0}^{+\infty}\sum_{q=0}^{+\infty}\left((qK)^2 D_p(t)u_q(t)\frac{1}{2}\{\cos[(p-q)Kx]+\cos[(p+q)Kx]\}\right)$$

$$-F_0 f_0\sum_{i=0}^{+\infty}u_i(t)e^{-(iK)^2\sigma^2}\cos(iKx)$$

$$-F_0\sum_{i=0}^{+\infty}\sum_{m=1}^{\infty}\frac{f_m}{2}\left[u_i(t)e^{-K^2(m-i)^2\sigma^2}\cos((m-i)Kx)+u_i(t)e^{-K^2(m+i)^2\sigma^2/2}\cos((m+i)Kx)\right]$$

(D.14)

The coefficients of the individual harmonics, which we have used in our expansions, must be identified. In this way we will produce a set of first order coupled differential equations. We work from the following equation

$$\sum_{i=0}^{+\infty}\frac{du_i(t)}{dt}\cos(iKx)=$$

$$\frac{1}{2}\sum_{m=0}^{+\infty}\sum_{n=0}^{+\infty}mnK^2 D_m(t)u_n(t)\cos[(m-n)Kx]-\frac{1}{2}\sum_{m=0}^{+\infty}\sum_{n=0}^{+\infty}mnK^2 D_m(t)u_n(t)\cos[(m+n)Kx]$$

$$-\frac{1}{2}\sum_{p=0}^{+\infty}\sum_{q=0}^{+\infty}(qK)^2 D_p(t)u_q(t)\cos[(p-q)Kx]-\frac{1}{2}\sum_{p=0}^{+\infty}\sum_{q=0}^{+\infty}(qK)^2 D_p(t)u_q(t)\cos[(p+q)Kx]$$

$$-F_0 f_0\sum_{i=0}^{+\infty}u_i(t)e^{-(iK)^2\sigma^2}\cos(iKx)$$

$$-F_0\sum_{i=0}^{+\infty}\sum_{m=1}^{\infty}\frac{f_m}{2}\left[u_i(t)e^{-K^2(m-i)^2\sigma^2}\cos((m-i)Kx)+u_i(t)e^{-K^2(m+i)^2\sigma^2/2}\cos((m+i)Kx)\right]$$

(D.15)

Examining the harmonics separately we start with the coefficient of $\cos(0)=1$:

$$\frac{du_0(t)}{dt} = \frac{1}{2}\sum_{m=0}^{+\infty} m^2K^2D_m(t)u_m(t) - \frac{1}{2}\sum_{p=0}^{+\infty} (pK)^2 D_p(t)u_p(t) - F_0 f_0 u_0(t) - \frac{F_0}{2}\sum_{m=1}^{+\infty} f_m u_m(t)$$

(D.16)

$$\frac{du_0(t)}{dt} + F_0 f_0 u_0(t) + \frac{F_0}{2}\sum_{m=1}^{+\infty} f_m u_m(t) = 0$$

(D.17)

The coefficient of the $\cos(Kx)$ harmonic must be found next. Starting from equation (D.15):

$$\frac{du_1(t)}{dt} =$$

$$\frac{1}{2}\sum_{n=0}^{+\infty} (n+1)nK^2D_{n+1}(t)u_n(t) + \frac{1}{2}\sum_{n=0}^{+\infty} (n-1)nK^2D_{n-1}(t)u_n(t) - \frac{1}{2}\sum_{n=0}^{+\infty} (1-n)nK^2D_{1-n}(t)u_n(t)$$

$$-\frac{1}{2}\sum_{q=0}^{+\infty} (qK)^2 D_{q-1}(t)u_q(t) - \frac{1}{2}\sum_{q=0}^{+\infty} (qK)^2 D_{q-1}(t)u_q(t) - \frac{1}{2}\sum_{q=0}^{+\infty} (qK)^2 D_{1-q}(t)u_q(t)$$

$$- F_0 f_0 u_1(t)e^{-(K)^2\sigma^2} - F_0\frac{f_1}{2}u_0(t)e^{-K^2\sigma^2}$$

$$- F_0\sum_{i=0}^{+\infty} \frac{f_{1-i}}{2}u_i(t)e^{-K^2\sigma^2} - F_0\sum_{i=2}^{+\infty} \frac{f_{i-1}}{2}u_i(t)e^{-K^2\sigma^2}$$

(D.18)

We proceed to carry out some algebraic manipulation described below.

$$\frac{\partial u_1(t)}{\partial t} + F_0 f_0 u_1(t) e^{-(K)^2\sigma^2} + F_0 \frac{f_1}{2} u_0(t) e^{-K^2\sigma^2} +$$

$$+ F_0 \sum_{i=0}^{+\infty} \frac{f_{1+i}}{2} u_i(t) e^{-K^2\sigma_i^2/2} + F_0 \sum_{i=2}^{+\infty} \frac{f_{i-1}}{2} u_i(t) e^{-K^2\sigma/2} =$$

$$\frac{1}{2} \sum_{n=1}^{+\infty} (n+1) nK^2 D_{n-1}(t) u_n(t) + \frac{1}{2} \sum_{n=1}^{+\infty} (n-1) nK^2 D_{n-1}(t) u_n(t)$$

$$- \frac{1}{2} \sum_{q=1}^{+\infty} (qK)^2 D_{q+1}(t) u_q(t) - \frac{1}{2} \sum_{q=1}^{+\infty} (qK)^2 D_{q-1}(t) u_q(t) - \frac{K^2 D_0(t) u_1(t)}{2}$$

(D.19)

This is the generalized (untruncated) first order coefficient. The full general coefficient for the j^{th} term must be found. The coefficient of the $\cos(jKx)$ harmonic must be extracted. Once again starting from Equation (D.15):

$$\frac{du_j(t)}{dt} = -F_0 f_0 u_j(t) e^{-(jK)^2\sigma^2}$$

$$- F_0 \sum_{i=0}^{+\infty} \frac{f_{j+i}}{2} \left[u_i(t) e^{-K^2 j^2 \sigma^2} \cos((m-i)Kx) \right] - F_0 \sum_{i=1+j}^{+\infty} \frac{f_{i-j}}{2} \left[u_i(t) e^{-K^2 j^2 \sigma^2} \cos((m-i)Kx) \right]$$

$$- F_0 \sum_{i=0}^{j-1} \frac{f_{j-i}}{2} \left[u_i(t) e^{-K^2 j^2 \sigma^2} \cos((m+i)Kx) \right]$$

$$+ \frac{1}{2} \sum_{n=0}^{+\infty} (n+j) nK^2 D_{n+j}(t) u_n(t) + \frac{1}{2} \sum_{n=0}^{+\infty} (n-j) nK^2 D_{n-j}(t) u_n(t)$$

$$- \frac{1}{2} \sum_{n=0}^{+\infty} (j-n) nK^2 D_{j-n}(t) u_n(t)$$

$$- \frac{1}{2} \sum_{q=0}^{+\infty} (qK)^2 D_{j+q}(t) u_q(t) - \frac{1}{2} \sum_{q=0}^{-\infty} (qK)^2 D_{q-j}(t) u_q(t) - \frac{1}{2} \sum_{q=0}^{-\infty} (qK)^2 D_{j-q}(t) u_q(t)$$

(D.20)

$$\frac{du_j(t)}{dt} = -F_0 f_0 u_j(t) e^{-(jK)^2\sigma^2/2}$$

$$-\frac{F_0 e^{-(jK)^2\sigma^2/2}}{2}\left\{\sum_{i=0}^{+\infty} f_{j+i}u_i(t) + \sum_{i=1+j}^{+\infty} f_{i-j}u_i(t) + \sum_{i=0}^{j-1} f_{j-i}u_i(t)\right\}$$

$$+\frac{K^2}{2}\sum_{n=1}^{+\infty} n^2 D_{n+j}(t)u_n(t) \quad +\frac{K^2}{2}\sum_{n=1}^{-\infty} jnD_{n+j}(t)u_n(t)$$

$$+\frac{K^2}{2}\sum_{n=1}^{+\infty} n^2 D_{n-j}(t)u_n(t) \quad -\frac{K^2}{2}\sum_{n=1}^{-\infty} jnD_{n-j}(t)u_n(t)$$

$$-\frac{K^2}{2}\sum_{q=1}^{+\infty} q^2 D_{j+q}(t)u_q(t) \qquad -\frac{K^2}{2}\sum_{q=1}^{-\infty} q^2 D_{q-j}(t)u_q(t)$$

$$-\frac{K^2}{2}\sum_{q=1}^{j} q^2 D_{j-q}(t)u_q(t)$$

(D.21)

$$\frac{du_j(t)}{dt} = -F_0 f_0 u_j(t) e^{-(jK)^2\sigma^2/2}$$

$$-\frac{F_0 e^{-(jK)^2\sigma^2/2}}{2}\left\{\sum_{i=0}^{+\infty} f_{j+i}u_i(t) + \sum_{i=1+j}^{+\infty} f_{i-j}u_i(t) + \sum_{i=0}^{j-1} f_{j-i}u_i(t)\right\}$$

$$+j\frac{K^2}{2}\sum_{n=1}^{+\infty} nD_{n-j}(t)u_n(t) - j\frac{K^2}{2}\sum_{n=1}^{+\infty} nD_{n-j}(t)u_n(t)$$

$$-j\frac{K^2}{2}\sum_{n=1}^{j-1} nD_{j-n}(t)u_n(t) + \frac{K^2}{2}\sum_{n=1}^{j-1} n^2 D_{j-n}(t)u_n(t)$$

$$-\frac{K^2}{2}\sum_{q=0}^{j-1} q^2 D_{j-q}(t)u_q(t) - \frac{K^2}{2} j^2 D_0(t)u_j(t)$$

(D.22)

$$\frac{du_j(t)}{dt} = -F_0 f_0 u_j(t) e^{-(jK)^2\sigma^2/2} - \frac{F_0 e^{-(jK)^2\sigma^2/2}}{2}\left\{ \sum_{i=0}^{+\infty} f_{j+i}u_i(t) + \sum_{i=1+j}^{+\infty} f_{i-j}u_i(t) + \sum_{i=0}^{j-1} f_{j-i}u_i(t) \right\} + j\frac{K^2}{2}\sum_{n=1}^{+\infty} nD_{n-j}(t)u_n(t) - j\frac{K^2}{2}\sum_{n=1}^{+\infty} nD_{n-j}(t)u_n(t) - j\frac{K^2}{2}\sum_{n=1}^{j-1} nD_{j-n}(t)u_n(t) - \frac{K^2}{2}j^2 D_0(t)u_j(t)$$

(D.23)

$$\frac{du_j(t)}{dt} + \left[\frac{K^2}{2}j^2 D_0(t)\right]u_j(t) + j\frac{K^2}{2}\sum_{n=1}^{j-1} nD_{j-n}(t)u_n(t) = -F_0 f_0 u_j(t) e^{-(jK)^2\sigma^2} - \frac{F_0 e^{-(jK)^2\sigma^2}}{2}\left\{ \sum_{i=0}^{+\infty} f_{j+i}u_i(t) + \sum_{i=1+j}^{+\infty} f_{i-j}u_i(t) + \sum_{i=0}^{j-1} f_{j-i}u_i(t) \right\} + j\frac{K^2}{2}\sum_{n=1}^{+\infty} \left\{nD_{n+j}(t)u_n(t) - nD_{n-j}(t)u_n(t)\right\}$$

(D.24)

$$\frac{du_j(t)}{dt} + \left[\frac{K^2}{2}j^2 D_0(t)\right]u_j(t) + j\frac{K^2}{2}\sum_{n=1}^{j-1} nD_{j-n}(t)u_n(t) = -F_0 f_0 u_j(t) e^{-(jK)^2\sigma^2/2} - \frac{F_0 e^{-(jK)^2\sigma^2}}{2}\left\{ \sum_{i=0}^{+\infty} f_{j+i}u_i(t) + \sum_{i=1+j}^{+\infty} f_{i-j}u_i(t) + \sum_{i=0}^{j-1} f_{j-i}u_i(t) \right\}$$

$$+ j\frac{K^2}{2}\sum_{n=1}^{-\infty}\left\{nD_{n+j}(t)u_n(t) - (n+j)D_n(t)u_{n+j}(t)\right\} - j\frac{K^2}{2}\left[(j)D_0(t)u_j(t)\right]$$

(D.25)

Which gives the completely general result, for any form of intensity dependence, any diffusion and any polymerisation.

$$\frac{du_j(t)}{dt} + (jK)^2 D_0(t)u_j(t) + j\frac{K^2}{2}\sum_{n=1}^{j-1} nD_{j-n}(t)u_n(t) = -F_0 f_0 u_j(t)e^{-(jK)^2\sigma^2}$$

$$-\frac{F_0 e^{-(jK)^2\sigma^2}}{2}\left\{\sum_{i=0}^{-\infty} f_{j-i}u_i(t) + \sum_{i=1-j}^{+\infty} f_{i-j}u_i(t) + \sum_{i=0}^{j-1} f_{j-i}u_i(t)\right\}$$

$$+ j\frac{K^2}{2}\sum_{n=1}^{+\infty}\left\{nD_{n+j}(t)u_n(t) - (n+j)D_n(t)u_{n+j}(t)\right\}$$

(D.26)

In the next section we will use equation (D.26) to derive a set of coupled differential equations when the monomer concentration depends on the square root of the intensity as pointed out by Kwon et al. [Kwon, 99].

Appendix E: Non-local Kwon Model

We wish to present a truncated set of coupled first-order differential equations, which can be solved numerically. In order to do so we must first decide on the number of monomer terms, which we wish to retain in our analysis, see Equation (D.6). We must also decide on the number of terms that we wish to retain in our diffusion coefficient expansion, see Equation (D.7).

Following Zhao and Mouroulis [Zhao, 94], we assume it is sufficient to retain the first four terms in the monomer expansion, that is $u_0(t), u_1(t), u_2(t)$, and $u_3(t)$. Furthermore we assume that is sufficient to retain only the two first terms in the diffusion constant expansion, that is $D_0(t)$, and $D_1(t)$. From equation (D.17) we get that

$$\frac{du_0(t)}{dt} + F_0 f_0 u_0(t) + \frac{F_0}{2}\left[f_1 u_1(t) + f_2 u_2(t) + f_3 u_3(t)\right] = 0 \tag{E.1}$$

From equation (D.19) we get that

$$\begin{aligned}\frac{\partial u_1(t)}{\partial t} &+ F_0 f_0 u_1(t) e^{-(K)^2\sigma^2/2} + F_0 \frac{f_1}{2} u_0(t) e^{-K^2\sigma^2/2} + \\ &+ \frac{F_0 e^{-K^2\sigma^2/2}}{2}\left[f_1 u_0(t) + f_2 u_1(t) + f_3 u_2(t) + f_4 u_3(t)\right] \\ &+ \frac{F_0 e^{-K^2\sigma^2/2}}{2}\left[f_1 u_2(t) + f_2 u_3(t)\right] + \left[K^2 D_0(t)\right] u_1(t) \\ &+ \frac{K^2}{2}\left[2D_1(t) u_2(t)\right] = 0\end{aligned} \tag{E.2}$$

Giving that:

$$\frac{\partial u_1(t)}{\partial t} + F_0 e^{-K^2\sigma/2} f_1 u_0(t) + \left\{ F_0 e^{-K^2\sigma 2} \left[f_0 + \frac{f_2}{2} \right] + K^2 D_0(t) \right\} u_1(t) +$$

$$+ \left\{ \frac{F_0 e^{-K^2\sigma 2}}{2} [+ f_3 + f_1] + K^2 D_1(t) \right\} u_2(t) + \frac{F_0 e^{-K^2\sigma/2}}{2} [f_4 + f_2] u_3(t) = 0$$

(E.3)

From Equation (D.26) we get for the second coupled equation:

$$\frac{du_2(t)}{dt} + \left[(2K)^2 D_0(t) \right] u_2(t) + K^2 \sum_{n=1}^{1} n D_{2-n}(t) u_n(t) = - F_0 f_0 u_2(t) e^{-(2K)^2\sigma/2}$$

$$- \frac{F_0 e^{-(2K)^2\sigma/2}}{2} \left\{ \sum_{i=0}^{\infty} f_{2-i} u_i(t) + \sum_{i=1-2}^{\infty} f_{i-2} u_i(t) + \sum_{i=0}^{1} f_{2-i} u_i(t) \right\}$$

$$+ K^2 \sum_{n=1}^{+\infty} \{ n D_{n-2}(t) u_n(t) - (n+2) D_n(t) u_{n-2}(t) \}$$

(E.4)

$$\frac{du_2(t)}{dt} + \left[(2K)^2 D_0(t) \right] u_2(t) + K^2 D_1(t) u_1(t) = - F_0 f_0 u_2(t) e^{-(2K)^2\sigma 2}$$

$$- \frac{F_0 e^{-(2K)^2\sigma/2}}{2} \left\{ [f_2 u_0(t) + f_3 u_1(t) + f_4 u_2(t) + f_5 u_3(t)] + [f_1 u_3(t)] + [f_2 u_0(t) + f_1 u_1(t)] \right\}$$

$$+ K^2 \{ - (3) D_1(t) u_3(t) \}$$

(E.5)

Therefore:

$$\frac{du_2(t)}{dt} + \left\{ F_0 e^{-(2K)^2\sigma/2} f_2 \right\} u_0(t) + \left\{ \frac{F_0 e^{-(2K)^2\sigma/2}}{2} [f_3 + f_1] + K^2 D_1(t) \right\} u_1(t)$$

$$+ \left\{ (2K)^2 D_0(t) + F_0 f_0 e^{-(2K)^2/2} \left[f_0 + \frac{f_4}{2} \right] \right\} u_2(t)$$

$$+\left\{3K^2 D_1(t)+F_0 f_0 e^{-(2K)^2/2}\left[\frac{f_5}{2}+\frac{f_1}{2}\right]\right\}u_3(t)$$

(E.6)

From Equation (D.26) we get for the third differential equation:

$$\frac{du_3(t)}{dt}+\left[(3K)^2 D_0(t)\right]u_3(t)+3\frac{K^2}{2}\sum_{n=1}^{2} nD_{3-n}(t)u_n(t)=-F_0 f_0 u_3(t)e^{-(3K)^2\sigma^2/2}$$

$$-\frac{F_0 e^{-(3K)^2\sigma^2/2}}{2}\left\{\sum_{i=0}^{+\infty} f_{3+i}u_i(t)+\sum_{i=4}^{+\infty} f_{i-3}u_i(t)+\sum_{i=0}^{2} f_{3-i}u_i(t)\right\}$$

$$+3\frac{K^2}{2}\sum_{n=1}^{+\infty}\left\{nD_{n+3}(t)u_n(t)-(n+3)D_n(t)u_{n+3}(t)\right\}$$

$$\frac{du_3(t)}{dt}+\left[(3K)^2 D_0(t)\right]u_3(t)+3\frac{K^2}{2}\left[2D_1(t)u_2(t)\right]=-F_0 f_0 u_3(t)e^{-(3K)^2\sigma^2/2}$$

$$-\frac{F_0 e^{-(3K)^2\sigma^2/2}}{2}\left\{\left[f_3 u_0(t)+f_4 u_1(t)+f_5 u_2(t)+f_6 u_3(t)\right]+\left[f_3 u_0(t)+f_2 u_1(t)+f_1 u_2(t)\right]\right\}$$

(E.7)

Therefore:

$$\frac{du_3(t)}{dt}+F_0 e^{-(3K)^2\sigma^2/2} f_3 u_0(t)+\frac{F_0 e^{-(3K)^2\sigma^2/2}}{2}(f_4+f_2)u_1(t)$$

$$+\left\{\frac{F_0 e^{-(3K)^2\sigma^2/2}}{2}(f_5+f_1)+3K^2 D_1(t)\right\}u_2(t)$$

$$+\left\{(3K)^2 D_0(t)+F_0 e^{-(3K)^2\sigma^2/2}\left[f_0+\frac{f_6}{2}\right]\right\}u_3(t)=0$$

(E.8)

Appendix F: Parameters and Units

This section contains a list of all the parameters that appear in this study along with their units.

D	Diffusion coefficient	cm^2/s
C, u(x,t)	concentration	mol/l
I(x,t)	Intensity	Wm^{-2}
κ		$m^2/W/s$
R(x,x')		1/m
R(x,x',t,t')		1/m/s
F_0	rate of polymerisation	1/s
σ	non-local variance	m^2
R		Dimensionless
N(x,t)		mol/l
$N_m(\xi)$		mol/l
C		l/mol
d	thickness	m
λ	wavelength	m
x	length	m
dt		s
dx		m
V	visibility	Dimensionless
ξ	exposure energy	Dimensionless
S		Dimensionless
n_{av}, n_m. n(x,t)		Dimensionless
η	diffraction efficiency	Dimensionless
W, B, A, L		Dimensionless
a_n, T, f_i		Dimensionless
k_i, k_t, k_p	rates	l/mol/s
Φ	quantum yield	Dimensionless

Publications

Reviewed Journal Papers

J. R. Lawrence, F. T. O'Neill, J. T. Sheridan, "Photopolymer material parameter estimation using diffusion based analytic formula", accepted for publication, Journal of Applied Physics, (2001).

J. R. Lawrence, F. T. O'Neill, J. T. Sheridan, "Adjusted intensity dependence non-local diffusion model of holographic grating formation in photopolymer", accepted for publication, JOSA B, (2001).

F. T. O'Neill, *J. R. Lawrence*, J. T. Sheridan, "Thickness variation of a self-processing acrylamide-based photopolymer and reflection holography", Optical Engineering, Vol. 40, No. 4, Pg. 533-539, (2001).

F. T. O'Neill, *J. R. Lawrence*, J. T. Sheridan, "Improvement of a holographic recording material using a aerosol sealant", J. European Optical Society A., Vol. 3, No 1, Pg. 20-25, (2001).

F. T. O'Neill, *J. R. Lawrence*, J. T. Sheridan, "Automated recording and testing of holographic optical element arrays",, Optik, Vol. 111, No. 10, Pg. 459-467, (2000).

J. T. Sheridan, *J. R. Lawrence*, "Non-local response diffusion model of holographic recording in photopolymer", JOSA. A., Vol. 17, No. 6, Pg. 1108-1114, (2000).

Conference Proceedings

V. Moreau, *J. R. Lawrence*, S. Soler-Hernandez, B. Tilkens, Y. Renotte, Y. Lion, "Optimisation of holograms recorded in DuPont photopolymer", to be published, Proc. SPIE, (2000).

Poster Presentations

J. R. Lawrence, S. Martin. J.T. Sheridan, "A self processing material for holographic recording", poster presentation, 51st Irish Universities Chemistry Research Colloquium, Dublin, (1999)

J. R. Lawrence, F. T. O'Neill, V. Toal, "A self processing photopolymer film for holographic recording", poster presentation, COST P2, Workshop on applications of non-linear optical phenomena and related industrial perspectives, Amalfi, Italy, 7-8 October (1999).